NIST Technical Note 1865

Impact Characterization of Line Pipe Steels by Means of Standard, Sub-Size and Miniaturized Charpy Specimens

Enrico Lucon
Chris N. McCowan
Ray L. Santoyo

http://dx.doi.org/10.6028/NIST.TN.1865

National Institute of Standards and Technology
U.S. Department of Commerce

NIST Technical Note 1865

Impact Characterization of Line Pipe Steels by Means of Standard, Sub-Size and Miniaturized Charpy Specimens

Enrico Lucon
Chris N. McCowan
Ray L. Santoyo

Applied Chemicals and Materials Division
Material Measurement Laboratory

This publication is available free of charge from:
http://dx.doi.org/10.6028/NIST.TN.1865

February 2015

U.S. Department of Commerce
Penny Pritzker, Secretary

National Institute of Standards and Technology
Willie May, Acting Under Secretary of Commerce for Standards and Technology and Acting Director

National Institute of Standards and Technology Technical Note 1865
Natl. Inst. Stand. Technol. Tech. Note 1865, 60Pages (February 2015)
CODEN: NTNOEF

This publication is available free of charge from:
http://dx.doi.org/10.6028/NIST.TN.1865

Abstract

In this investigation, we performed instrumented Charpy tests in order to characterize the impact properties of four line pipe steels with significantly different mechanical properties. For each of the steels, tests were performed on standard E23 Charpy specimens, sub-size specimens of two types (⅔-size and ½-size), and miniaturized specimens of two types (KLST and RHS). For every combination of steel and specimen type, full transition curves and corresponding transition temperatures were established for absorbed energy, lateral expansion and shear fracture appearance.

Topics addressed in this study on the basis of the results obtained include:

- comparisons between conventional Charpy data obtained from different specimen types;
- comparisons between different measures of ductile-to-brittle transition temperature;
- comparisons between characteristic instrumented forces obtained from different specimen types;
- normalization of characteristic instrumented forces;
- relationship between different measures of absorbed energy; and
- correlations between transition temperatures and upper shelf energies calculated from different specimen types.

The results of our investigation confirm the applicability and usefulness of both sub-size and miniaturized Charpy specimens for the characterization of line pipe steels, be they of past or recent production, whenever the thickness of the pipe doesn't allow testing full-size specimens. Although commonly used codes and procedures for line pipe steels only envisage the use of sub-size specimens, we demonstrated that miniaturized samples can also provide useful results and should also be considered. Reliable empirical correlations between transition temperatures and upper shelf energies measured from specimens of different type can be established, in substantial agreement with other studies available in the literature. This applies to steels of very high toughness and ductility also, such as X65 and X70 in this investigation, even though a substantial portion of the absorbed energy in a Charpy test is dissipated via plastic bending of the sample and interactions with the machine anvil/supports.

Keywords

ductile-to-brittle transition temperature; instrumented Charpy tests; Line pipe steels; miniaturized Charpy specimens; shear fracture appearance; size-normalization; sub-size Charpy specimens; upper shelf energy.

Table of Contents

1. Introduction

Line pipe steels, particularly of the most recent generations (X80, X100), are characterized by a continuously increasing ratio between ductility and mechanical strength, which makes it difficult to interpret the results of conventional mechanical characterization tests, such as Charpy impact tests. In these modern steels, the improvement in fracture resistance is due to various refinements of the manufacturing process, which lead to smaller grain sizes, reduced inclusion contents, a fine bainitic structure, etc. For steels exhibiting this combination of toughness and ductility, the usefulness and significance of conventional mechanical tests are nowadays seriously questioned, as well as the possibility of predicting ductile fracture scenarios in actual line pipes in full-scale tests based on the outcome of small-scale laboratory tests.

According to current Charpy test standards (ASTM E23-12c and ISO 148-1:2009), absorbed energy (*KV*) results from partially fractured test specimens can be averaged with the results from fully fractured specimens. However, most researchers agree that if a specimen does not fully fracture at the end of a Charpy test, a significant fraction of the work spent was employed to bend/plastically deform the sample rather than fracture it. Therefore, in principle *KV* results from partially and fully fractured specimens are not directly comparable and should not be averaged. In the case of very high-ductility materials such as modern line pipe steels, the situation is exacerbated by the very limited amount of tearing (actual fracture) observed on tested specimens. The extremely high *KV* values recorded from these tests can be associated mostly to bending of the sample and friction between specimen and anvils. The reliability and usefulness of conventional Charpy tests under these circumstances are therefore questionable.

In the work presented here, we characterized the impact properties of four line pipe steels ranging from a 50-year-old service-exposed steel (X52) to modern high-toughness and high-ductility steels (X65, X70, X100). X65 and X70 exhibit a high ductility-to-strength ratio and ductile specimens hardly fracture, whereas X100 has a lower ductility-to-strength ratio and fractures completely even under fully ductile conditions.

For each of the steels investigated, we performed tests on standard full-size Charpy specimens (10 × 10 × 55 mm), sub-size specimens corresponding to different fractions of the thickness of a standard Charpy specimen (⅔, ½), and miniaturized specimens, where all dimensions are scaled or reduced (KLST and RHS). All tests were performed as instrumented impact tests, recording the force applied to the specimen during impact, at temperatures ranging from lower shelf conditions (fully brittle behavior) to upper shelf conditions (fully ductile behavior). Ductile-to-Brittle Transition Temperatures (*DBTT*s) calculated from absorbed energy, lateral expansion, and shear fracture appearance were compared among the different specimen types, and empirical correlations between full-size, sub-size, and miniaturized specimens were established.

For high-ductility/high-toughness materials, it is often very difficult to correctly interpret the fracture surface when performing optical measurements of Shear Fracture Appearance (*SFA*) due to the complex appearance of the microstructure and the intermixing of brittle (cleavage) and ductile features. Under these circumstances, the conventional method of *SFA* measurement is associated with a very high degree of uncertainty and the availability of an instrumented test record is extremely useful. Characteristic force values, corresponding to specific events such as general yield, maximum force, initiation of brittle fracture and crack arrest, can be correlated to the percentage of ductility on the fracture surface, so that reasonable estimates of *SFA* can be obtained by correlating these characteristic force values.

2. Materials and experimental

Four commercial line pipe steels (X52, X65, X70, X100) were selected for this investigation, representing a variety of different material behaviors and manufacturing processes. X52 was produced in the early 60s and put in service in 1964 in a natural gas pipeline, which was extracted from the ground after 40 years of operation. X65 and X70 represent more modern and very high ductility and toughness materials. X100, although of recent production, exhibits a lower ratio between ductility and mechanical strength. The chemical composition of the steels is shown in Table 1, while Table 2 provides their tensile properties at room temperature.

Table 1 - Chemical composition (weight %) of the investigated line pipe steels.

Steel	C	Mn	Si	S	P	Al	Cu	Ni	Cr	Mo	Sn	Nb	Ti	V	N
X52	0.24	0.96	0.06	0.021	0.011	0.002	0.085	0.05	0.01	0.004	n/a	0.001	0.002	0.002	0.003
X65	0.05	1.42	0.28	0.003	0.011	0.024	0.137	0.05	0.04	0.01	0.007	0.042	0.009	n/a	0.007
X70	0.05	1.37	0.23	0.001	0.010	0.027	0.260	0.13	0.06	n/a	n/a	0.070	0.013	0.008	0.008
X100	0.07	1.83	0.11	0.005	0.005	0.042	0.303	0.52	0.03	0.27	n/a	0.027	0.009	n/a	0.004

Table 2 – Room temperature tensile properties (transverse direction) of the investigated line pipe steels.

Steel	Yield strength, σ_y (MPa)	Tensile strength, σ_{TS} (MPa)	Total elongation, ε_t (%)	$\frac{\varepsilon_t}{\sigma_{TS}}$
X52	325	526	15.0	0.03
X65	514	581	31.9	0.05
X70	503	608	23.8	0.04
X100	817	849	19.1	0.02

From Table 1, it can be noted that all steels except for X52 are microalloyed with Nb and Ti, which results in grain refinement during steel processing. The content of S is also higher by an order of magnitude in X52, and this is expected to cause a higher inclusion content. The high C content in X52 could also explain the poor ductility of the steel, indicated by the low total elongation in Table 2.

Charpy specimens of five different geometries were tested. Along with full-size standard specimens (thickness B and width W = 10 mm, length L = 55 mm), both sub-size (SCVN) and miniaturized (MCVN) specimens were used.

Sub-size Charpy specimens have the length and one of the cross-sectional dimensions identical to a standard specimen, while the other cross-sectional dimension (the specimen thickness) is reduced. In this investigation, we used ⅔-size (thickness = 6.67 mm) and ½-size (thickness = 5 mm) specimens. Both geometries are among those listed in ASTM A370-13 [1] and the only two sub-size Charpy specimens considered by API Specification 5L [2].

Two types of miniaturized Charpy specimens were used: KLST (3 × 4 × 27 mm) and RHS (4.83 × 4.83 × 24.13 mm). The former is the reference MCVN geometry of ISO 14556:2000 [3], while the latter is the reference specimen type of ASTM E2248-13 [4]. See also Figure 1.

All the specimens were machined in T-L direction.

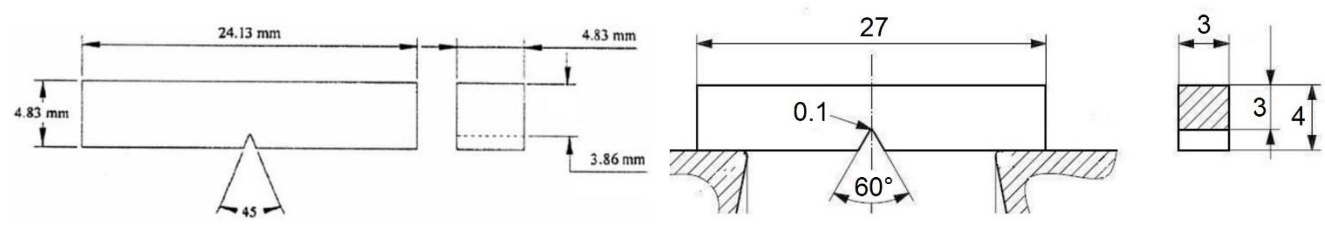

(a) (b)

Figure 1 - Dimensions of MCVN specimens: (a) RHS and (b) KLST.

For every material and specimen type, 12 instrumented Charpy tests (11 for X100) were performed at temperatures allowing a complete definition of transition curves for absorbed energy (*KV*), lateral expansion (*LE*) and shear fracture appearance (*SFA*).

CVN and SCVN tests were performed on a large-scale impact machine with capacity of 953.56 J and impact speed of 5.47 m/s. The machine was equipped with an instrumented striker conforming to ASTM E23-12c (radius of striking edge = 8 mm). For tests above room temperature, specimens were heated by means of an electric plate; for tests below room temperature and down to -90 °C, specimens were refrigerated by means of a cooling bath utilizing ethyl alcohol. Below -90 °C, specimens were positioned on a steel block partially immersed in liquid nitrogen inside an insulated container. In all cases, the transfer time of the specimen between removal from the conditioning medium to pendulum impact was well below 5 s (typically around 3 s). During conditioning, temperature was monitored by means of a dummy specimen instrumented with a K-type thermocouple.

In order to maintain the position of the center of strike when SCVN specimens were tested, shims were attached to the impact machine supports by means of double-sided tape. The thickness of the shims was 1.7 mm and 2.5 mm for ⅔-size and ½-size specimens, respectively, so that the centerline of the SCVN specimen at impact coincided with the centerline of a CVN specimen.

MCVN specimens were tested on a small-scale impact tester. When testing KLST specimens, the machine has a capacity of 50.15 J and an impact speed of 3.5 m/s, and is equipped with a 2-mm instrumented striker. When RHS specimens are tested, the capacity is 50.8 J, the impact speed is 3.5 m/s and the instrumented striker has a radius of 3.86 mm (nominal 4-mm striker, in accordance with E2248-13). For high temperature tests, specimens were heated by means of an electric plate. For low-temperature tests, the samples were individually immersed in liquid nitrogen until their temperature was stable between -180 °C and -190 °C. Using specially-made tongs, the specimen was removed from the LN_2 bath and positioned on the machine supports and anvils. When its temperature reached the desired test temperature (within approximately ± 3 °C), the hammer was released and the specimen impacted. The actual specimen temperature at the moment of impact was recorded[*]. Each sample was individually instrumented with a K-type thermocouple that had been spot-welded on the specimen surface, in the vicinity of the notch tip (within 1 mm). To minimize temperature gradients induced by the small size of the specimens, the anvils and supports of the machine were kept at low temperature (between -30 °C and -60 °C) by a constant flow of LN_2 vapors through copper blocks insulated with Styrofoam.

For all tests, absorbed energy (*KV*) values were provided by the machine encoder. Lateral expansion (*LE*) on CVN and SCVN specimens was measured by the use of a gage similar to the one recommended by ASTM E23-12c, Fig. 7. On MCVN specimens, *LE* measurements were executed with the aid of a caliper.

[*]The same procedure was followed for tests above room temperature.

Shear fracture appearance (*SFA*) was measured directly on the specimen fracture surface in accordance with ASTM E23-12c and ISO 148-1:2009. Optical measurements were also compared with estimates obtained from the instrumented test records, by means of empirical formulae that are included in both ISO 14556:2000 and ASTM E2298-13a [5]. These formulae utilize characteristic instrumented forces (general yield, maximum force, brittle fracture initiation and crack arrest) to quantify the percentage of brittle fracture for the specimen tested. Results and analyses are reported elsewhere [6].

3. Data analyses

3.1 Conventional Charpy parameters (*KV*, *LE*, *SFA*)

Absorbed energy, lateral expansion and shear fracture appearance values were fitted as a function of test temperature using the widely used hyperbolic tangent (TANH) model, given by:

$$Y = A + B \cdot \tanh\left[\frac{X - DBTT}{C}\right] \tag{1}$$

where the variables X and Y are temperature and *KV*/*LE*/*SFA* respectively, and A, B, $DBTT$, and C are fitting coefficients that are calculated by the least square method [7]. The fitting coefficients in eq.(1) have the following physical interpretation:

- $A + B$ corresponds to the upper shelf value (asymptotic Y level that the curve approaches for $X \to +\infty$);
- $A - B$ corresponds to the lower shelf value (asymptotic Y level that the curve approaches for $X \to -\infty$);
- C corresponds to the half-width of the transition region (portion of the curve between lower and upper shelf), in °C;
- *DBTT* (Ductile-to-Brittle Transition Temperature) corresponds to the X value of the midpoint between lower and upper shelf, in °C;
- B/C corresponds to the slope of the fitted curve in the transition region.

Data fitting for *KV* values was performed with the following constraints applied:

- the upper shelf energy ($USE = A + B$) was set as the average *KV* for all specimens having $SFA \geq 95$ %;
- the lower shelf energy ($A - B$) was set at 2.7 J for CVN specimens [8], and as the minimum recorded value for SCVN and MCVN specimens.

Data fitting for *LE* values was performed with the following constraints applied:

- the upper shelf level ($A + B$) was set as the average *LE* of all specimens having $SFA \geq 95$ %;
- the lower shelf energy level ($A - B$) was set as the minimum recorded value for all specimens.

Finally, data fitting for *SFA* values was performed with the following constraint applied:

- A and B were both set at 50 %, so that lower and upper shelf level always equal 0 % and 100 %, respectively; consequently, the value of *DBTT* (designated as $T_{50\%}$) always corresponds to $SFA = 50$ %.

For each data set analyzed (material/specimen type), the following parameters are reported:

- *DBTT*s calculated from the transition curves of absorbed energy ($DBTT_{KV}$), lateral expansion ($DBTT_{LE}$), and shear fracture appearance ($T_{50\%}$);
- upper shelf energy (*USE*).

3.2 Instrumented Charpy parameters

From the analysis of each instrumented Charpy test record, conducted in accordance with both ISO 14556:2000 and E2298-13a, the following values of force (*F*) and absorbed energy (*W*) were determined:

- general yield (F_{gy}, W_{gy});
- maximum force (F_m, W_m);
- initiation of brittle fracture (F_{bf}, W_{bf})†;
- crack arrest (F_a, W_a);
- test termination (W_t).

In case of fully brittle behavior (curve of Type A according to ASTM E2298-13a, curve of Type A or B according to ISO 14556:2000), F_{gy} is not defined. In case of fully ductile behavior (curve of Type A according to ASTM E2298-13a, curve of Type A or B according to ISO 14556:2000), F_{bf} and F_a are not defined.

Additionally, the ratio between the two independent measures of absorbed energy (KV/W_t) was calculated and reported. *KV* and W_t should ideally be in agreement within ± 15 % [5], and their ratio should be reasonably consistent from test to test and from material to material (since it only depends on the machine characteristics and the calibration of the instrumented striker).

4. Test results

4.1 Conventional Charpy parameters (*KV*, *LE*, *SFA*)

Conventional Test results for CVN, ⅔-size, ½-size, KLST and RHS specimens are provided in Tables 3 to 7.

Table 3 - Charpy test results for CVN specimens.

X52					X65				
Specimen id	**T (°C)**	**KV (J)**	**LE (mm)**	**SFA (%)**	**Specimen id**	**T (°C)**	**KV (J)**	**LE (mm)**	**SFA (%)**
C11	-80	2.40	0.058	0	C10	-150	5.27	0.036	0
C8	-50	4.13	0.046	0	C2	-90	10.13	0.094	4
C5	-35	4.13	0.058	6	C7	-65	198.68	1.895	54
C4	-15	10.21	0.074	16	C5	-50	98.50	1.240	26
C2	0	27.99	0.480	28	C1	-35	176.56	1.783	45
C10	10	34.25	0.676	39	C9	-20	268.81	2.035	68
C1	21	48.86	0.848	53	C11	0	229.11	2.080	81
C6	40	61.88	1.135	79	C8	5	422.98	1.918	86
C7	76	74.29	1.387	100	C3	10	428.76	2.007	100
C3	100	75.22	1.415	100	C4	21	431.78	1.963	100
C12	148	71.50	1.026	100	C6	100	404.14	1.941	100
C9	198	69.40	1.102	100	C12	150	391.04	2.418	100

†The identification used here and in the rest of this document ("*bf*") is from ASTM E2298-13a; ISO 14556:2000 uses "*iu*" as a subscript.

X70					X100				
Specimen id	**T (°C)**	**KV (J)**	**LE (mm)**	**SFA (%)**	**Specimen id**	**T (°C)**	**KV (J)**	**LE (mm)**	**SFA (%)**
C2	-150	5.95	0.076	4	C4	-149	7.09	0.051	4
C3	-125	7.54	0.043	4	C5	-90	32.11	0.399	21
C6	-112	18.14	0.157	7	C6	-80	33.46	0.399	15
C9	-99	205.42	1.842	67	C1	-75	163.24	1.656	50
C10	-98	30.52	0.320	14	C7	-70	125.99	1.328	52
C5	-90	327.65	1.867	100	C12	-50	148.54	1.364	70
C11	-80	406.42	1.704	100	C2	-50	183.76	1.417	69
C1	-70	339.31	1.697	100	C10	-35	225.93	1.948	100
C7	-70	410.12	1.770	100	C9	-20	226.99	1.867	100
C12	-50	462.33	1.971	100	C8	21	206.73	2.027	100
C8	-20	460.94	2.200	100	C3	100	248.20	2.320	100
C4	21	439.74	2.304	100					

Table 4 - Charpy test results for ⅔-size specimens.

X52					X65				
Specimen id	**T (°C)**	**KV (J)**	**LE (mm)**	**SFA (%)**	**Specimen id**	**T (°C)**	**KV (J)**	**LE (mm)**	**SFA (%)**
S1-8	-80	2.70	0.056	0	S1-11	-164	1.57	0.132	0
S1-7	-50	4.74	0.079	2	S1-2	-140	3.30	0.064	2
S1-5	-35	13.58	0.292	14	S1-5	-125	3.38	0.064	3
S1-2	-15	15.73	0.378	20	S1-10	-114	2.48	0.041	6
S1-3	0	19.76	0.589	31	S1-9	-95	5.04	0.074	9
S1-12	10	32.02	0.851	52	S1-7	-90	111.13	1.989	51
S1-1	21	38.17	1.052	71	S1-3	-70	121.95	1.816	61
S1-6	40	46.90	1.189	87	S1-4	-50	158.64	2.212	86
S1-10	75	47.96	1.316	100	S1-6	-35	261.16	1.862	97
S1-4	100	47.96	1.331	100	S1-12	-20	231.72	1.628	100
S1-9	152	46.09	1.293	100	S1-8	21	244.95	1.928	100
S1-11	199	47.31	1.293	100	S1-1	100	246.25	2.070	100
X70					**X100**				
Specimen id	**T (°C)**	**KV (J)**	**LE (mm)**	**SFA (%)**	**Specimen id**	**T (°C)**	**KV (J)**	**LE (mm)**	**SFA (%)**
S1-10	-163	2.93	0.028	2	S1-10	-162	3.46	0.114	4
S1-9	-136	1.87	0.197	3	S1-6	-124	9.67	0.030	4
S1-7	-111	10.36	0.066	8	S1-5	-90	34.98	0.559	26
S1-6	-105	8.23	0.127	6	S1-2	-80	86.12	1.415	73
S1-3	-100	199.06	1.829	100	S1-4	-75	78.70	1.514	74
S1-2	-95	179.07	2.042	100	S1-7	-70	89.23	1.529	62
S1-5	-90	181.43	2.098	100	S1-1	-50	93.99	1.455	82
S1-11	-70	221.89	2.027	100	S1-3	-40	101.90	1.760	100
S1-1	-60	239.35	1.806	100	S1-12	-20	117.15	1.852	100
S1-8	-50	278.14	1.745	100	S1-8	21	120.56	1.715	100
S1-12	-20	271.85	1.781	100	S1-9	100	130.66	2.169	100
S1-4	21	249.30	1.720	100					

Table 5 - Charpy test results for ½-size specimens.

X52					X65				
Specimen id	T (°C)	KV (J)	LE (mm)	SFA (%)	Specimen id	T (°C)	KV (J)	LE (mm)	SFA (%)
S2-10	-80	1.57	0.058	0	S2-12	-153	2.48	0.094	3
S2-7	-60	2.33	0.015	4	S2-10	-123	1.35	0.061	3
S2-6	-50	8.76	0.160	8	S2-8	-114	3.30	0.064	5
S2-3	-35	11.20	0.201	16	S2-6	-100	43.82	1.191	38
S2-2	-15	11.66	0.394	25	S2-3	-90	57.32	1.524	51
S2-4	0	18.06	0.660	45	S2-7	-70	80.49	1.951	69
S2-1	21	29.33	1.036	81	S2-11	-50	93.38	1.735	85
S2-8	42	36.57	1.214	100	S2-2	-40	82.36	1.608	81
S2-9	75	37.05	1.151	100	S2-9	-35	119.54	1.745	100
S2-5	100	36.81	1.245	100	S2-4	-20	127.74	1.709	100
S2-11	145	34.33	1.179	100	S2-1	21	113.01	1.979	100
S2-12	200	35.45	1.234	100	S2-5	100	121.96	1.699	100
X70					**X100**				
Specimen id	**T (°C)**	**KV (J)**	**LE (mm)**	**SFA (%)**	**Specimen id**	**T (°C)**	**KV (J)**	**LE (mm)**	**SFA (%)**
S2-1	-151	1.95	0.051	5	S2-3	-149	2.55	0.046	5
S2-7	-132	2.63	0.152	7	S2-10	-131	3.08	0.046	7
S2-11	-124	6.55	0.251	16	S2-11	-110	11.13	0.287	8
S2-6	-120	57.56	1.270	69	S2-7	-96	7.47	0.135	15
S2-9	-115	37.94	0.978	41	S2-5	-90	54.60	1.346	59
S2-10	-100	63.21	1.603	75	S2-2	-70	32.11	0.754	59
S2-3	-100	74.20	1.448	60	S2-1	-50	70.41	1.580	84
S2-2	-96	73.27	1.615	84	S2-8	-20	73.53	1.549	76
S2-5	-90	120.00	2.235	100	S2-9	10	89.48	2.047	100
S2-8	-50	122.77	1.994	100	S2-4	21	81.26	1.930	100
S2-12	-20	134.63	1.585	100	S2-6	100	70.33	1.697	100
S2-4	21	138.01	1.651	100					

Table 6 - Charpy test results for KLST specimens.

X52					X65				
Specimen id	T (°C)	KV (J)	LE (mm)	SFA (%)	Specimen id	T (°C)	KV (J)	LE (mm)	SFA (%)
K4	-188	0.08	0.05	2	K11	-190	0.20	0.09	4
K10	-150	0.18	0.04	8	K3	-174	0.30	0.13	6
K12	-122	0.16	0.03	2	K2	-150	4.18	0.45	21
K1	-76	0.21	0.10	10	K10	-147	1.39	0.13	10
K3	-50	0.63	0.09	29	K7	-122	0.96	0.19	6
K7	-40	1.69	0.21	44	K4	-111	6.63	0.77	54
K8	-35	2.32	0.31	54	K8	-100	4.35	0.55	30
K6	-26	2.97	0.40	67	K5	-84	9.53	0.94	100
K5	0	3.91	0.48	88	K12	-75	8.08	0.88	100
K2	20	4.49	0.57	100	K9	-50	9.57	0.96	100
K9	100	4.34	0.64	100	K6	0	9.37	1.00	100
K11	144	3.99	0.60	100	K1	20	9.33	1.02	100

X70					X100				
Specimen id	**T (°C)**	**KV (J)**	**LE (mm)**	**SFA (%)**	**Specimen id**	**T (°C)**	**KV (J)**	**LE (mm)**	**SFA (%)**
K11	-190	0.20	0.10	5	K9	-191	0.27	0.07	4
K12	-169	0.33	0.12	7	K5	-150	0.94	0.07	13
K4	-150	0.95	0.08	6	K6	-126	2.05	0.15	13
K5	-140	0.67	0.21	7	K2	-121	2.71	0.23	16
K6	-134	9.19	0.81	100	K3	-112	7.34	0.63	n/a[‡]
K3	-130	9.28	0.83	100	K1	-100	7.96	0.67	93
K9	-115	9.82	0.86	100	K10	-75	8.23	0.72	n/a[‡]
K10	-100	10.34	0.93	100	K4	-50	8.67	0.74	100
K7	-77	10.22	0.99	100	K7	-10	9.20	0.85	100
K8	-50	9.57	1.00	100	K12	0	N/A	0.84	100
K2	0	9.94	1.00	100	K8	20	8.89	0.80	100
K1	20	9.86	1.00	100					

Table 7 - Charpy test results for RHS specimens.

X52					X65				
Specimen id	**T (°C)**	**KV (J)**	**LE (mm)**	**SFA (%)**	**Specimen id**	**T (°C)**	**KV (J)**	**LE (mm)**	**SFA (%)**
R3	-184	0.20	0.04	2	R1	-180	0.55	0.04	3
R2	-150	0.22	0.08	1	R2	-150	0.47	0.00	3
R1	-125	0.31	0.06	4	R7	-135	1.60	0.03	4
R4	-101	0.38	0.09	1	R3	-124	4.21	0.16	8
R8	-70	0.64	0.07	3	R4	-119	20.75	0.92	45
R7	-50	2.00	0.11	4	R10	-112	32.58	0.88	100
R9	-25	2.09	0.12	25	R6	-112	1.66	0.12	7
R5	-16	4.85	0.31	39	R5	-101	42.48	0.73	100
R10	-5	4.81	0.34	46	R9	-90	39.97	0.84	88
R12	21	13.14	0.70	100	R11	-75	47.40	1.03	100
R11	100	11.66	0.74	100	R8	-40	45.88	1.03	100
R6	149	12.13	0.72	100	R12	21	44.03	1.07	100

X70					X100				
Specimen id	**T (°C)**	**KV (J)**	**LE (mm)**	**SFA (%)**	**Specimen id**	**T (°C)**	**KV (J)**	**LE (mm)**	**SFA (%)**
R1	-180	0.53	0.03	4	R2	-184	1.21	0.05	3
R2	-150	2.26	0.09	5	R1	-153	2.16	0.06	9
R7	-136	2.08	0.05	7	R12	-123	4.49	0.13	8
R5	-129	4.89	0.22	10	R3	-110	3.62	0.33	9
R3	-125	39.98	1.06	100	R8	-105	6.30	0.25	14
R6	-120	42.60	0.91	100	R4	-102	19.16	0.67	88
R12	-115	8.13	0.45	61	R9	-100	29.37	0.93	96
R4	-115	45.37	0.92	100	R6	-76	24.27	0.90	100
R9	-100	47.93	0.70	100	R10	-70	29.60	0.99	100
R8	-31	48.41	1.16	100	R5	-35	29.76	1.04	100
R10	21	46.61	1.13	100	R7	21	31.73	1.06	100
R11	21	N/A	1.13	100					

[‡]For these tests, it was not possible to estimate the value of *SFA* through optical measurements. Furthermore, the instrumented signal was not recorded, and therefore no estimate of *SFA* is available either.

The values of $DBTT_{KV}$, USE, $DBTT_{LE}$, and $T_{50\%}$ calculated from the transition curves for all materials and specimen types are summarized in Table 8.

Table 8 - Values of *DBTT* and *USE* calculated from the transition curves.

Steel	Specimen type	$DBTT_{KV}$ (°C)	USE (J)	$DBTT_{LE}$ (°C)	$T_{50\%}$ (°C)
X52	CVN	11.7	72.6	8.4	17.8
	⅔-size	0.2	47.3	-0.8	9.0
	½-size	-4.3	36.0	-5.2	0.3
	KLST	-35.1	4.2	-29.6	-36.6
	RHS	-5.6	12.3	-4.8	-8.0
X65	CVN	-34.8	415.7	-75.7	-40.0
	⅔-size	-70.1	246.0	-94.6	-78.8
	½-size	-80.5	120.6	-102.6	-85.4
	KLST	-111.0	9.5	-110.9	-102.8
	RHS	-111.6	44.0	-114.1	-114.2
X70	CVN	-94.5	419.8	-100.3	-97.4
	⅔-size	-100.3	252.1	-104.3	-103.9
	½-size	-103.8	128.9	-117.2	-113.8
	KLST	-136.6	10.0	-136.2	-139.1
	RHS	-126.6	47.1	-123.5	-128.5
X100	CVN	-69.6	233.7	-74.0	-67.7
	⅔-size	-82.7	122.8	-85.2	-83.7
	½-size	-76.7	78.7	-78.6	-78.5
	KLST	-117.8	8.9	-115.5	-113.0
	RHS	-103.0	28.9	-103.0	-103.6

Figure 2 compares values of $DBTT_{KV}$ measured from the different specimen types. The same information is presented in terms of USE, $DBTT_{LE}$, and $T_{50\%}$ in Figures 3, 4, and 5 respectively. A general trend of decreasing transition temperatures and upper shelf energies with decreasing specimen size/cross section is observed.

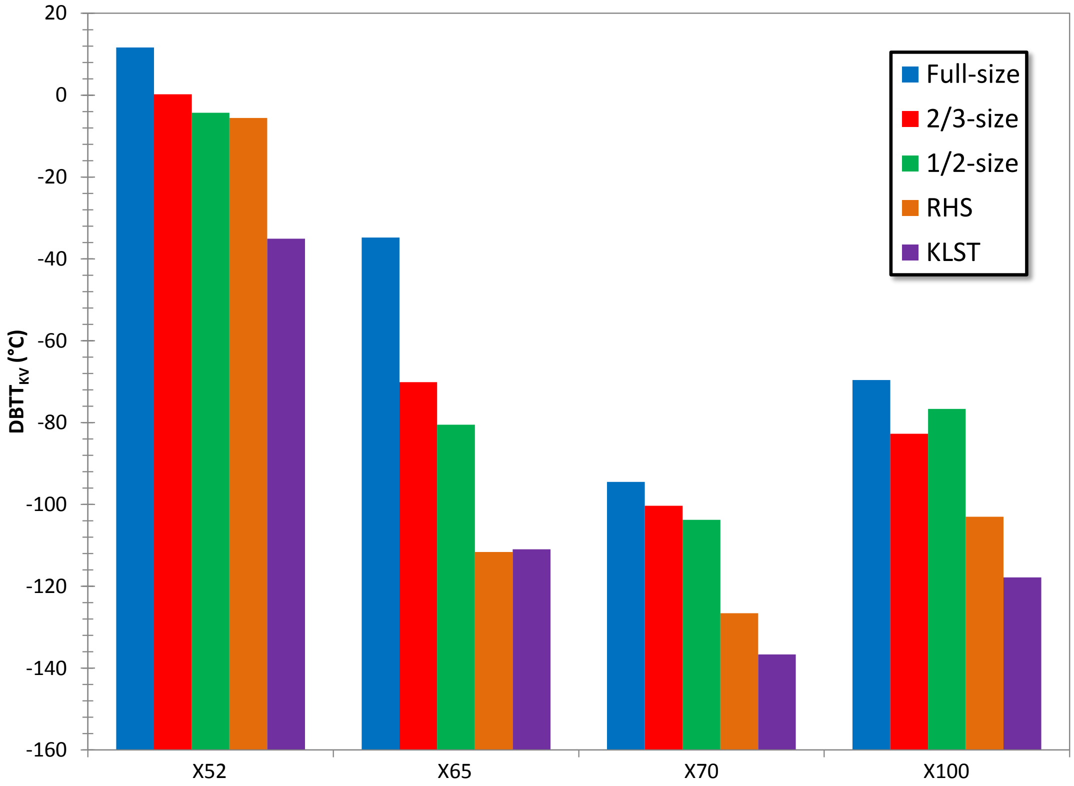

Figure 2 - *DBTT$_{KV}$* values measured from different specimen types.

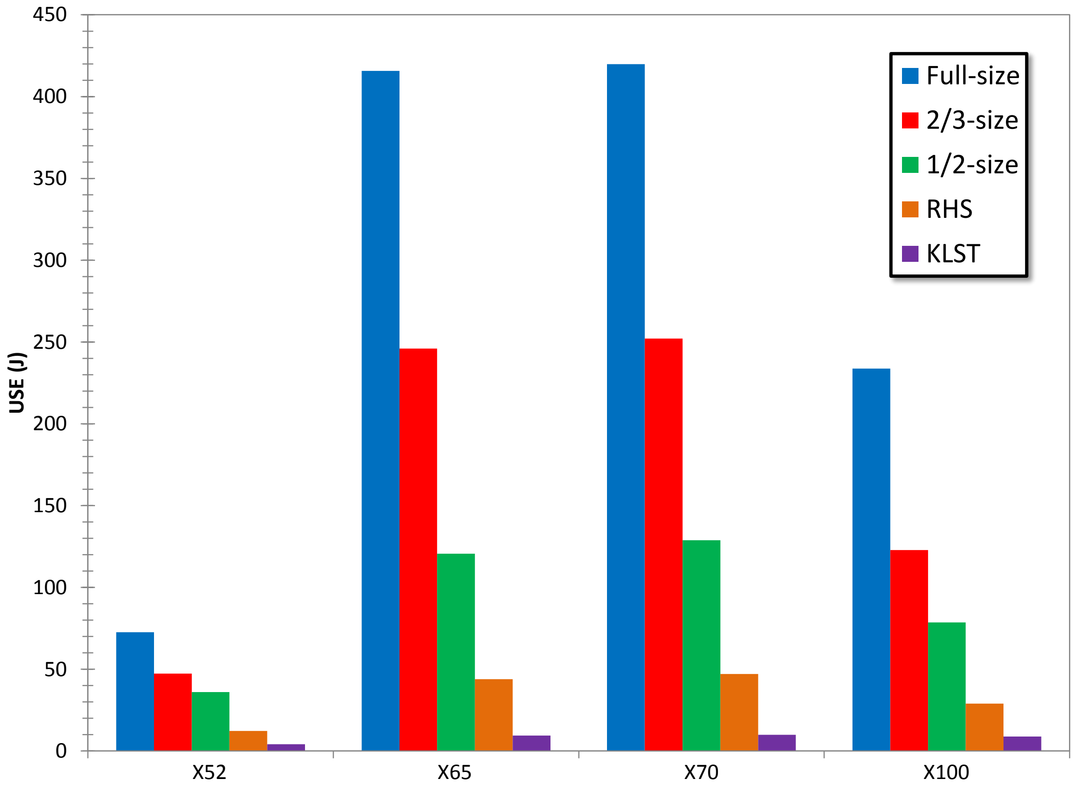

Figure 3 - *USE* values measured from different specimen types.

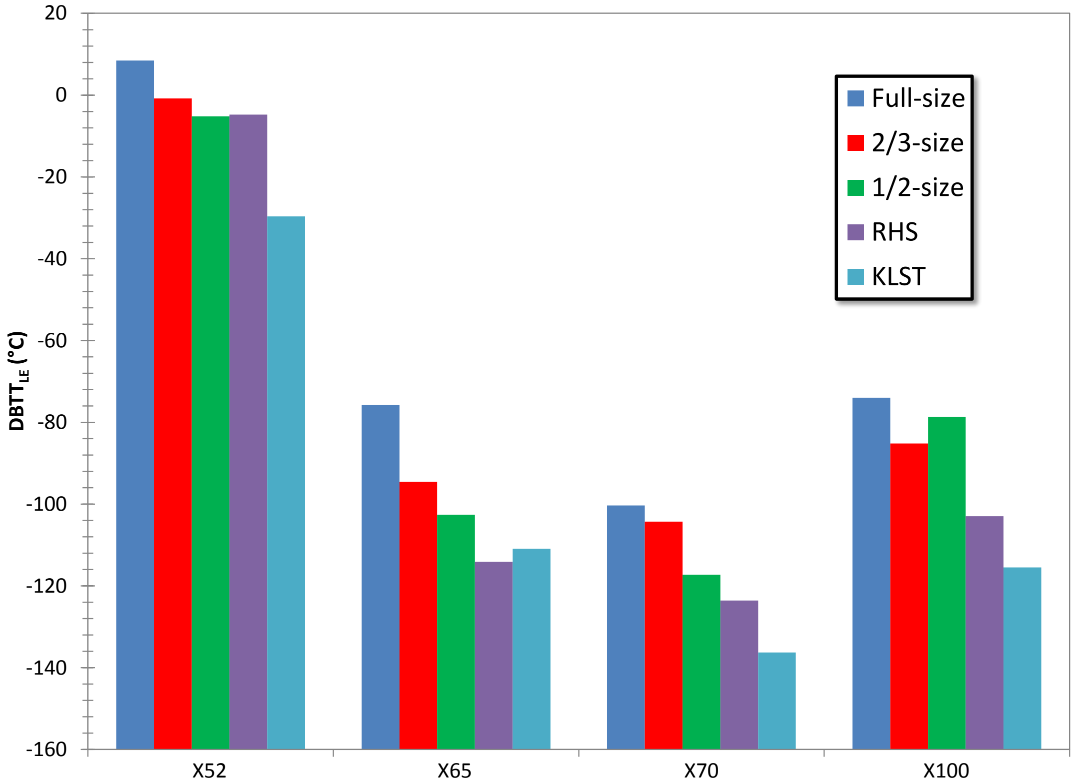

Figure 4 - *$DBTT_{LE}$* values measured from different specimen types.

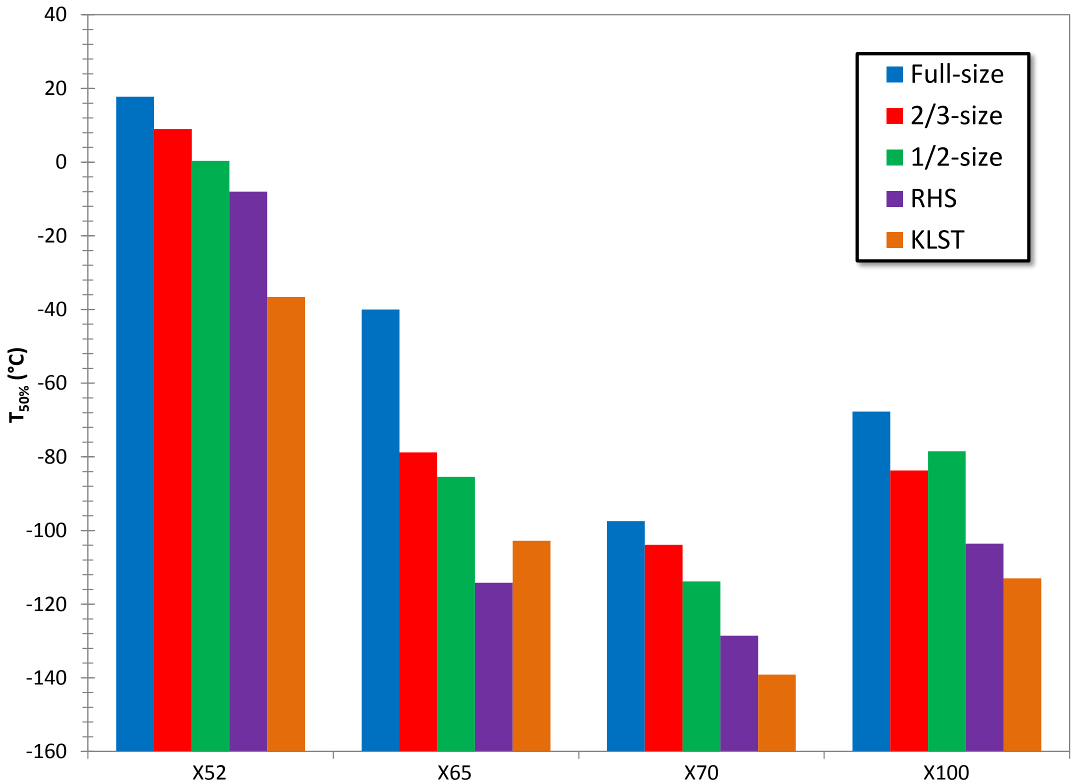

Figure 5 - *$T_{50\%}$* values measured from different specimen types.

Figure 6 compares values of ductile-to-brittle transition temperature measured from absorbed energy ($DBTT_{KV}$), lateral expansion ($DBTT_{LE}$) and shear fracture appearance ($T_{50\%}$). In the Figure, dotted and dashed lines correspond to ± 10 °C and ± 25 °C tolerance bounds respectively. In 90 % of the cases (possible combinations of material and specimen type), transition temperatures calculated from *LE* and *SFA* measurements agree with *KV*-based *DBTT*s within ± 10 °C. Only in one case ($DBTT_{LE}$ from CVN specimens for X65), the difference is larger than 25 °C. It's interesting to note that all the data points corresponding to MVCN test results (red symbols for KLST and yellow symbols for RHS) fall inside the ± 10 °C lines. Among the different specimen types, the ½-size samples (blue symbols) provide most of the data points falling below the -10 °C line.

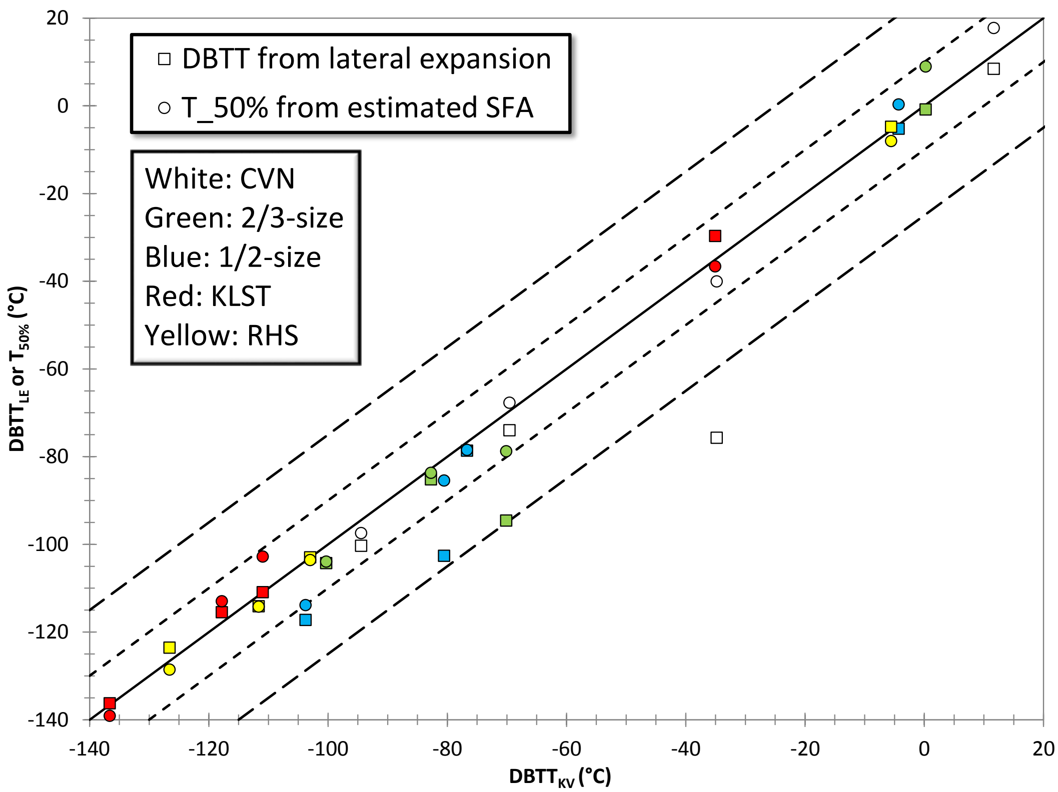

Figure 6 - Comparison between different measures of ductile-to-brittle transition temperature.

The comparisons between CVN transition curves, shown in Figure 7 (*KV*), Figure 8 (*LE*), and Figure 9 (*SFA*), lead to the following observations:

- the least tough steel is X52 (highest *DBTT*s and lowest *USE*);
- the toughest steel is X70 (lowest *DBTT*s and highest *USE*);
- X65 has almost the same *USE* as X70, but its *DBTT*s are the second highest after X52;
- X100 has lower *USE* than X65 or X70, but its *DBTT*s are better (*i.e.*, lower) than X65;
- the upper shelf lateral expansion is similar for X65, X70, and X100;
- X70 has the steepest transition, while X52 has the most shallow;
- X65 and X70 exhibit more data scatter than X100 or X52 in the transition region.

All the remarks above remain valid when considering data from other specimen types.

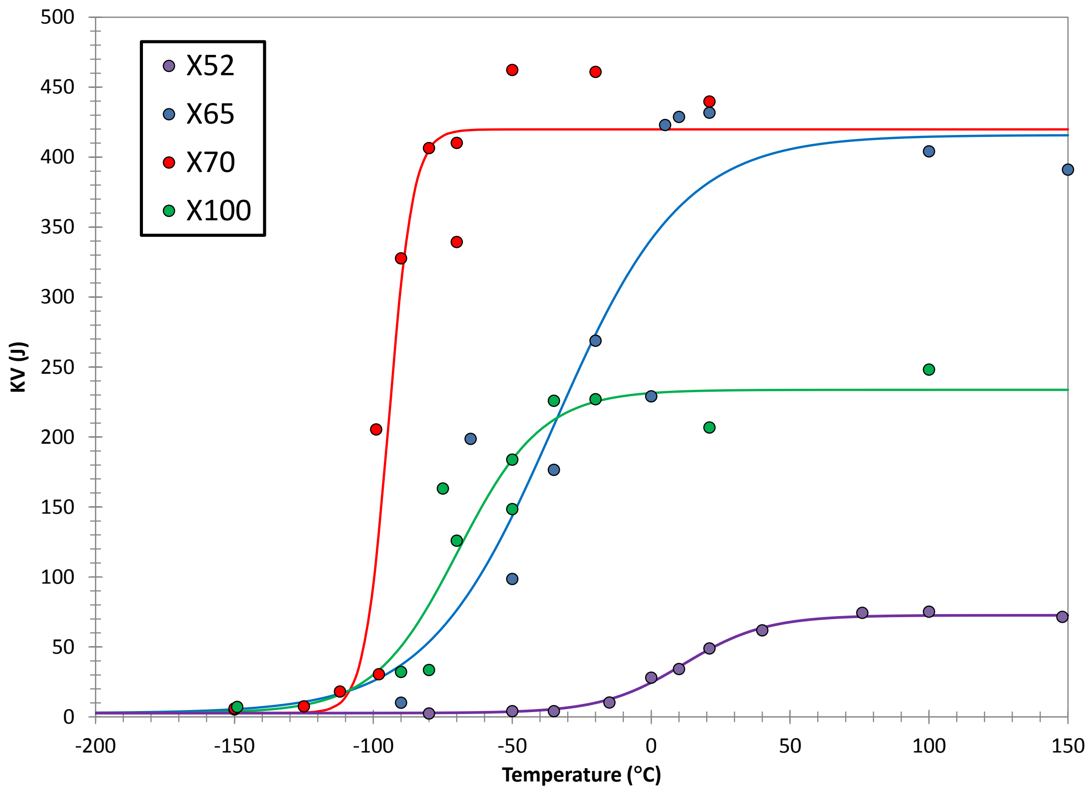

Figure 7 - Comparison between CVN transition curves for absorbed energy.

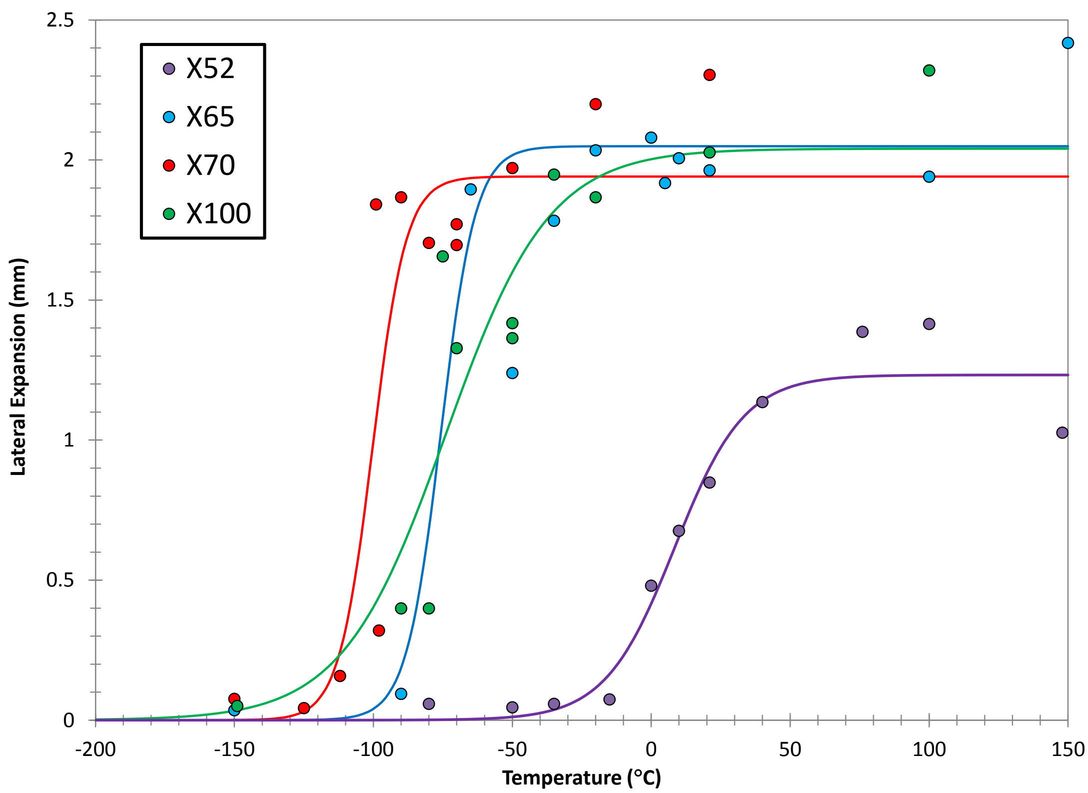

Figure 8 - Comparison between CVN transition curves for lateral expansion.

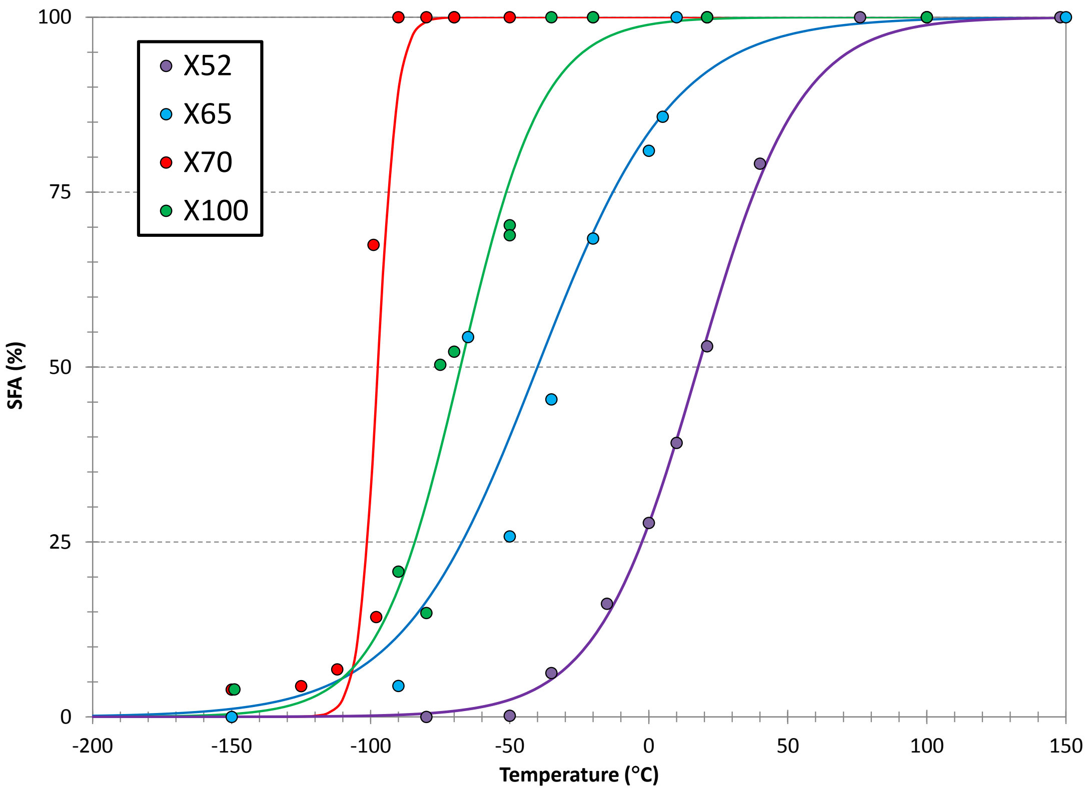

Figure 9 - Comparison between CVN transition curves for shear fracture appearance.

4.2 Instrumented Charpy parameters

Characteristic force and absorbed energy values are reported in Tables 9 to 13 for the different specimen types. Tables also include the ratio between the two measures of absorbed energy (KV/W_t).

Table 9 - Instrumented impact results obtained from CVN specimens.

X52									
Specimen id	**T (°C)**	F_{gy} **(kN)**	F_m **(kN)**	F_{bf} **(kN)**	F_a **(kN)**	W_m **(J)**	W_t **(J)**	KV **(J)**	$\frac{KV}{W_t}$
C11	-80	9.90	9.90	9.90	0.00	1.65	1.99	2.40	1.21
C8	-50	*No instrumented data available*							
C5	-35	12.12	13.9	13.90	0.00	2.53	3.47	4.13	1.19
C4	-15	13.42	13.62	13.62	0.00	6.63	9.93	10.21	1.03
C2	0	12.38	15.72	15.45	1.08	21.89	28.78	27.99	0.97
C10	10	11.67	15.55	15.36	4.55	22.94	34.08	34.25	1.00
C1	21	11.23	15.07	14.52	8.29	26.23	51.43	48.86	0.95
C6	40	*No instrumented data available*							
C7	76	9.47	14.21	-	-	26.52	71.84	74.29	1.03
C3	100	9.03	14.15	-	-	27.31	72.36	75.22	1.04
C12	148	8.41	13.38	-	-	25.74	70.03	71.50	1.02
C9	198	8.22	12.89	-	-	24.76	68.31	69.40	1.02

X65									
Specimen id	**T (°C)**	F_{gy} **(kN)**	F_m **(kN)**	F_{bf} **(kN)**	F_a **(kN)**	W_m **(J)**	W_t **(J)**	KV **(J)**	$\frac{KV}{W_t}$
C10	-150	29.15	29.15	29.15	0.00	3.91	4.92	5.27	1.07
C2	-90	15.45	18.14	16.68	0.00	5.91	6.50	10.13	1.56
C7	-65	15.18	21.42	11.83	4.65	76.17	194.52	198.68	1.02
C5	-50	14.56	20.93	19.91	7.59	62.60	97.53	98.50	1.01
C1	-35	13.71	20.48	10.04	5.92	67.92	172.29	176.56	1.02
C9	-20	13.62	19.83	13.69	11.53	68.11	259.14	268.81	1.04
C11	0	13.00	19.45	13.91	12.87	70.96	220.06	229.11	1.04
C8	5	12.65	19.50	-	-	74.98	396.58	422.98	1.07
C3	10	12.47	19.28	-	-	73.42	400.06	428.76	1.07
C4	21	12.17	19.20	-	-	74.12	403.42	431.78	1.07
C6	100	10.81	17.60	-	-	69.53	372.77	404.14	1.08
C12	150	10.44	16.74	-	-	68.87	361.91	391.04	1.08
X70									
Specimen id	**T (°C)**	F_{gy} **(kN)**	F_m **(kN)**	F_{bf} **(kN)**	F_a **(kN)**	W_m **(J)**	W_t **(J)**	KV **(J)**	$\frac{KV}{W_t}$
C2	-150	19.18	19.18	19.18	0.00	3.93	5.54	5.95	1.07
C3	-125	19.36	19.36	19.36	0.00	3.88	6.87	7.54	1.10
C6	-112	17.02	21.70	21.37	0.00	15.30	17.09	18.14	1.06
C9	-99	17.67	24.09	18.93	15.06	74.07	203.87	205.42	1.01
C10	-98	16.63	20.58	20.55	2.06	15.88	29.43	30.52	1.04
C5	-90	16.61	23.22	13.66	12.50	76.91	320.68	327.65	1.02
C11	-80	15.71	23.03	-	-	76.71	388.49	406.42	1.05
C1	-70	16.40	22.51	-	-	76.01	328.92	339.31	1.03
C7	-70	15.58	22.54	-	-	77.36	393.35	410.12	1.04
C12	-50	14.81	21.83	-	-	78.02	436.33	462.33	1.06
C8	-20	13.85	20.82	-	-	78.10	431.72	460.94	1.07
C4	21	12.82	19.92	-	-	75.43	414.89	439.74	1.06
X100									
Specimen id	**T (°C)**	F_{gy} **(kN)**	F_m **(kN)**	F_{bf} **(kN)**	F_a **(kN)**	W_m **(J)**	W_t **(J)**	KV **(J)**	$\frac{KV}{W_t}$
C4	-149	19.53	19.53	19.53	0.00	5.96	6.75	7.09	1.05
C5	-90	23.11	25.92	23.80	5.20	13.93	32.18	32.11	1.00
C6	-80	22.92	23.05	23.05	9.05	7.68	34.62	33.46	0.97
C1	-75	21.17	29.88	24.93	18.99	77.32	166.84	163.24	0.98
C7	-70	22.59	29.85	29.32	25.41	70.48	130.78	125.99	0.96
C12	-50	22.29	29.19	27.65	24.71	73.40	153.08	148.54	0.97
C2	-50	22.08	29.19	25.55	21.71	77.91	186.54	183.76	0.99
C10	-35	21.38	28.56	23.25	21.96	81.60	224.99	225.93	1.00
C9	-20	20.99	27.76	21.01	19.64	78.37	224.29	226.99	1.01
C8	21	20.68	26.93	20.83	19.10	75.82	207.20	206.73	1.00
C3	100	16.33	24.81	-	-	70.68	242.46	248.20	1.02

Table 10 - Instrumented impact results obtained from ⅔-size specimens.

X52									
Specimen id	**T (°C)**	F_{gy} **(kN)**	F_m **(kN)**	F_{bf} **(kN)**	F_a **(kN)**	W_m **(J)**	W_t **(J)**	***KV*** **(J)**	$\frac{KV}{W_t}$
S1-8	-80	7.67	7.67	7.67	0.00	1.29	2.36	2.70	1.14
S1-7	-50	*No instrumented data available*							
S1-5	-35	9.35	10.53	10.35	0.00	11.56	12.25	13.58	1.11
S1-2	-15	8.40	10.29	10.04	0.57	12.74	16.62	15.73	0.95
S1-3	0	7.96	10.00	10.00	1.85	13.96	19.75	19.76	1.00
S1-12	10	*No instrumented data available*							
S1-1	21	7.36	9.42	8.66	5.15	15.03	37.44	38.17	1.02
S1-6	40	7.76	10.94	10.25	7.58	20.19	59.41	46.90	0.79
S1-10	75	6.16	8.9	-	-	16.3	46.14	47.96	1.04
S1-4	100	5.57	8.37	-	-	15.31	45.52	47.96	1.05
S1-9	152	5.31	8.25	-	-	15.63	44.24	46.09	1.04
S1-11	199	5.15	7.95	-	-	15.56	43.96	47.31	1.08
X65									
Specimen id	**T (°C)**	F_{gy} **(kN)**	F_m **(kN)**	F_{bf} **(kN)**	F_a **(kN)**	W_m **(J)**	W_t **(J)**	***KV*** **(J)**	$\frac{KV}{W_t}$
S1-11	-164	8.00	8.00	8.00	0.00	1.23	1.55	1.57	1.01
S1-2	-140	14.14	14.14	14.14	0.00	2.63	3.24	3.30	1.02
S1-5	-125	13.26	13.26	13.26	0.00	2.16	3.34	3.38	1.01
S1-10	-114	11.79	11.79	11.79	0.00	1.45	1.83	2.48	1.36
S1-9	-95	12.71	12.71	12.71	0.06	1.87	3.29	5.04	1.53
S1-7	-90	10.84	13.56	9.76	5.26	41.81	106.87	111.13	1.04
S1-3	-70	10.26	13.19	9.65	6.86	41.83	117.10	121.95	1.04
S1-4	-50	9.77	12.77	7.96	6.35	43.26	149.80	158.64	1.06
S1-6	-35	9.41	12.52	-	-	44.76	236.34	261.16	1.11
S1-12	-20	8.96	12.15	-	-	44.86	211.90	231.72	1.09
S1-8	21	8.51	11.83	-	-	44.23	223.92	244.95	1.09
S1-1	100	7.03	10.65	-	-	41.89	219.83	246.25	1.12
X70									
Specimen id	**T (°C)**	F_{gy} **(kN)**	F_m **(kN)**	F_{bf} **(kN)**	F_a **(kN)**	W_m **(J)**	W_t **(J)**	***KV*** **(J)**	$\frac{KV}{W_t}$
S1-10	-163	13.53	13.53	13.53	0.00	2.16	2.75	2.93	1.07
S1-9	-136	5.98	5.98	5.98	0.00	1.45	1.79	1.87	1.04
S1-7	-111	11.12	13.68	12.97	0.00	8.16	10.36	10.36	1.00
S1-6	-105	8.91	10.52	10.52	1.15	3.23	8.60	8.23	0.96
S1-3	-100	11.36	14.65	-	-	39.68	187.35	199.06	1.06
S1-2	-95	11.04	14.43	9.00	8.32	43.43	169.93	179.07	1.05
S1-5	-90	10.68	14.15	10.21	9.37	46.02	170.57	181.43	1.06
S1-11	-70	9.99	13.61	-	-	42.75	201.80	221.89	1.10
S1-1	-60	10.39	13.47	-	-	48.75	221.21	239.35	1.08
S1-8	-50	9.76	13.32	-	-	45.19	253.06	278.14	1.10
S1-12	-20	8.94	12.79	-	-	46.79	246.41	271.85	1.10
S1-4	21	8.18	12.13	-	-	45.22	226.77	249.30	1.10

X100									
Specimen id	T (°C)	F_{gy} (kN)	F_m (kN)	F_{bf} (kN)	F_a (kN)	W_m (J)	W_t (J)	KV (J)	$\frac{KV}{W_t}$
S1-10	-162	13.67	13.67	13.67	0.00	2.29	3.44	3.46	1.01
S1-6	-124	21.21	21.21	21.21	0.00	6.53	7.76	9.67	1.25
S1-5	-90	12.65	18.29	18.09	0.03	29.8	32.78	34.98	1.07
S1-2	-80	12.77	18.03	17.67	16.59	40.34	86.71	86.12	0.99
S1-4	-75	12.15	17.41	12.75	8.04	33.06	80.00	78.7	0.98
S1-7	-70	12.49	17.90	16.77	15.86	39.19	86.94	89.23	1.03
S1-1	-50	11.96	17.53	14.55	10.67	39.27	94.24	93.99	1.00
S1-3	-40	12.48	17.76	16.92	15.62	42.75	101.63	101.9	1.00
S1-12	-20	11.73	17.08	-	-	42.33	114.22	117.15	1.03
S1-8	21	11.12	16.38	-	-	38.63	118.57	120.56	1.02
S1-9	100	10.54	15.38	-	-	37.58	126.25	130.66	1.03

Table 11 - Instrumented impact results obtained from ½-size specimens.

X52									
Specimen id	T (°C)	F_{gy} (kN)	F_m (kN)	F_{bf} (kN)	F_a (kN)	W_m (J)	W_t (J)	KV (J)	$\frac{KV}{W_t}$
S2-10	-80	6.85	6.85	6.85	0.00	0.98	1.31	1.57	1.20
S2-7	-60	7.82	8.25	8.14	0.00	1.32	2.1	2.33	1.11
S2-6	-50	6.96	7.93	7.93	0.33	7.85	8.15	8.76	1.07
S2-3	-35	6.45	7.74	7.73	0.28	9.56	10.9	11.2	1.03
S2-2	-15	6.20	7.23	7.23	0.58	8.83	11.28	11.66	1.03
S2-4	0	5.90	6.99	6.99	2.17	10.56	18.08	18.06	1.00
S2-1	21	5.47	6.77	4.15	3.44	9.17	28.25	29.33	1.04
S2-8	42	5.03	6.52	-	-	10.73	34.83	36.57	1.05
S2-9	75	4.4	6.39	-	-	12.04	34.79	37.05	1.06
S2-5	100	4.33	6.34	-	-	11.88	35.18	36.81	1.05
S2-11	145	4.08	6.01	-	-	11.07	33.56	34.33	1.02
S2-12	200	3.74	5.63	-	-	11.11	32.8	35.45	1.08
X65									
Specimen id	T (°C)	F_{gy} (kN)	F_m (kN)	F_{bf} (kN)	F_a (kN)	W_m (J)	W_t (J)	KV (J)	$\frac{KV}{W_t}$
S2-12	-153	12.57	12.57	12.57	0.00	1.77	2.29	2.48	1.08
S2-10	-123	6.87	6.87	6.87	0.00	1.19	1.35	1.35	1.00
S2-8	-114	8.32	10.22	10.22	0.37	2.19	3.04	3.30	1.09
S2-6	-100	8.40	9.98	9.04	3.65	23.97	43.81	43.82	1.00
S2-3	-90	7.94	9.69	7.94	4.35	25.31	56.79	57.32	1.01
S2-7	-70	7.26	9.30	5.09	2.08	26.32	75.47	80.49	1.07
S2-11	-50	9.04	9.04	4.71	3.00	26.7	87.02	93.38	1.07
S2-2	-40	6.58	8.82	5.02	3.94	26.8	75.07	82.36	1.10
S2-9	-35	6.81	8.88	-	-	28.09	109.89	119.54	1.09
S2-4	-20	6.65	8.71	-	-	29.44	116.02	127.74	1.10
S2-1	21	5.95	8.25	-	-	26.71	104.6	113.01	1.08
S2-5	100	5.03	7.54	-	-	25.49	109.21	121.96	1.12

X70									
Specimen id	**T (°C)**	***F_{gy}* (kN)**	***F_m* (kN)**	***F_{bf}* (kN)**	***F_a* (kN)**	***W_m* (J)**	***W_t* (J)**	***KV* (J)**	$\frac{KV}{W_t}$
S2-1	-151	*No instrumented data available*							
S2-7	-132	10.00	10.00	10.00	0.00	1.31	2.50	2.63	1.05
S2-11	-124	15.21	15.21	15.21	0.00	4.28	6.08	6.55	1.08
S2-6	-120	8.55	10.65	6.21	2.75	24.10	57.47	57.56	1.00
S2-9	-115	8.71	10.74	10.38	7.30	23.91	39.38	37.94	0.96
S2-10	-100	8.41	10.45	9.06	7.12	25.31	63.54	63.21	0.99
S2-3	-100	8.25	10.22	7.17	5.40	26.02	69.94	74.20	1.06
S2-2	-96	8.08	10.18	5.64	4.29	25.71	70.41	73.27	1.04
S2-5	-90	7.84	9.93	-	-	27.26	111.33	120.00	1.08
S2-8	-50	7.07	9.40	-	-	27.19	113.56	122.77	1.08
S2-12	-20	6.36	9.10	-	-	28.28	123.44	134.63	1.09
S2-4	21	5.95	8.46	-	-	29.97	124.88	138.01	1.11
X100									
Specimen id	**T (°C)**	***F_{gy}* (kN)**	***F_m* (kN)**	***F_{bf}* (kN)**	***F_a* (kN)**	***W_m* (J)**	***W_t* (J)**	***KV* (J)**	$\frac{KV}{W_t}$
S2-3	-149	10.59	10.59	10.59	0.00	1.65	2.53	2.55	1.01
S2-10	-131	11.70	11.70	11.70	0.00	1.98	3.01	3.08	1.02
S2-11	-110	9.07	12.85	12.70	0.00	9.85	10.31	11.13	1.08
S2-7	-96	11.74	12.70	12.70	0.48	3.36	5.66	7.47	1.32
S2-5	-90	9.27	12.73	9.72	7.62	21.92	52.57	54.6	1.04
S2-2	-70	8.23	11.36	10.92	6.32	15.73	27.4	32.11	1.17
S2-1	-50	9.46	12.63	8.65	7.45	22.99	67.16	70.41	1.05
S2-8	-20	8.49	11.9	10.24	9.53	24.57	69.47	73.53	1.06
S2-9	10	8.29	11.71	-	-	25.97	85.66	89.48	1.04
S2-4	21	8.19	11.35	-	-	22.45	78.05	81.26	1.04
S2-6	100	8.41	11.42	-	-	20.27	67.55	70.33	1.04

Table 12 - Instrumented impact results obtained from KLST specimens.

X52									
Specimen id	**T (°C)**	***F_{gy}* (kN)**	***F_m* (kN)**	***F_{bf}* (kN)**	***F_a* (kN)**	***W_m* (J)**	***W_t* (J)**	***KV* (J)**	$\frac{KV}{W_t}$
K4	-188	0.98	0.98	0.98	0.00	0.03	0.12	0.08	0.67
K10	-150	1.83	1.83	1.83	0.00	0.10	0.15	0.18	1.20
K12	-122	1.14	1.14	1.14	0.00	0.10	0.18	0.16	0.89
K1	-76	1.24	1.24	1.24	0.00	0.12	0.17	0.21	1.24
K3	-50	1.04	1.17	1.17	0.00	1.15	1.7	0.63	0.37
K7	-40	0.93	1.12	0.98	0.28	0.86	2.39	1.69	0.71
K8	-35	0.96	1.13	0.98	0.40	0.92	3.03	2.32	0.77
K6	-26	0.93	1.07	0.68	0.54	0.86	4.02	2.97	0.74
K5	0	0.75	1.05	-	-	1.17	4.67	3.91	0.84
K2	20	0.87	1.05	-	-	1.17	4.67	4.49	0.96
K9	100	0.74	0.96	-	-	1.42	4.47	4.34	0.97
K11	144	0.66	0.87	-	-	1.21	4.10	3.99	0.97

X65									
Specimen id	**T (°C)**	F_{gy} **(kN)**	F_m **(kN)**	F_{bf} **(kN)**	F_a **(kN)**	W_m **(J)**	W_t **(J)**	KV **(J)**	$\frac{KV}{W_t}$
K11	-190	1.63	1.63	1.63	0.00	0.08	0.18	0.20	1.11
K3	-174	2.08	2.08	2.08	0.00	0.19	0.24	0.30	1.25
K2	-150	1.57	1.59	1.42	0.09	2.12	4.37	4.18	0.96
K10	-147	1.31	1.74	1.50	0.00	0.64	1.42	1.39	0.98
K7	-122	1.12	1.54	1.52	0.00	0.55	0.88	0.96	1.09
K4	-111	1.36	1.47	1.03	0.54	2.2	7.05	6.63	0.94
K8	-100	1.39	1.48	1.38	0.33	2.19	4.87	4.35	0.89
K5	-84	1.4	1.43	-	-	2.4	10.27	9.53	0.93
K12	-75	1.31	1.4	-	-	1.95	8.78	8.08	0.92
K9	-50	1.15	1.33	-	-	2.79	9.87	9.57	0.97
K6	0	0.98	1.22	-	-	2.67	9.55	9.37	0.98
K1	20	0.85	1.2	-	-	2.63	9.52	9.33	0.98
X70									
Specimen id	**T (°C)**	F_{gy} **(kN)**	F_m **(kN)**	F_{bf} **(kN)**	F_a **(kN)**	W_m **(J)**	W_t **(J)**	KV **(J)**	$\frac{KV}{W_t}$
K11	-190	1.70	1.70	1.70	0.00	0.13	0.36	0.20	0.56
K12	-169	1.79	1.79	1.79	0.00	0.15	0.31	0.33	1.06
K4	-150	1.47	1.77	1.77	0.00	0.56	1.06	0.95	0.90
K5	-140	1.40	1.56	1.50	0.00	0.32	0.71	0.67	0.94
K6	-134	1.30	1.58	0.92	0.82	0.98	9.55	9.19	0.96
K3	-130	1.48	1.63	0.82	0.78	1.52	9.58	9.28	0.97
K9	-115	1.47	1.56	0.76	0.66	2.27	10.15	9.82	0.97
K10	-100	1.34	1.52	-	-	1.66	10.8	10.34	0.96
K7	-77	1.24	1.48	-	-	2.61	10.79	10.22	0.95
K8	-50	1.17	1.43	-	-	2.06	10.7	9.57	0.89
K2	0	0.99	1.27	-	-	2.46	10.11	9.94	0.98
K1	20	1	1.25	-	-	3.69	10.11	9.86	0.98
X100									
Specimen id	**T (°C)**	F_{gy} **(kN)**	F_m **(kN)**	F_{bf} **(kN)**	F_a **(kN)**	W_m **(J)**	W_t **(J)**	KV **(J)**	$\frac{KV}{W_t}$
K9	-191	0.81	0.81	0.81	0.00	0.08	0.16	0.27	1.69
K5	-150	1.61	2.17	2.06	0.00	0.78	0.93	0.94	1.01
K6	-126	1.73	2.09	1.94	0.30	0.98	2.39	2.05	0.86
K2	-121	1.76	2.04	2.04	0.17	2.39	2.87	2.71	0.94
K3	-112	*No instrumented data available*							
K1	-100	1.84	1.97	1.66	1.49	2.54	8.41	7.96	0.95
K10	-75	*No instrumented data available*							
K4	-50	1.59	1.83	1.22	1.10	2.54	8.93	8.67	0.97
K7	-10	1.47	1.75	-	-	2.43	9.63	9.20	0.96
K12	0	1.45	1.73	-	-	2.46	9.23	N/A	N/A
K8	20	1.54	1.79	-	-	2.24	9.17	8.89	0.97

Table 13 - Instrumented impact results obtained from RHS specimens.

X52									
Specimen id	**T (°C)**	F_{gy} (kN)	F_m (kN)	F_{bf} (kN)	F_a (kN)	W_m (J)	W_t (J)	KV (J)	$\frac{KV}{W_t}$
R3	-184	3.21	3.21	3.21	0.00	0.15	0.23	0.20	0.87
R2	-150	2.76	2.76	2.76	0.00	0.25	0.31	0.22	0.71
R1	-125	2.89	2.89	2.89	0.00	0.28	0.41	0.31	0.76
R4	-101	2.99	2.99	2.99	0.00	0.56	0.66	0.38	0.58
R8	-70	4.20	4.42	4.39	0.00	0.95	1.07	0.64	0.60
R7	-50	1.09	1.29	1.29	0.00	1.00	3.97	2.00	0.50
R9	-25	3.44	3.66	3.66	0.51	1.73	2.39	2.09	0.87
R5	-16	1.60	1.95	1.94	0.41	3.62	8.20	4.85	0.59
R10	-5	1.48	1.80	1.77	0.89	2.56	10.65	4.81	0.45
R12	21	2.84	3.72	-	-	4.05	13.25	13.14	0.99
R11	100	0.92	1.26	-	-	2.95	31.72	11.66	0.37
R6	149	1.01	1.62	-	-	4.19	23.56	12.13	0.51

X65									
Specimen id	**T (°C)**	F_{gy} (kN)	F_m (kN)	F_{bf} (kN)	F_a (kN)	W_m (J)	W_t (J)	KV (J)	$\frac{KV}{W_t}$
R1	-180	3.97	3.97	3.70	0.00	0.6	0.83	0.55	0.66
R2	-150	4.11	4.11	4.11	0.00	0.49	0.61	0.47	0.77
R7	-135	3.00	3.00	2.84	0.04	1.42	3.08	1.60	0.52
R3	-124	2.37	2.57	2.48	0.00	4.07	9.01	4.21	0.47
R4	-119	2.34	2.66	2.24	1.25	7.45	38.28	20.75	0.54
R10	-112	2.25	2.64	-	-	8.26	48.74	32.58	0.67
R6	-112	2.56	3.18	3.06	0.07	1.37	2.73	1.66	0.61
R5	-101	2.24	2.57	-	-	8.37	50.39	42.48	0.84
R9	-90	2.16	2.55	1.42	1.21	9.00	50.39	39.97	0.79
R11	-75	2.08	2.5	-	-	9.57	50.39	47.40	0.94
R8	-40	1.73	2.37	-	-	9.36	50.39	45.88	0.91
R12	21	1.57	2.23	-	-	9.89	44.03	44.03	1.00

X70									
Specimen id	**T (°C)**	F_{gy} (kN)	F_m (kN)	F_{bf} (kN)	F_a (kN)	W_m (J)	W_t (J)	KV (J)	$\frac{KV}{W_t}$
R1	-180	*No instrumented data available*							
R2	-150	4.83	5.65	5.65	1.43	2.54	3.08	2.26	0.73
R7	-136	4.21	5.94	5.94	0.39	2.35	2.90	2.08	0.72
R5	-129	2.48	2.81	2.81	0.37	3.92	8.37	4.89	0.58
R3	-125	2.41	2.84	-	-	9.05	50.39	39.98	0.79
R6	-120	2.44	2.88	-	-	8.82	50.39	42.60	0.85
R12	-115	1.75	2.22	2.22	1.17	4.41	20.82	8.13	0.39
R4	-115	2.35	2.84	-	-	8.74	50.39	45.37	0.90
R9	-100	2.23	2.75	-	-	9.78	50.39	47.93	0.95
R8	-31	1.8	2.53	-	-	10.25	50.39	48.89	0.97
R10	21	1.63	2.37	-	-	10.24	46.61	46.61	1.00
R11	21	1.75	2.40	-	-	10.08	46.35	n/a	n/a

X100									
Specimen id	**T (°C)**	**F_{gy} (kN)**	**F_m (kN)**	**F_{bf} (kN)**	**F_a (kN)**	**W_m (J)**	**W_t (J)**	**KV (J)**	**$\frac{KV}{W_t}$**
R2	-184	3.37	5.08	4.72	0.20	1.47	1.63	1.21	0.74
R1	-153	*No instrumented data available*							
R12	-123	2.99	3.62	3.62	0.31	3.49	8.63	4.49	0.73
R3	-110	2.47	3.08	2.72	0.04	2.31	8.11	3.62	0.72
R8	-105	2.45	2.91	2.91	0.48	3.96	15.66	6.30	0.58
R4	-102	2.73	3.58	3.20	2.67	8.30	37.00	19.16	0.79
R9	-100	3.37	4.19	3.91	3.69	11.72	43.57	29.37	0.85
R6	-76	*No instrumented data available*							
R10	-70	2.62	3.33	1.85	1.59	9.14	47.96	29.60	0.62
R5	-35	2.71	3.48	1.85	1.71	8.86	48.37	29.76	0.62
R7	21	2.37	3.04	-	-	8.76	31.73	31.73	1.00

Force values at general yield (F_{gy}) and maximum forces (F_m) are plotted as a function of test temperature for the investigated steels in Figures 10-17. In the Figures, data points are fitted by 3rd or 4th order polynomials as a guide for the eye.

As expected, characteristic forces tend to decrease with the specimen cross-section and test temperature, often after reaching a peak at low temperatures.

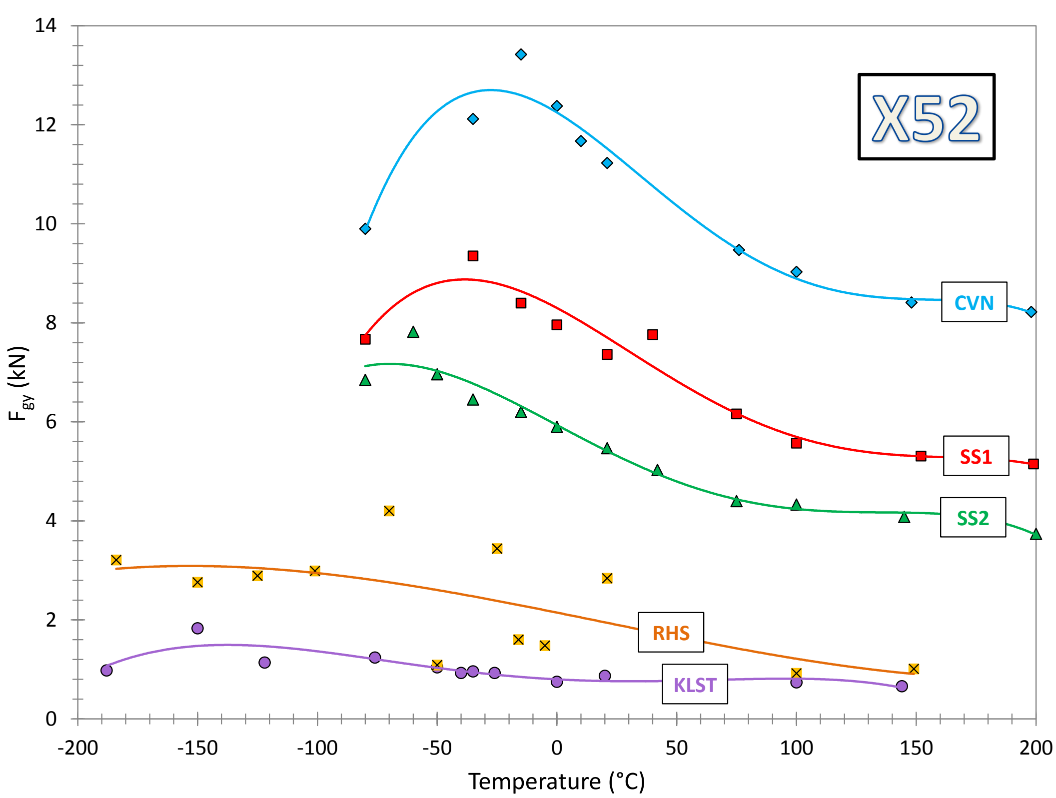

Figure 10 - Forces at general yield for steel X52.

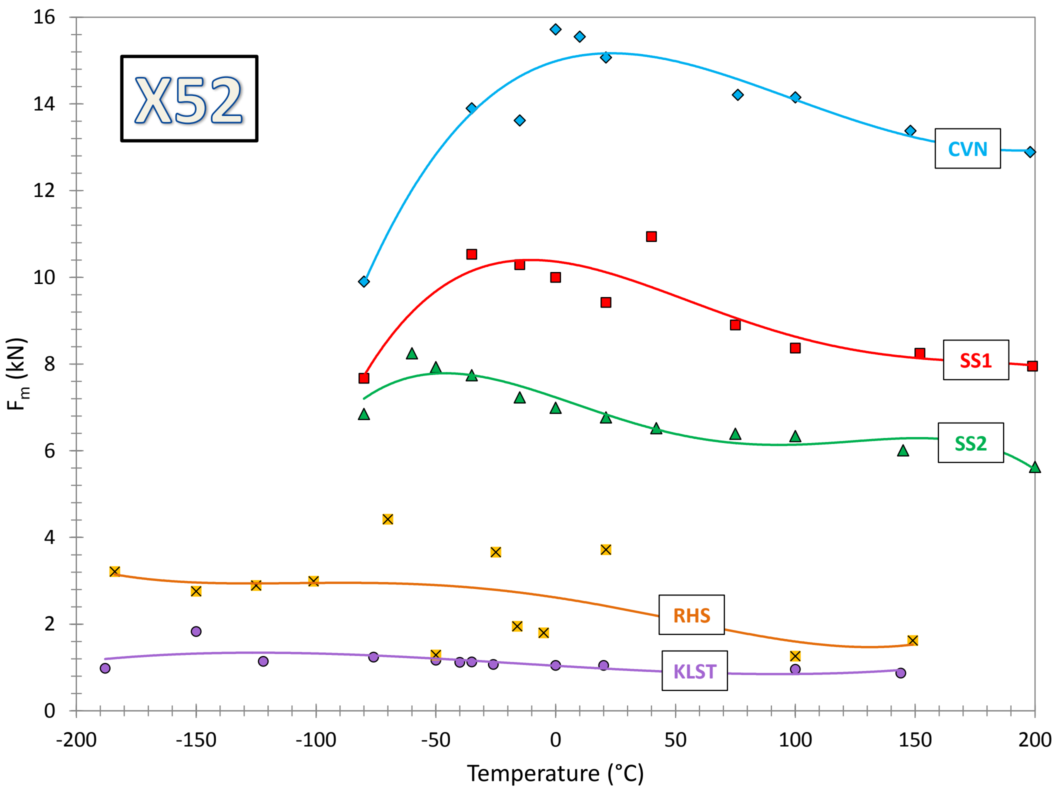

Figure 11 – Maximum forces for steel X52.

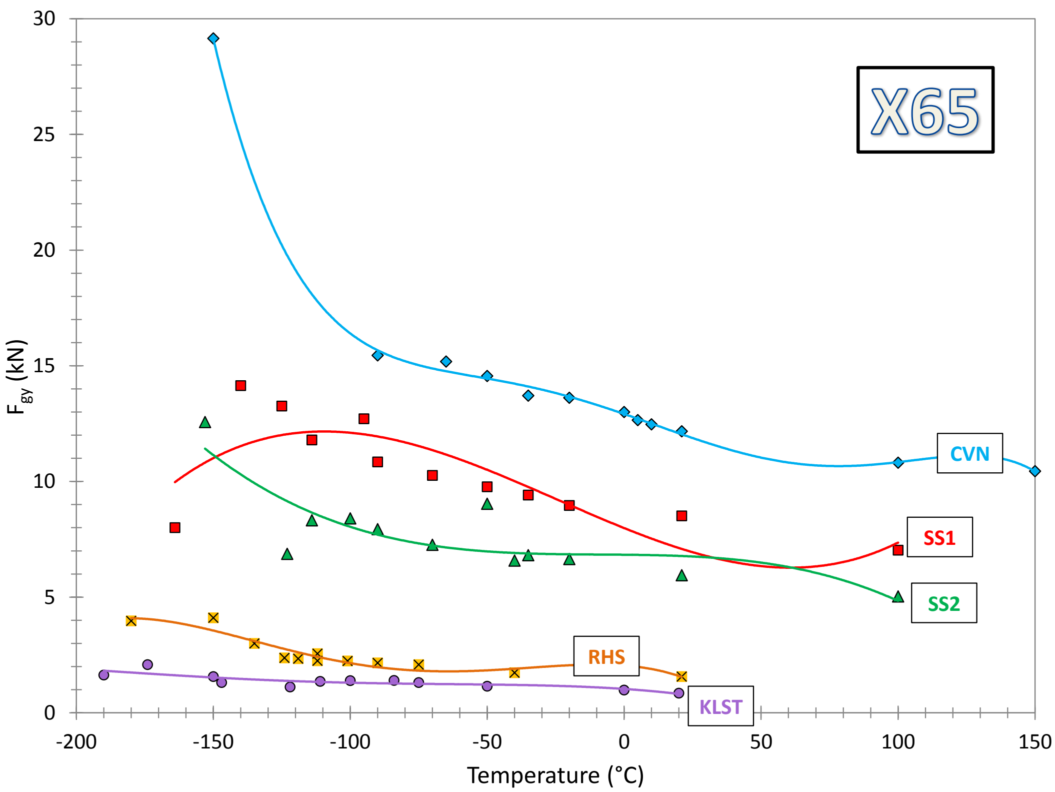

Figure 12 - Forces at general yield for steel X65.

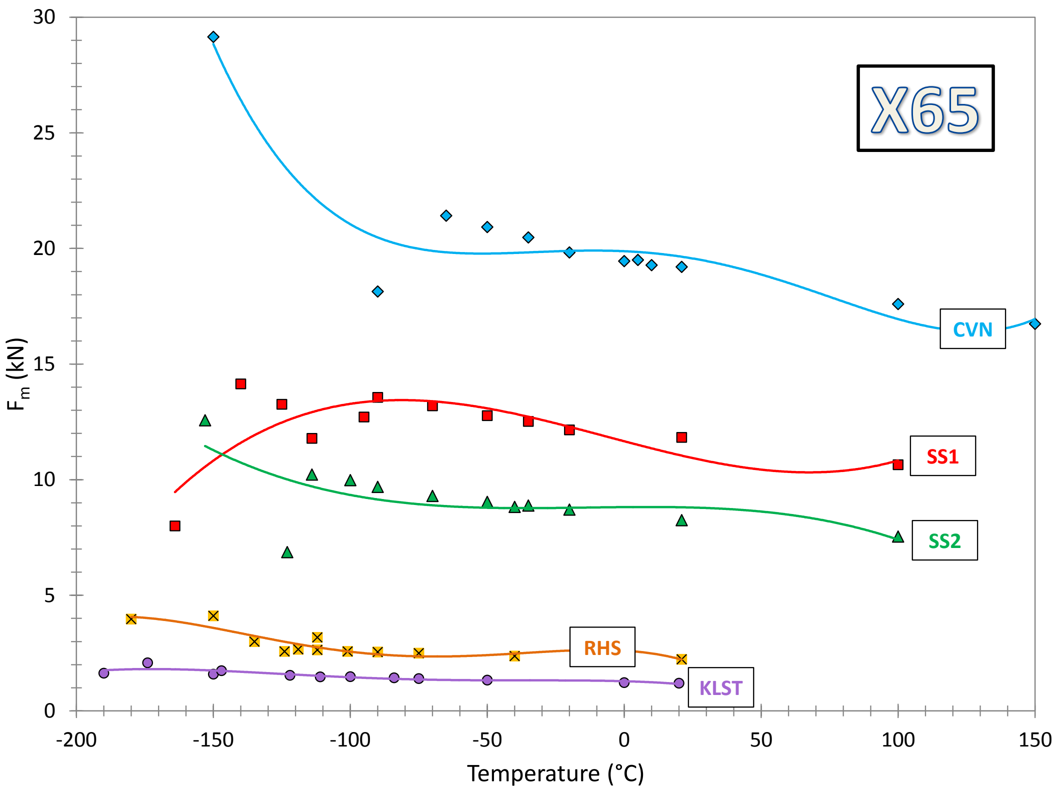

Figure 13 – Maximum forces for steel X65.

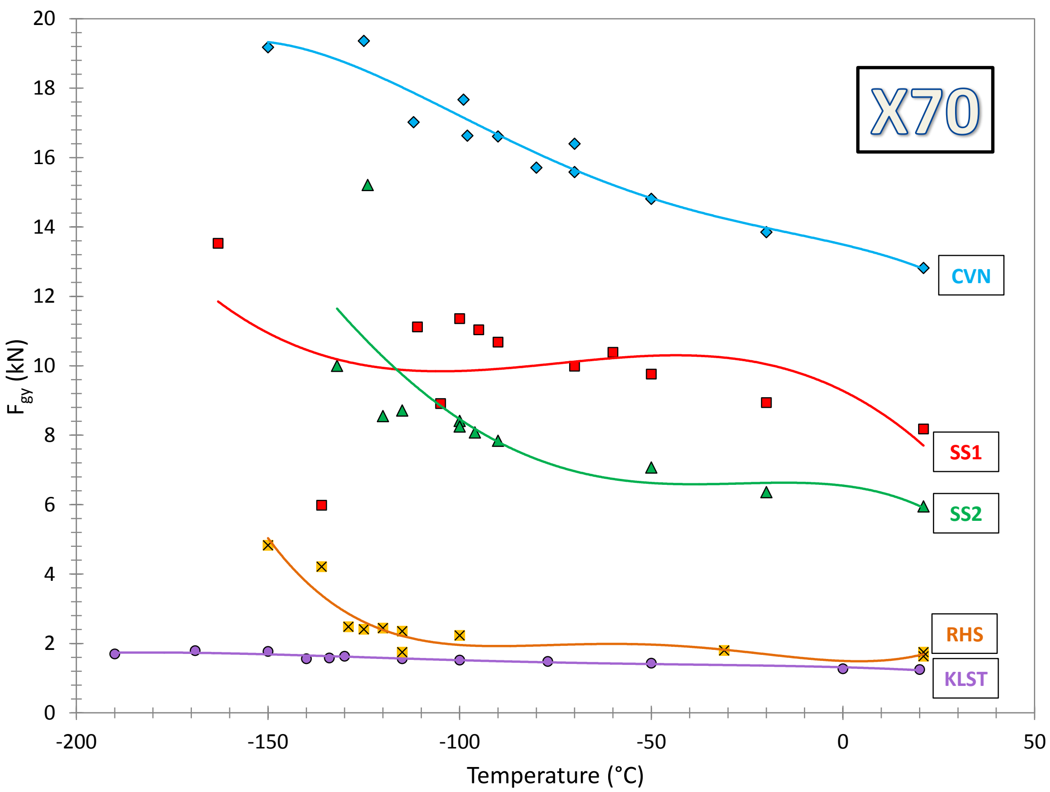

Figure 14 - Forces at general yield for steel X70.

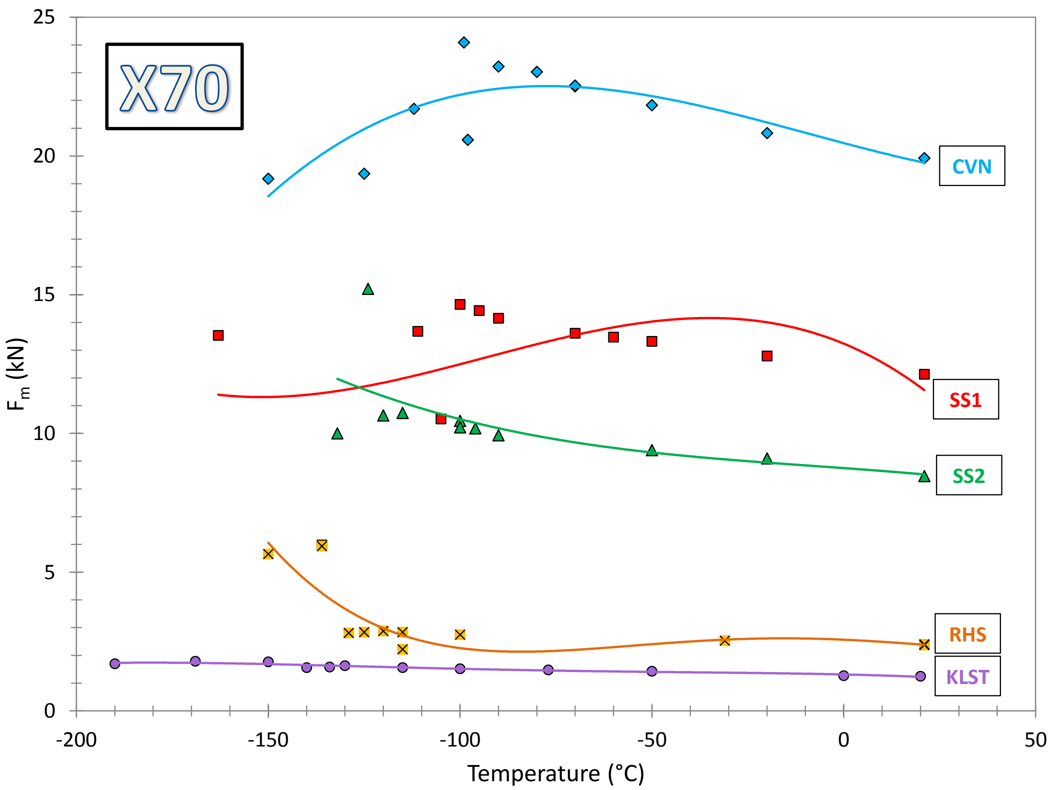

Figure 15 – Maximum forces for steel X70.

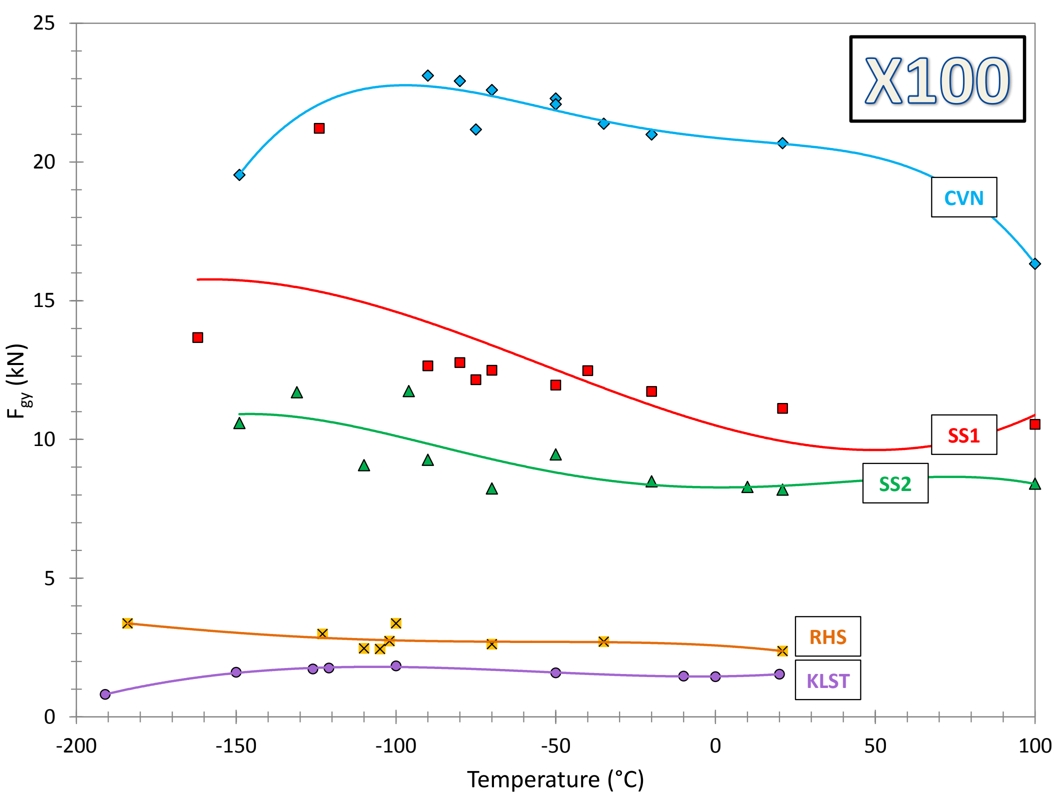

Figure 16 - Forces at general yield for steel X100.

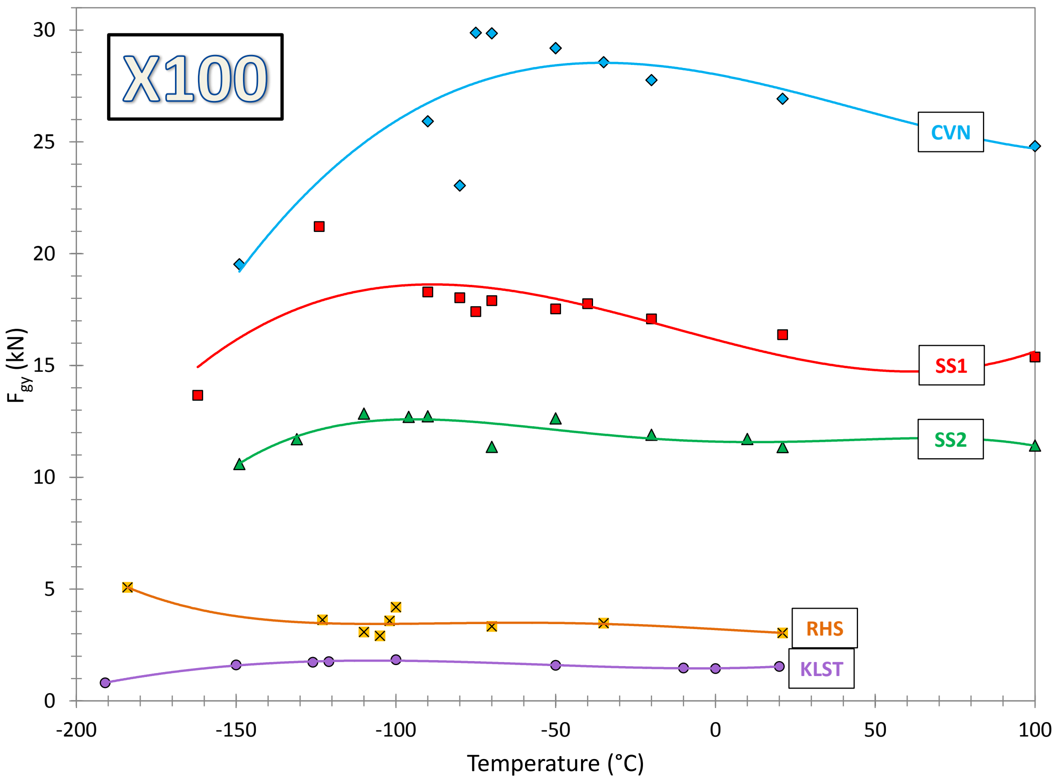

Figure 17 – Maximum forces for steel X100.

4.2.1 Normalization of characteristic forces

We applied several normalization procedures to general yield and maximum forces measured from SCVN and MCVN specimens, in order to verify if any of these approaches is successful in bringing together force values obtained from specimens of different size and geometry.

The general approach we followed was the use of the ratio between the following geometrical parameters, as several researchers have already proposed for correlating upper shelf energies between miniaturized and full-size Charpy specimens (see also Section 5.2):

(a) ratio of nominal fracture areas, expressed as $B \cdot b$, where B is the specimen thickness and b is the specimen width below the notch (unnotched ligament size);
(b) ratio of nominal fracture volumes, expressed as $B \cdot b^2$;
(c) ratio of nominal fracture volumes, expressed as $(B \cdot b)^{3/2}$.

The values of the above quantities for the different specimen types are summarized in Table 14; the corresponding normalization factors obtained for each specimen type are listed in Table 15.

Table 14 - Values of nominal fracture areas and volumes for the Charpy specimens used in this study.

Specimen type	$B \cdot b$ (mm²)	$B \cdot b^2$ (mm³)	$(B \cdot b)^{3/2}$ (mm³)
CVN	80	640	715.54
⅔-size	53.33	426.67	389.49
½-size	40	320	252.98
KLST	9	27	27
RHS	18.64	71.97	80.50

Table 15 – Normalization factors based on the ratio of nominal fracture areas and volumes for the SCVN and MCVN specimens used in this study.

<table>
<tr><th rowspan="2">Geometrical parameter</th><th colspan="4">Non-standard specimen type</th></tr>
<tr><th>⅔-size</th><th>½-size</th><th>KLST</th><th>RHS</th></tr>
<tr><td>Area, B·b</td><td rowspan="2">1.50</td><td rowspan="2">2.00</td><td>8.89</td><td>4.29</td></tr>
<tr><td>Volume, B·b²</td><td>23.70</td><td rowspan="2">8.89</td></tr>
<tr><td>Volume, (B·b)^{3/2}</td><td>1.84</td><td>2.83</td><td>26.50</td></tr>
</table>

Note that (Table 15):

- for sub-size specimens, since the ligament size is the same as for CVN, the normalization factors corresponding to $B{\cdot}b$ and $B{\cdot}b^2$ are identical;
- for RHS specimens, which are exactly scaled down with respect to CVN, the two volume-based normalization factors are identical.

The results of the force normalization process on F_{gy} and F_m values are illustrated in Figures 18-23 (X52), 24-29 (X65), 30-35 (X70), and 36-41 (X100).

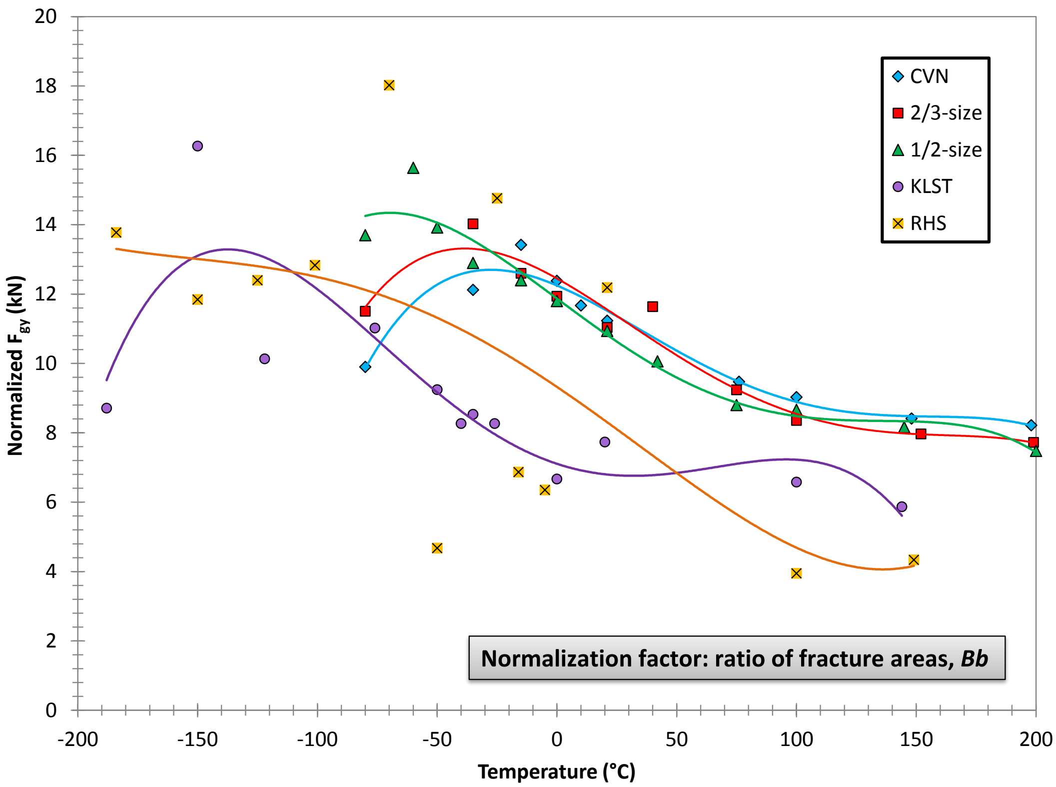

Figure 18 - Forces at general yield for X52, normalized by the ratio of fracture areas.

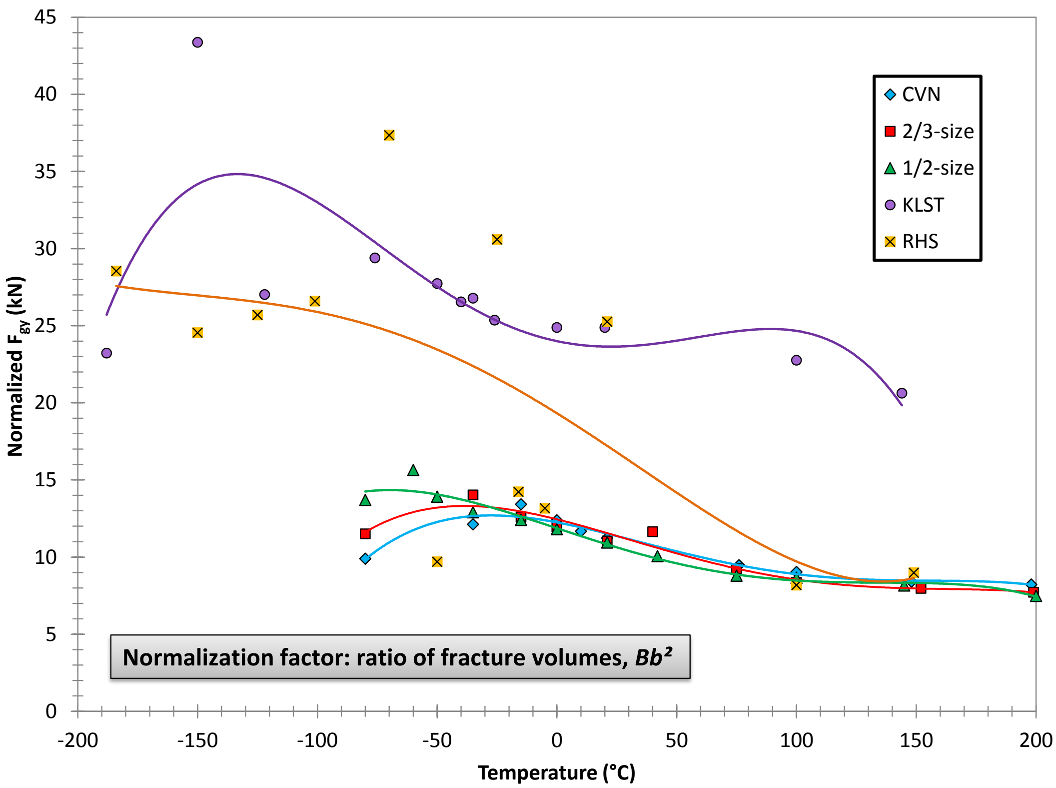

Figure 19 - Forces at general yield for X52, normalized by the ratio of fracture volumes, *Bb*².

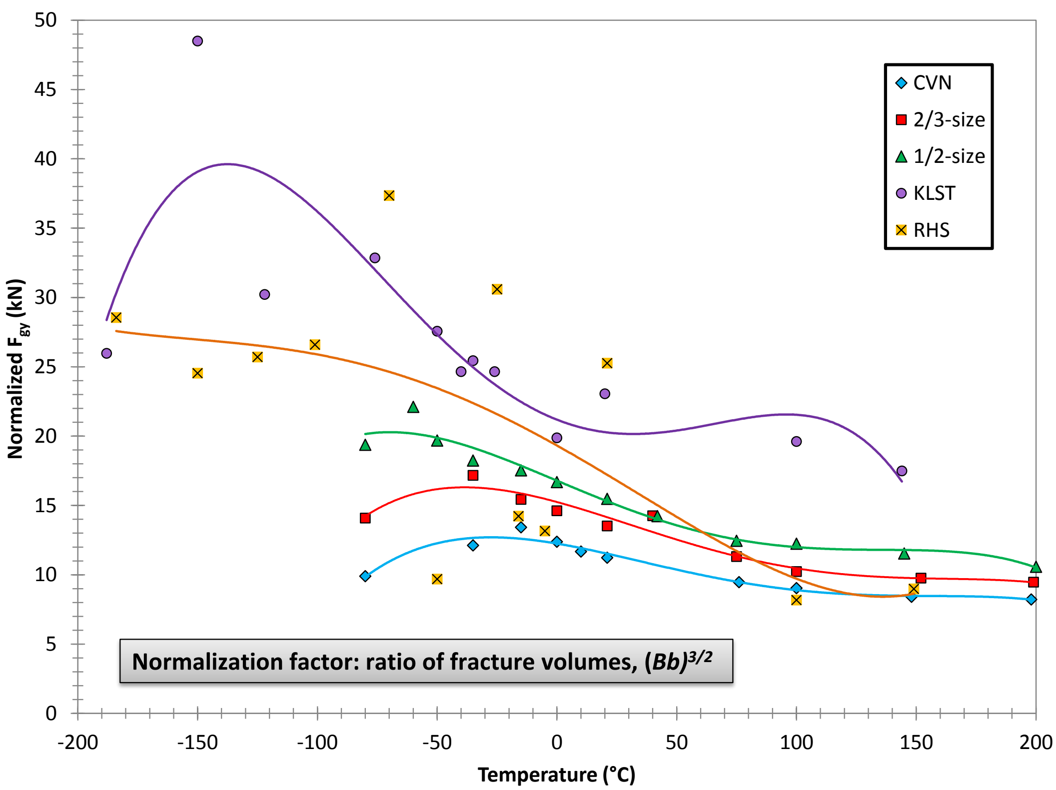

Figure 20 - Forces at general yield for X52, normalized by the ratio of fracture volumes, (*Bb*)$^{3/2}$.

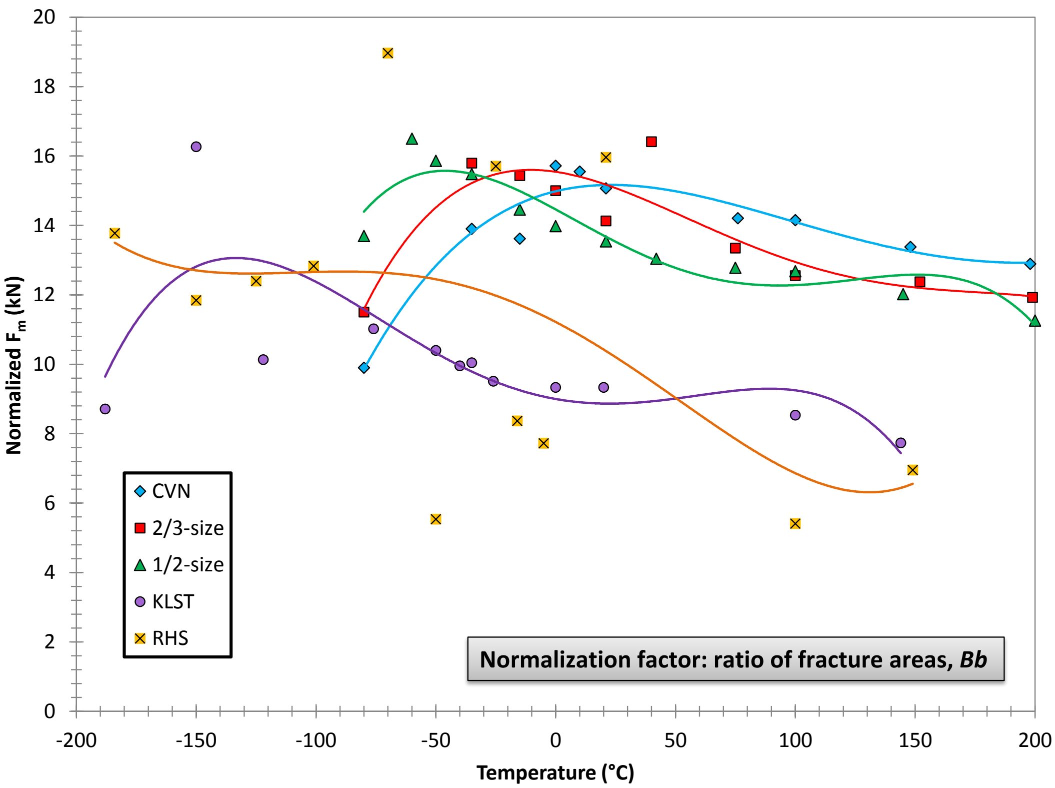

Figure 21 – Maximum forces for X52, normalized by the ratio of fracture areas.

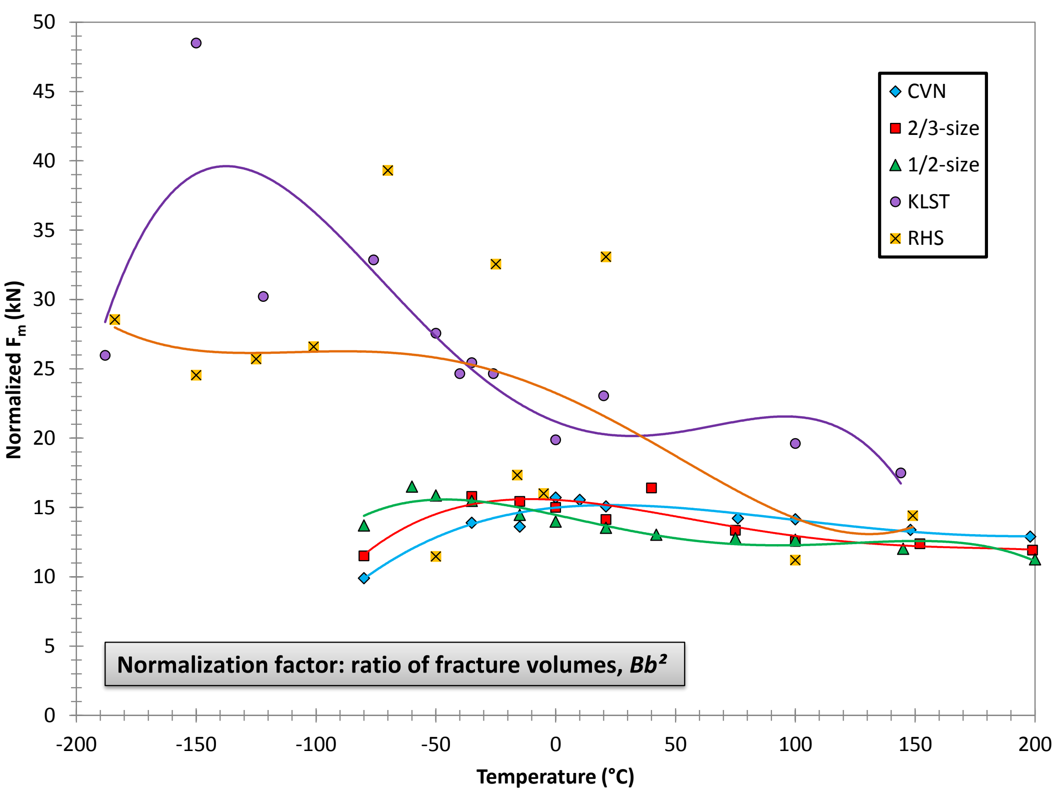

Figure 22 – Maximum forces for X52, normalized by the ratio of fracture volumes, *Bb*².

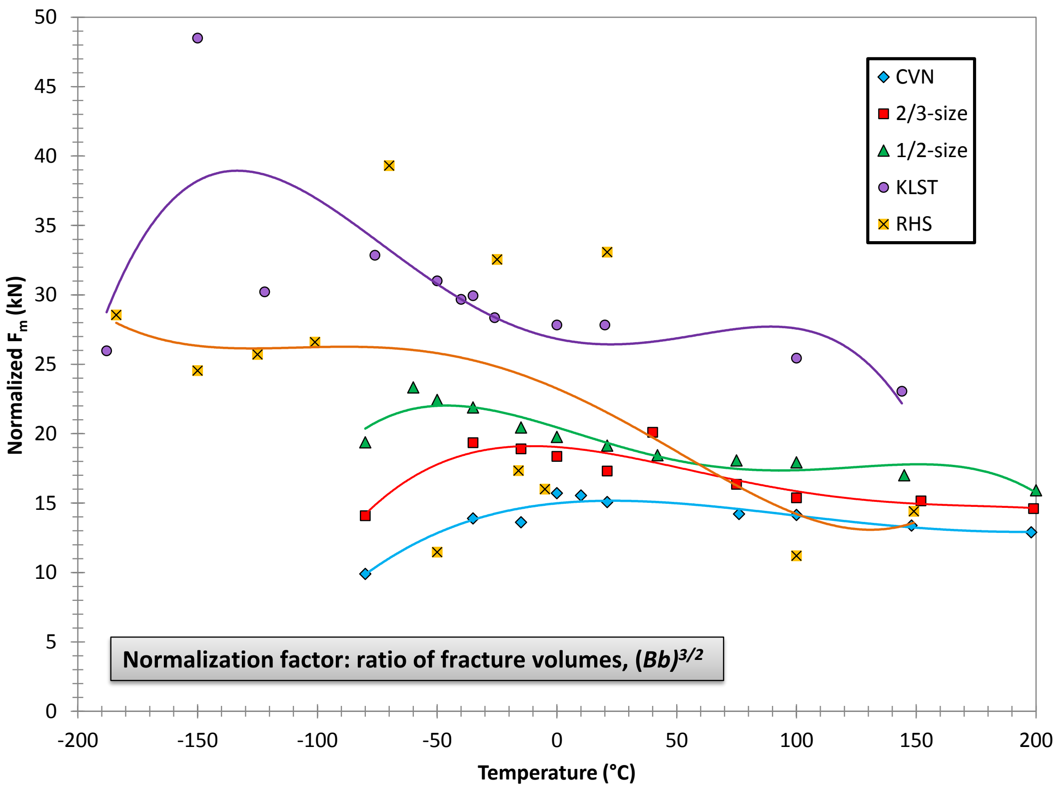

Figure 23 – Maximum forces for X52, normalized by the ratio of fracture volumes, $(Bb)^{3/2}$.

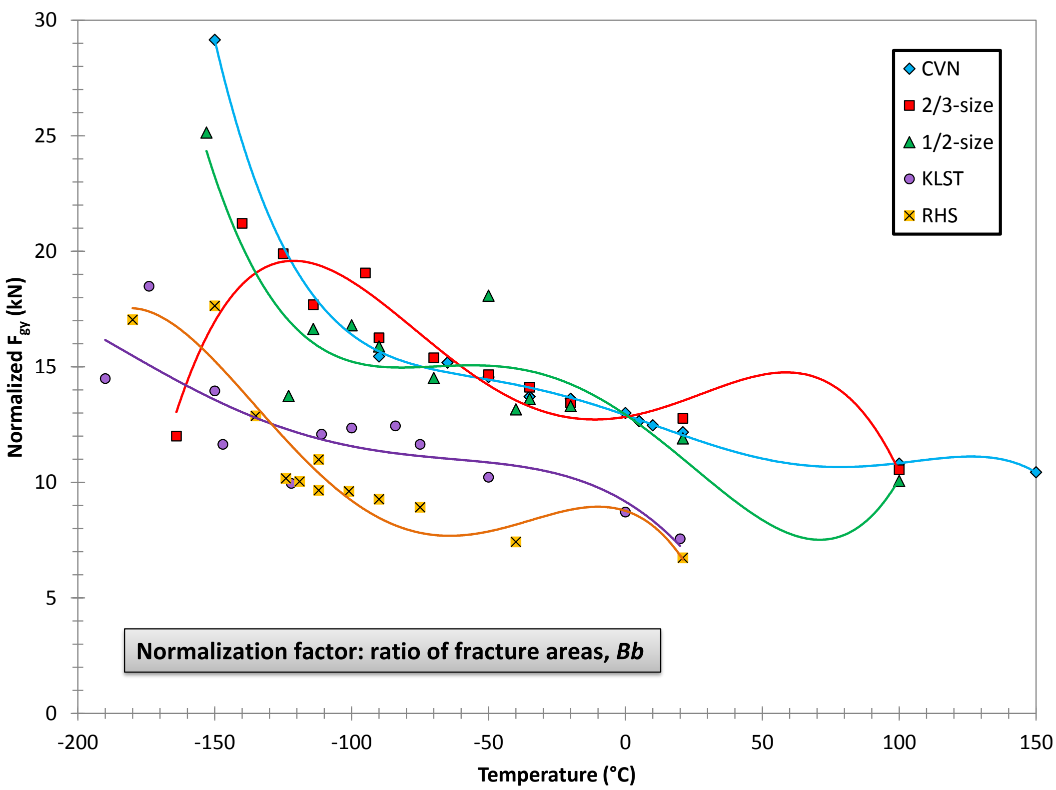

Figure 24 - Forces at general yield for X65, normalized by the ratio of fracture areas.

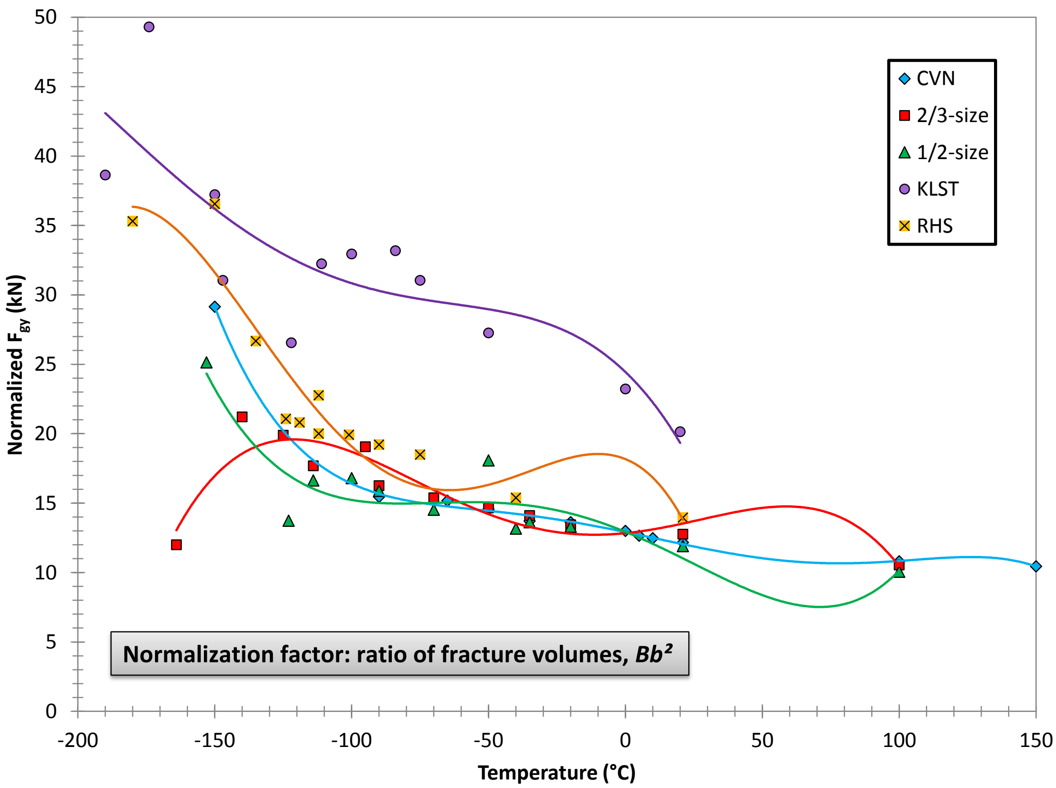

Figure 25 - Forces at general yield for X65, normalized by the ratio of fracture volumes, *Bb*².

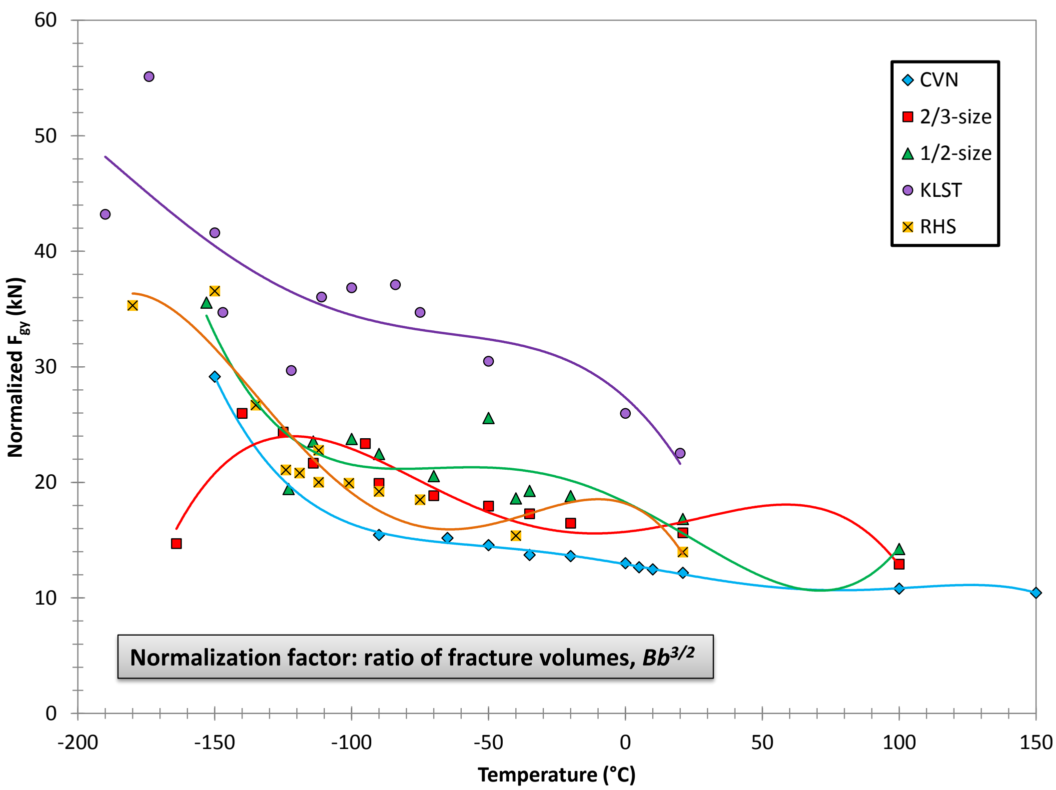

Figure 26 - Forces at general yield for X65, normalized by the ratio of fracture volumes, (*Bb*)$^{3/2}$.

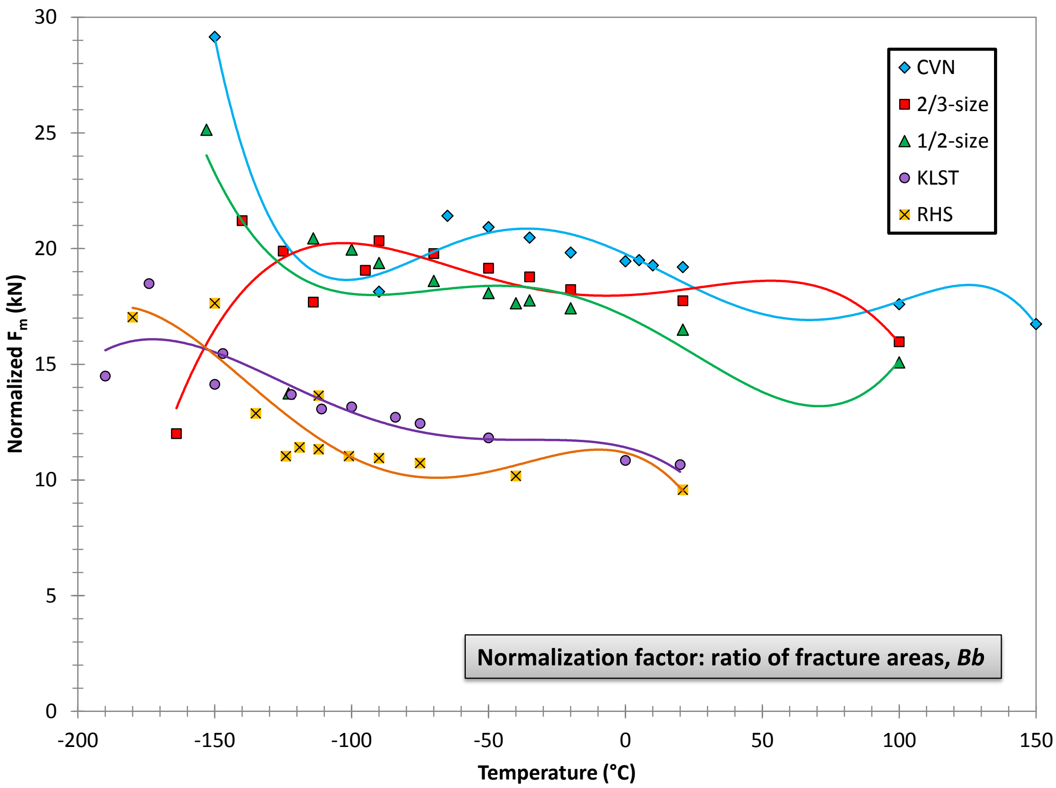

Figure 27 – Maximum forces for X65, normalized by the ratio of fracture areas.

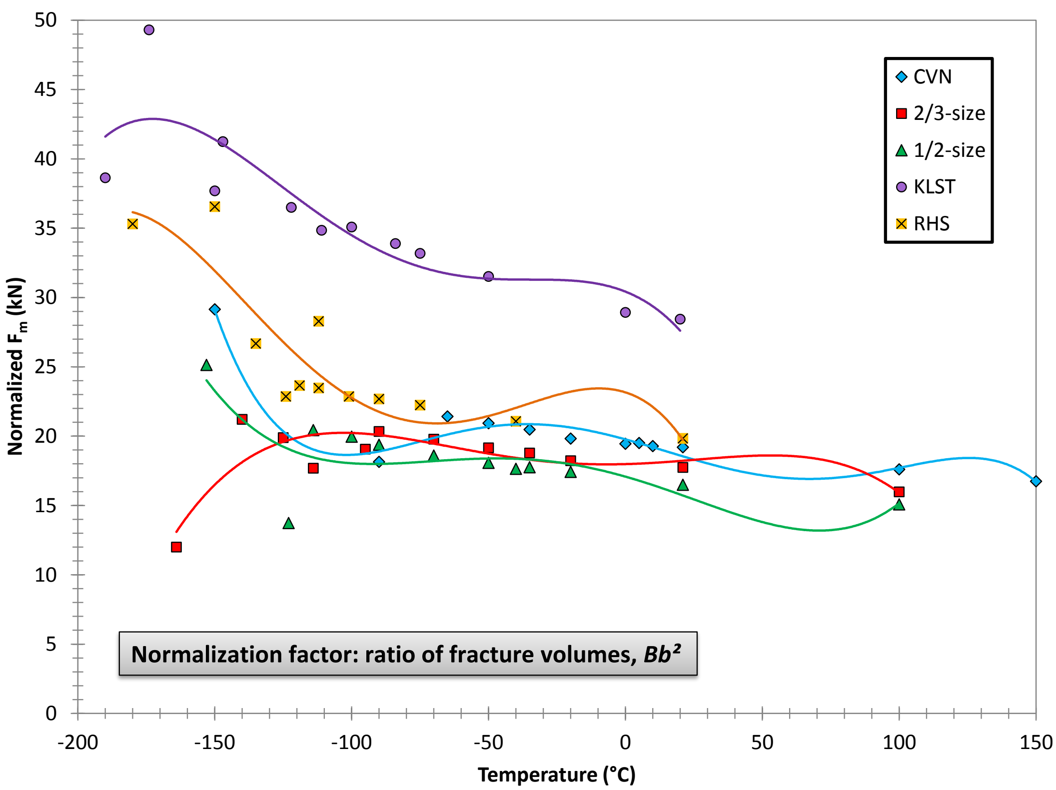

Figure 28 – Maximum forces for X65, normalized for by ratio of fracture volumes, *Bb*²\.

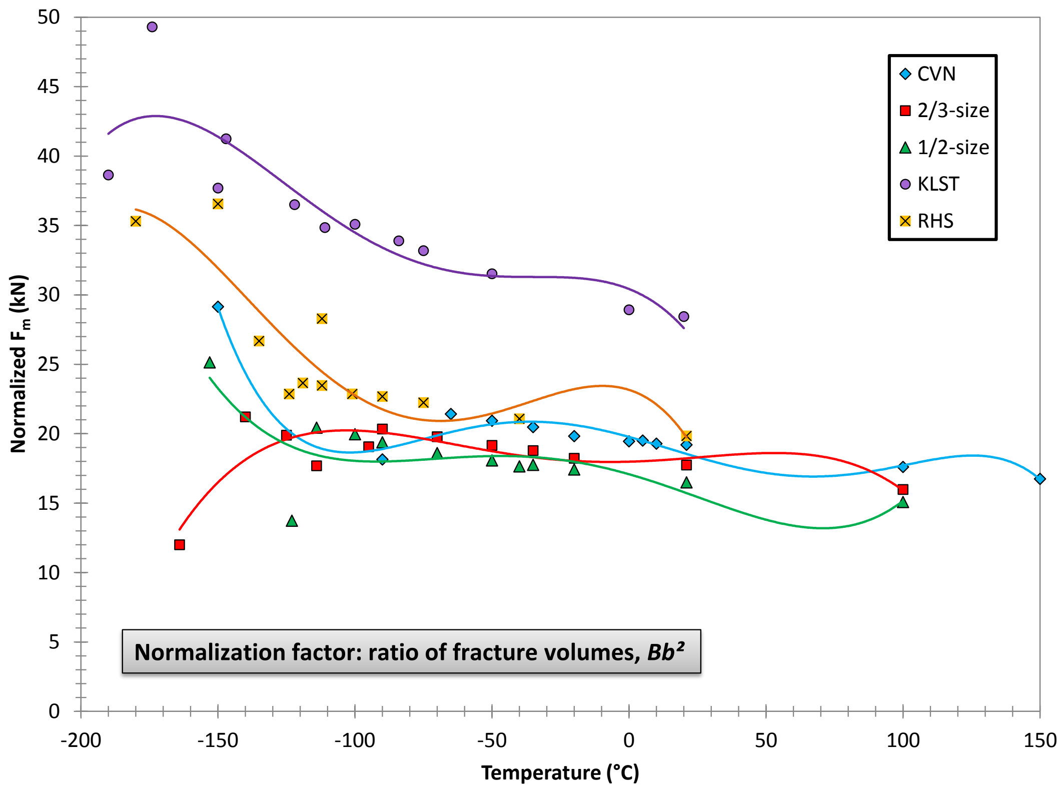

Figure 29 – Maximum forces for X65, normalized by the ratio of fracture volumes, $(Bb)^{3/2}$.

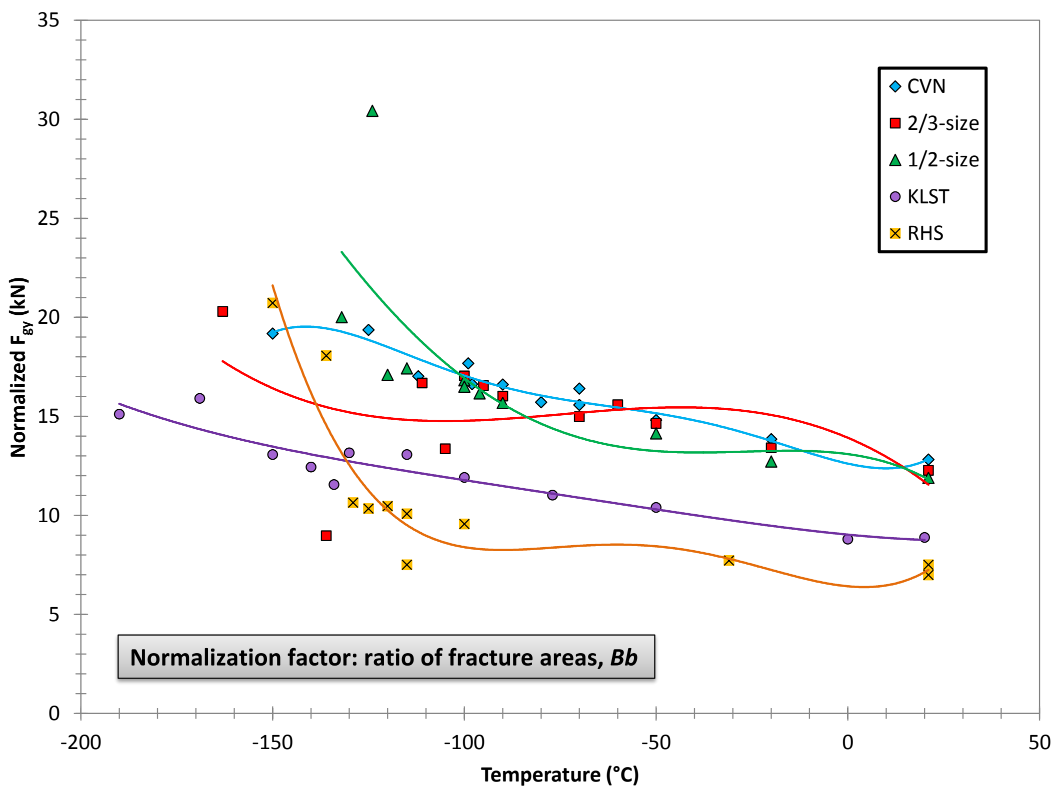

Figure 30 - Forces at general yield for X70, normalized by the ratio of fracture areas.

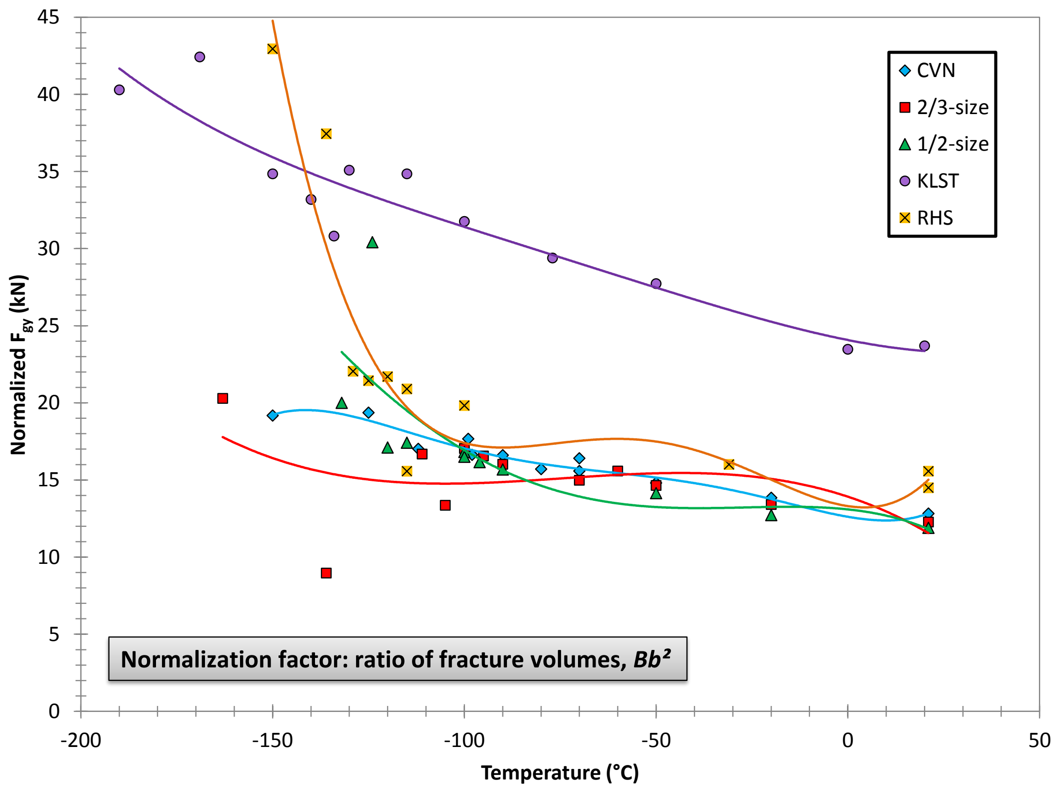

Figure 31 - Forces at general yield for X70, normalized by the ratio of fracture volumes, *Bb*².

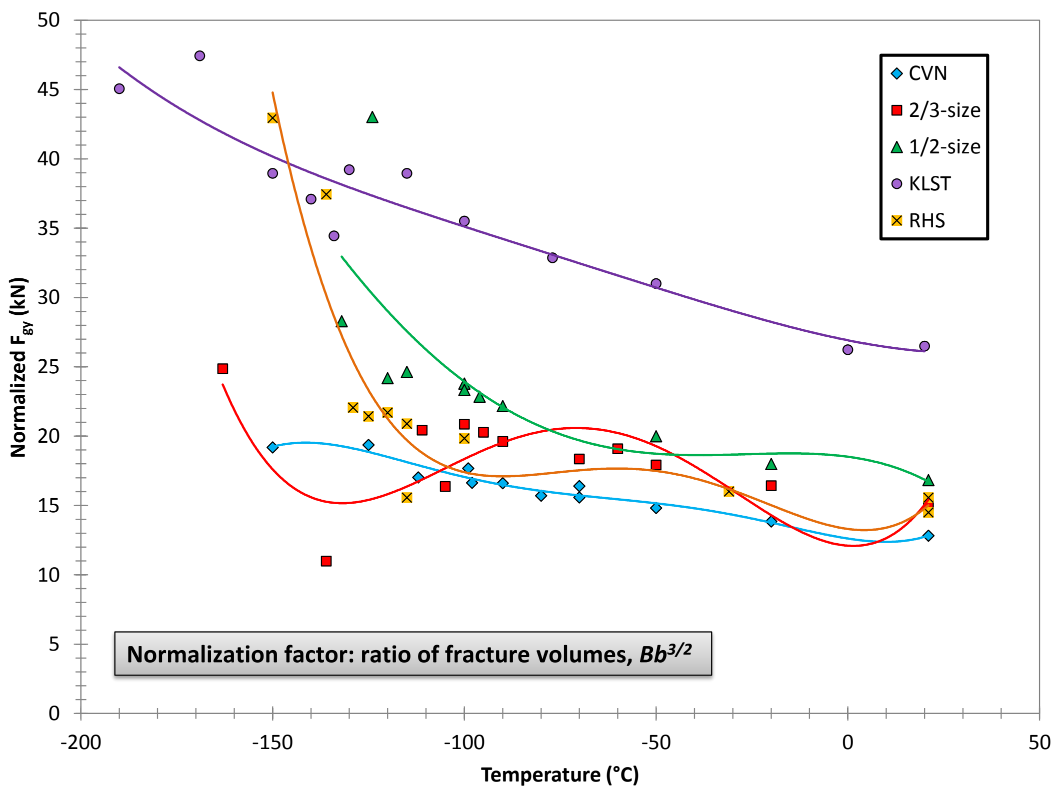

Figure 32 - Forces at general yield for X70, normalized by the ratio of fracture volumes, (*Bb*)$^{3/2}$.

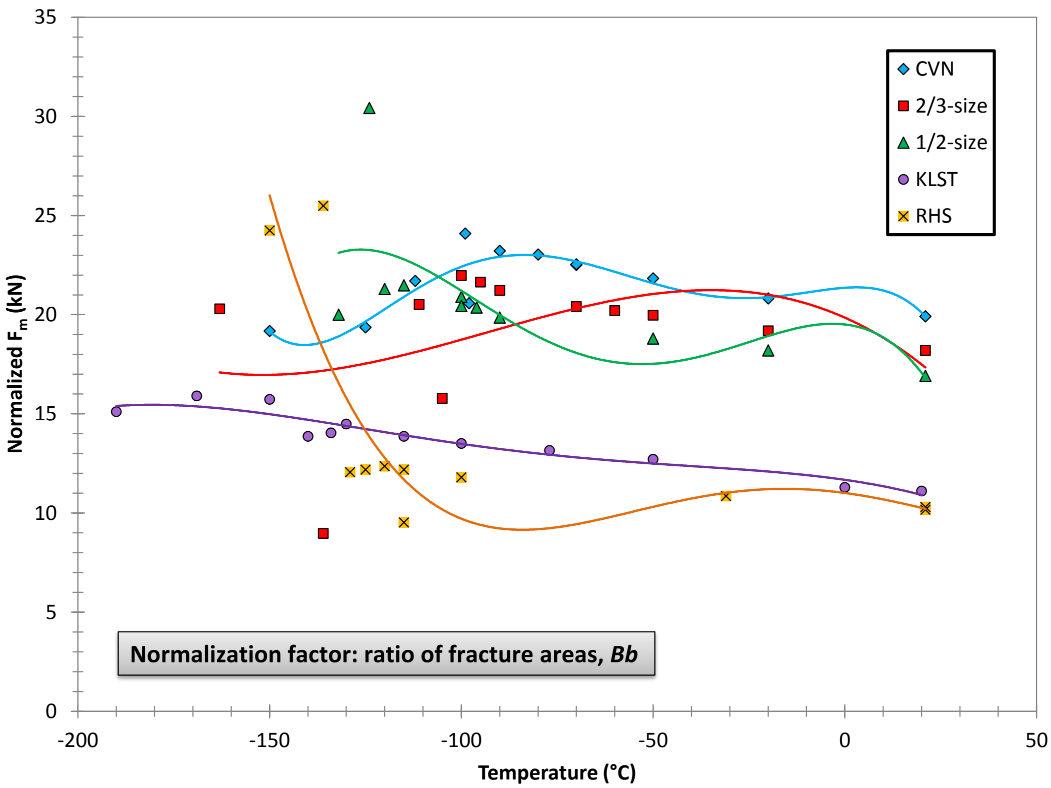

Figure 33 – Maximum forces for X70, normalized by the ratio of fracture areas.

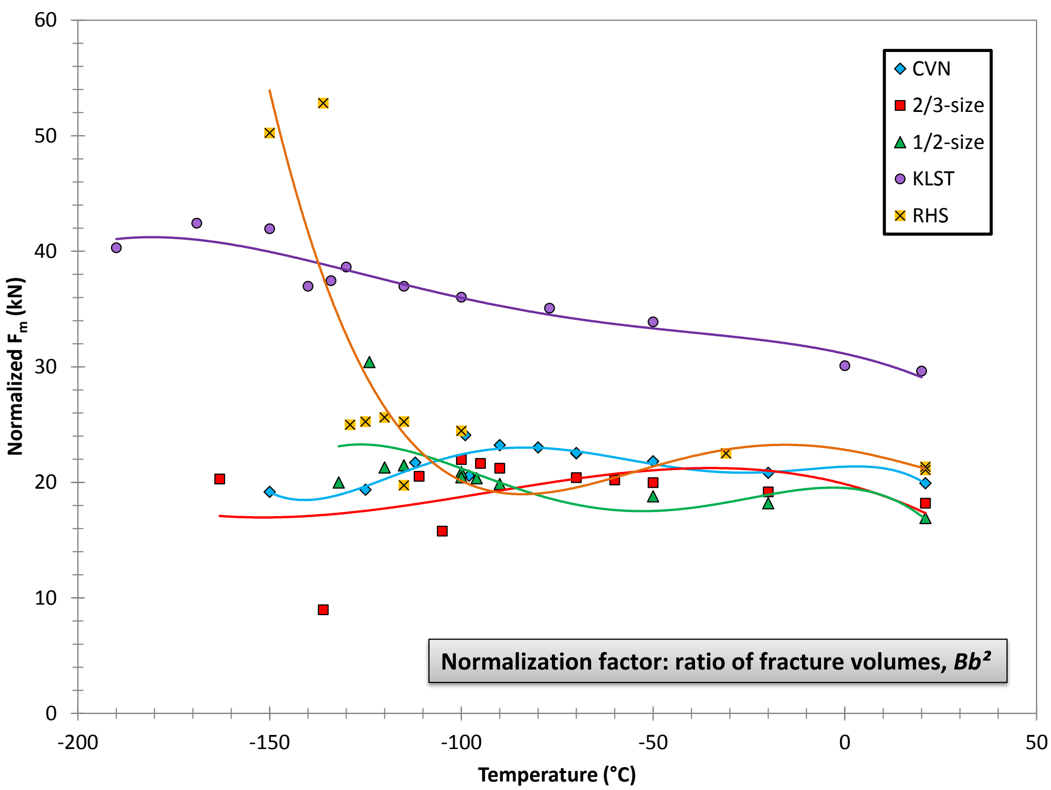

Figure 34 – Maximum forces for X70, normalized by the ratio of fracture volumes, *Bb*².

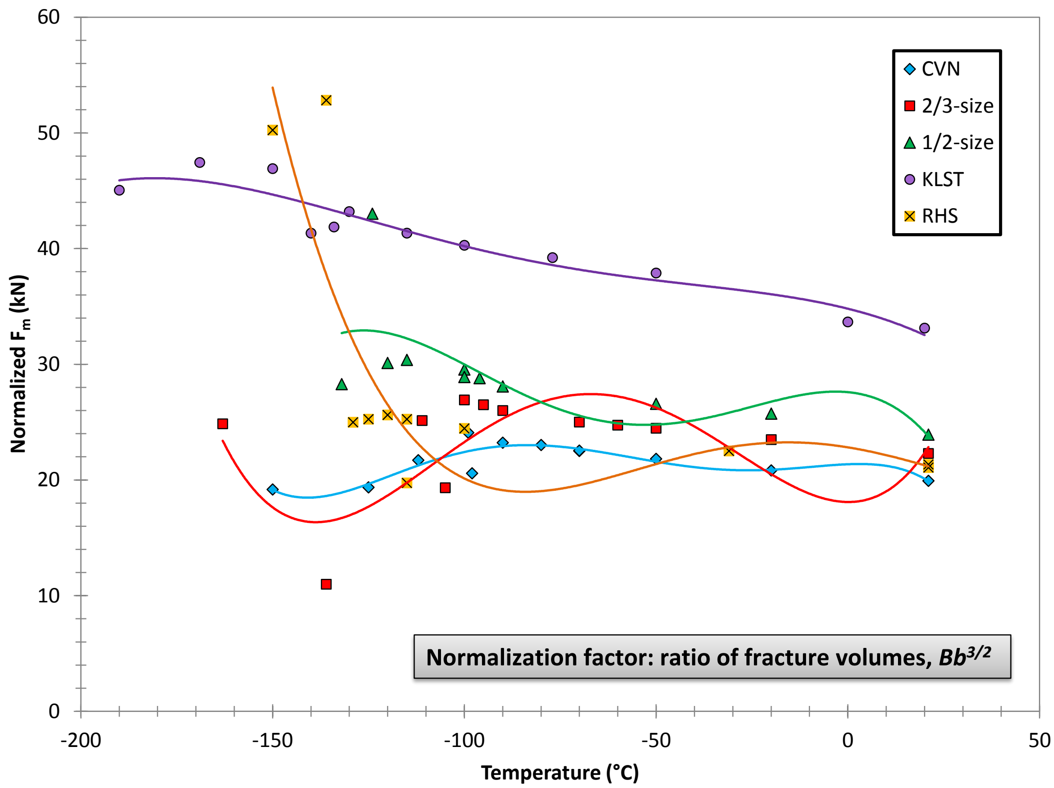

Figure 35 – Maximum forces for X70, normalized by the ratio of fracture volumes, $(Bb)^{3/2}$.

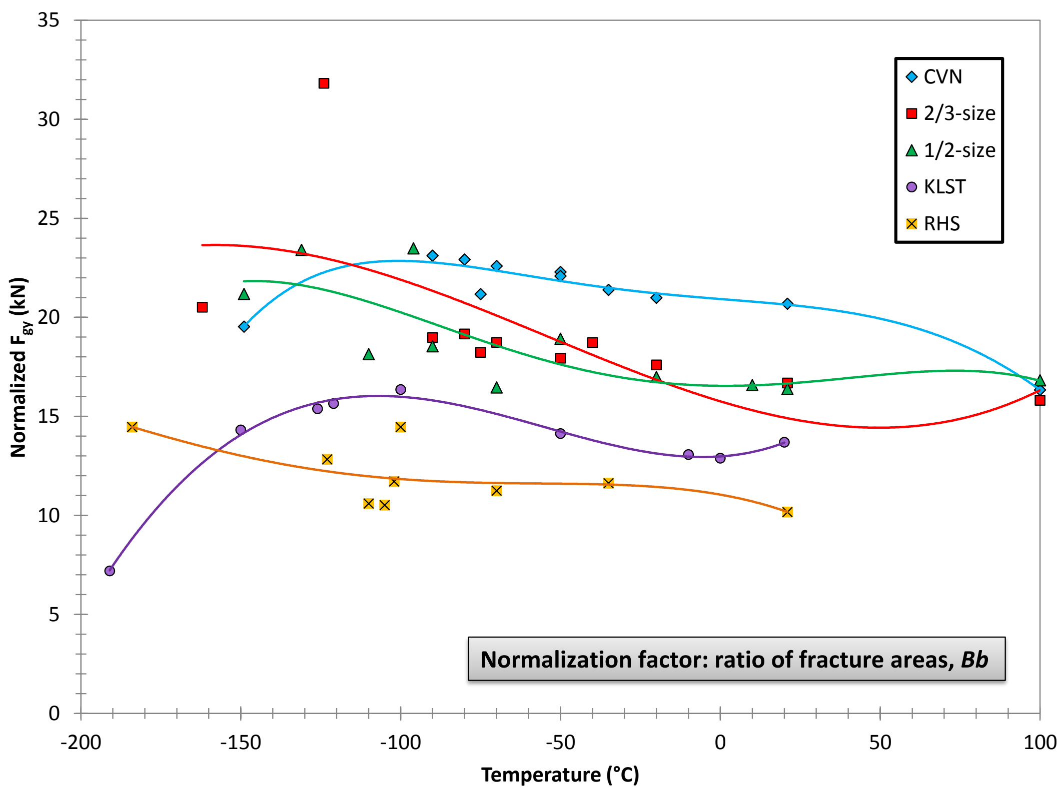

Figure 36 - Forces at general yield for X100, normalized by the ratio of fracture areas.

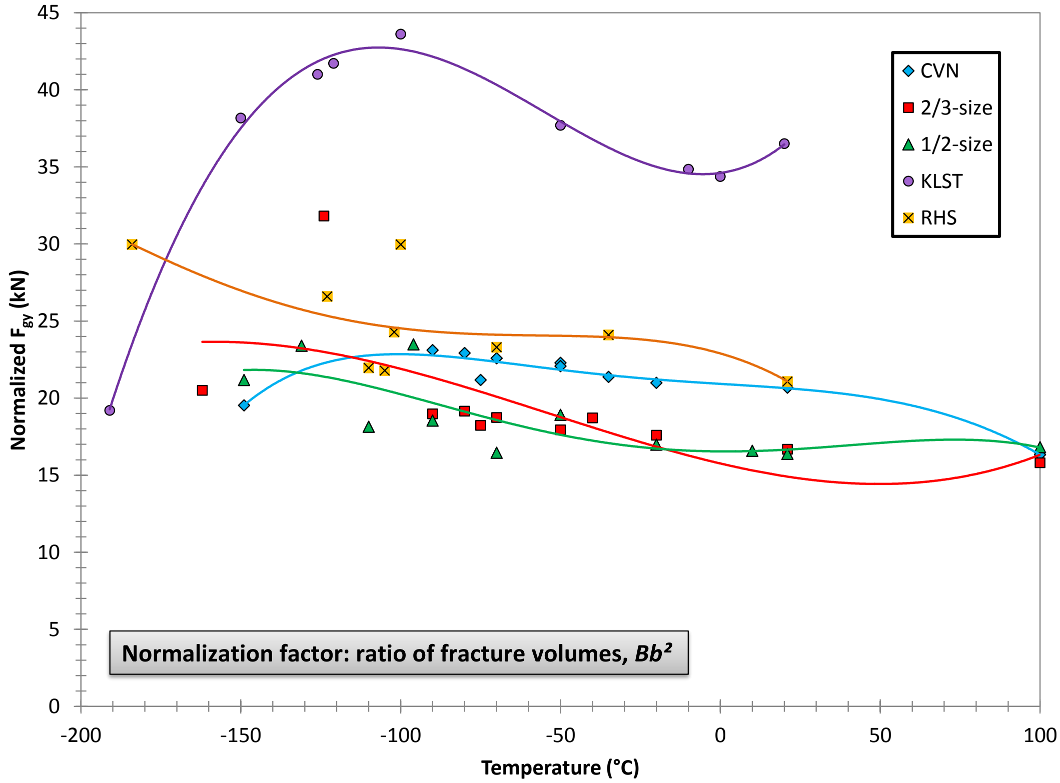

Figure 37 - Forces at general yield for X100, normalized by the ratio of fracture volumes, *Bb*².

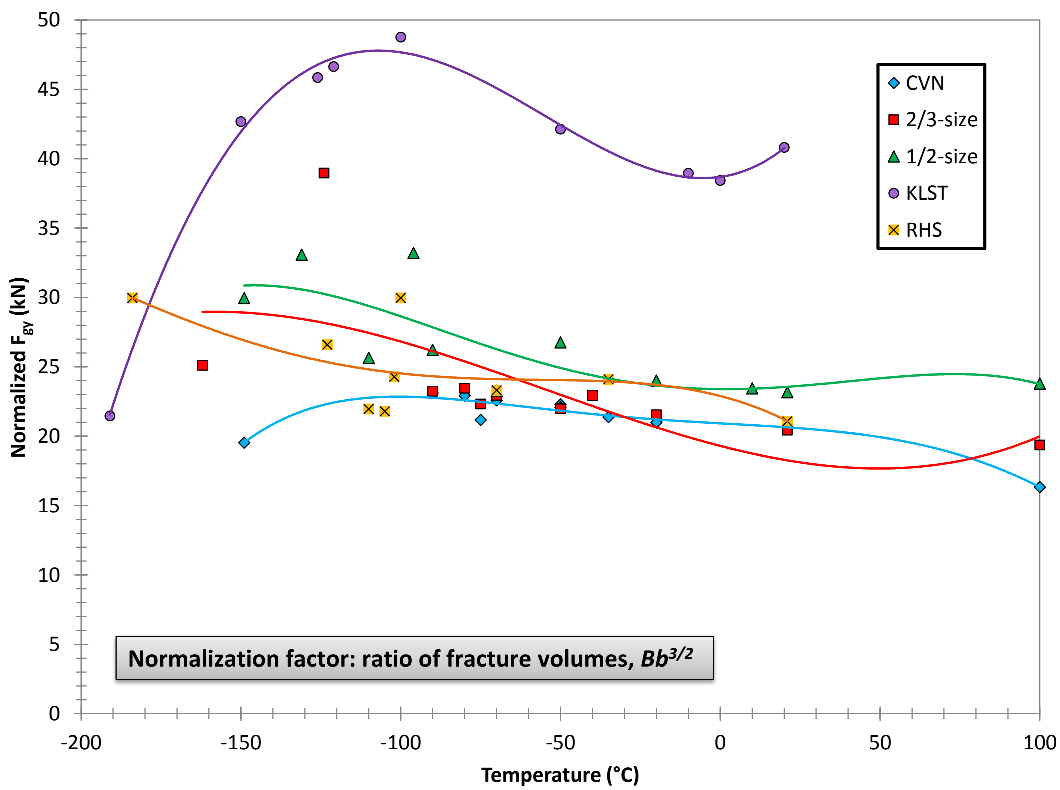

Figure 38 - Forces at general yield for X100, normalized by the ratio of fracture volumes, (*Bb*)$^{3/2}$.

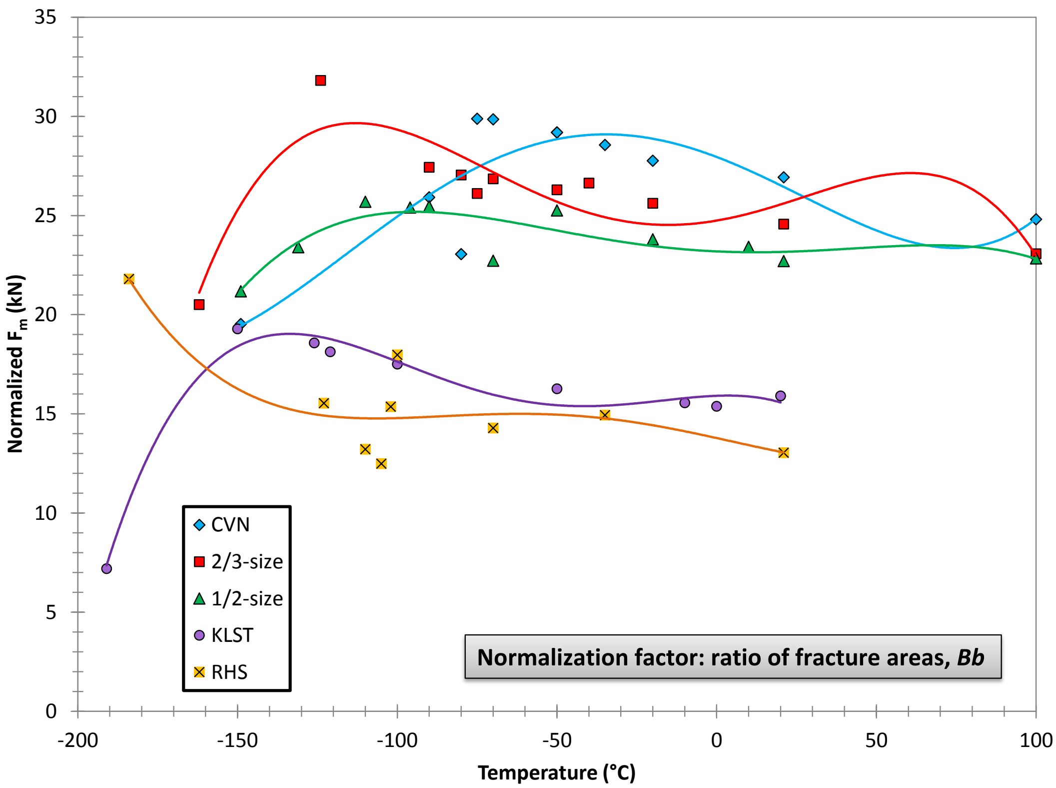

Figure 39 – Maximum forces for X100, normalized by the ratio of fracture areas.

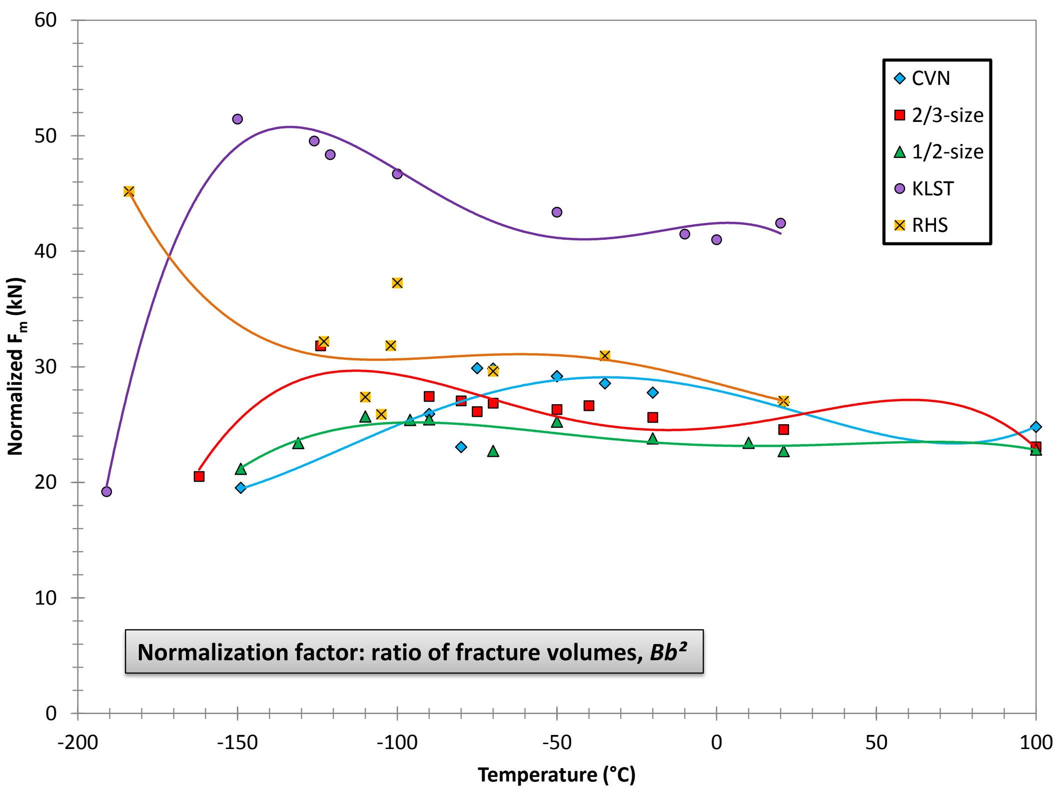

Figure 40 – Maximum forces for X100, normalized by the ratio of fracture volumes, *Bb*².

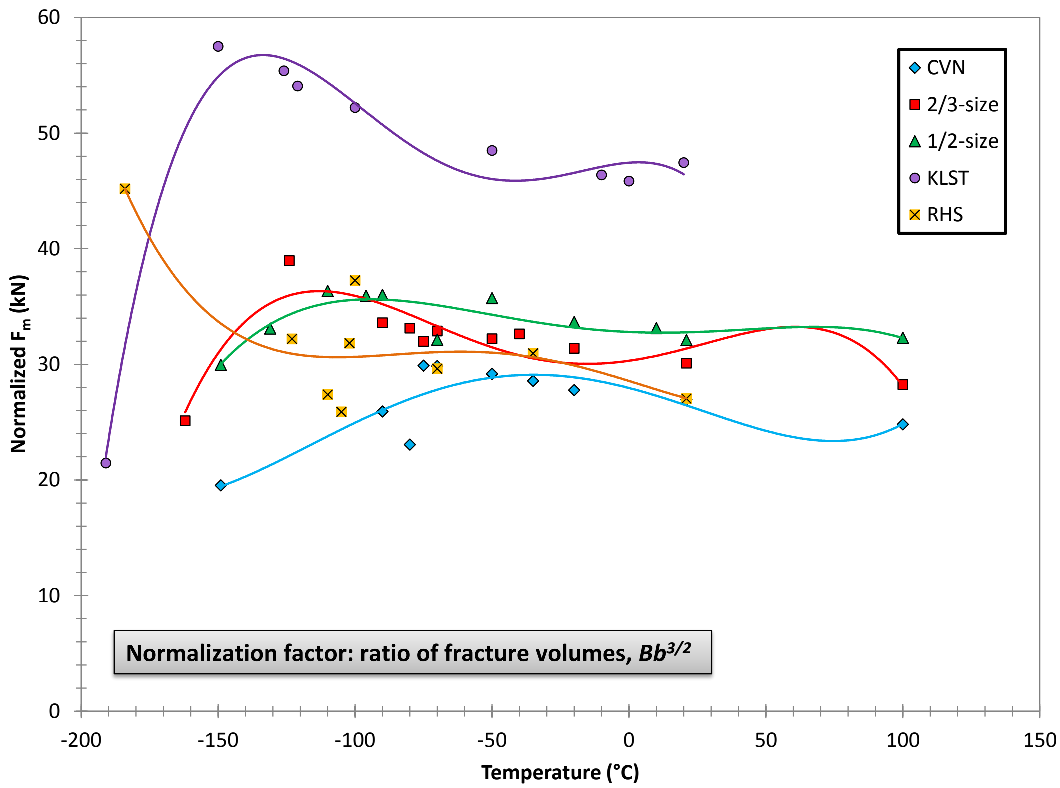

Figure 41 – Maximum forces for X100, normalized by the ratio of fracture volumes, $(Bb)^{3/2}$.

Examination of Figures 18 to 41 leads to the following conclusions:

(a) In the case of SCVN specimens (⅔-size and ½-size), normalization by the ratio of fracture areas (***Bb***) is quite effective for forces at general yield, but less effective (but still more than acceptable) for maximum forces. This might be expected, since at general yield the specimen is predominantly elastic and fracture area normalization has been shown to work well only when elastic conditions are prevailing [8]. At maximum force, plastic deformation is no more negligible and the effectiveness of fracture area normalization is reduced (normalized forces are slightly too low).

(b) Normalization by the ratio of fracture areas (***Bb***) does not work well for either type of MCVN specimen (RHS or KLST), where plastic deformation in the specimen is exacerbated by the loss of constraint. For the reasons mentioned under (a) above, the underestimation is more pronounced for F_m.

(c) Normalization by the ratio of fracture volumes ($\boldsymbol{Bb^2}$) is inadequate for KLST specimens, where it produces grossly overestimated normalized force values. In the case of RHS specimens, results are acceptable except at the lowest test temperatures, and in general for the least tough material (X52). However, even for the latter steel this normalization approach works satisfactorily under the most ductile conditions (*i.e.*, the highest temperatures).

(d) Normalization by the ratio of fracture volumes $(\boldsymbol{Bb})^{3/2}$ tends to overcorrect instrumented forces for SCVN specimens. This overcorrection tends to increase with decreasing specimen cross section.

(e) For KLST specimens, normalization by the ratio of fracture volumes $(\boldsymbol{Bb})^{3/2}$ also yields gross overcorrection of F_{gy} and F_m values.

None of the normalization factors seems to work for KLST specimens, also due to the non-proportionality of this geometry with respect to the standard Charpy geometry. We therefore attempted to optimize a KLST-specific normalization factor based on the ratio of fracture volumes, expressed as αBb^2, where $\alpha < 1$ is an empirical coefficient which minimizes the differences between (normalized) characteristic forces for CVN and KLST specimens. Based on the data shown in Figures 42 to 45, we have found that the optimum values of α for the line pipe steels investigated are 0.55 for F_{gy} and 0.63 for F_m. The need to use two different values of α can be explained by the larger amount of plasticity (and therefore larger fracture volume) occurring in the specimen at maximum force.

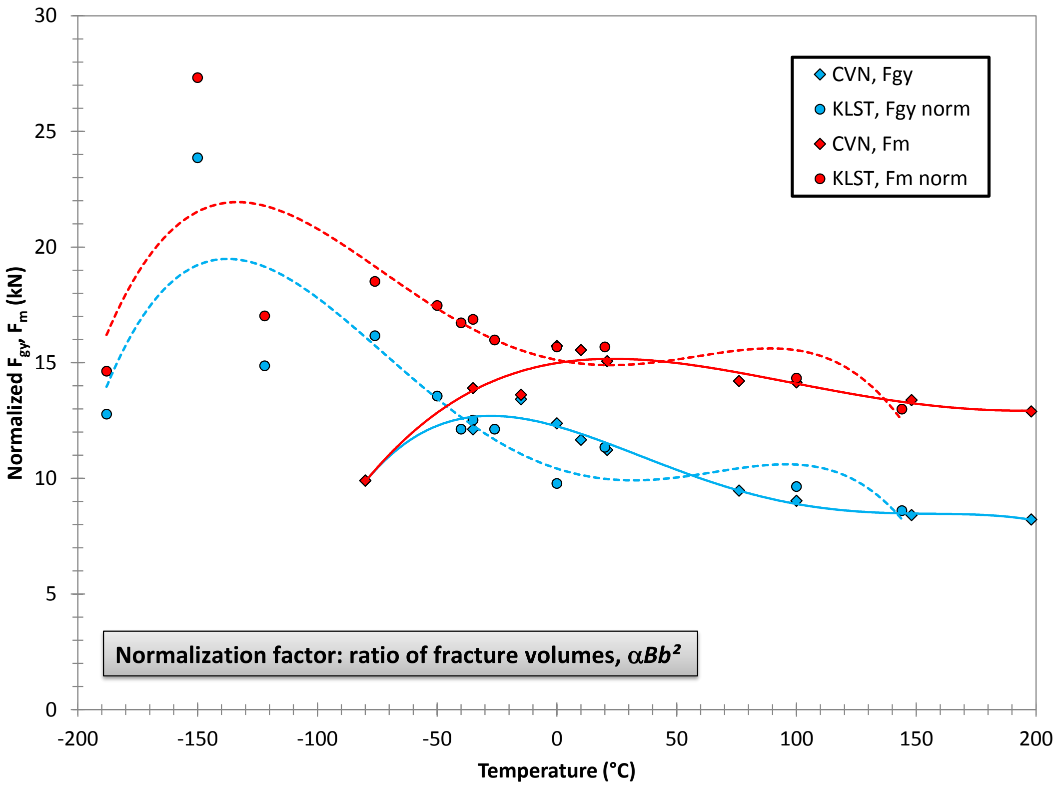

Figure 42 - Normalization of F_{gy} and F_m for KLST specimens of X52 steel with an optimized ratio of fracture volumes. Trendlines for CVN specimens are solid, trendlines for KLST specimens are dotted.

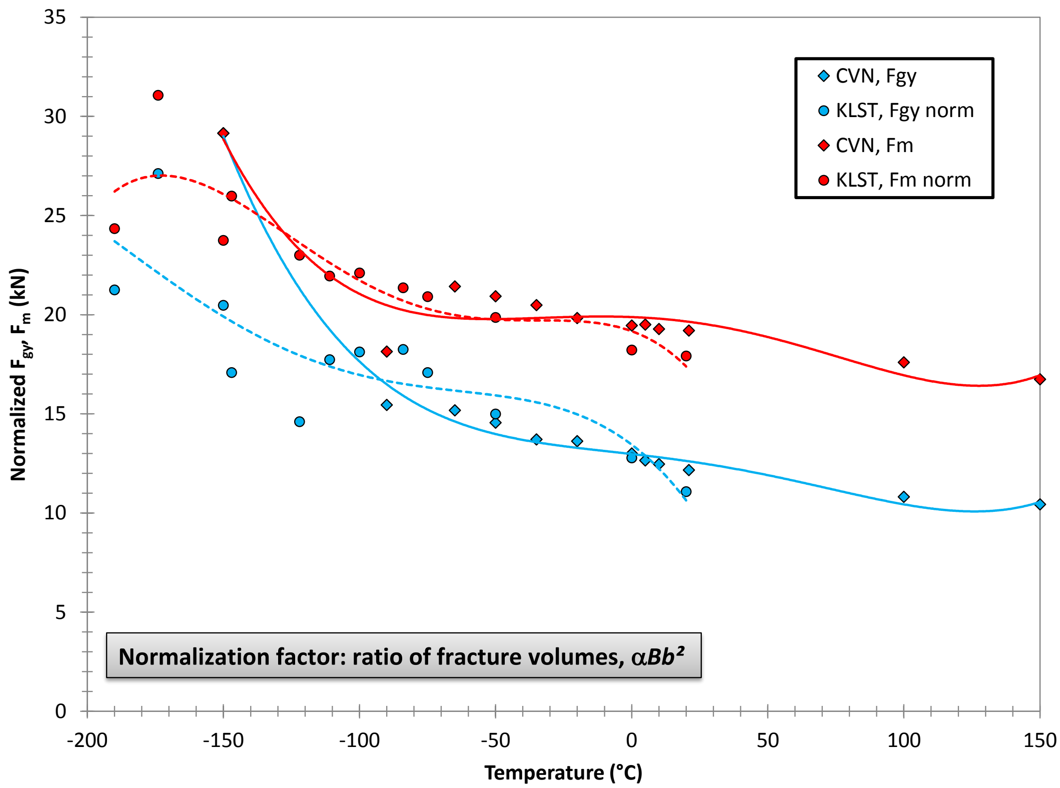

Figure 43 - Normalization of F_{gy} and F_m for KLST specimens of X65 steel with an optimized ratio of fracture volumes. Trendlines for CVN specimens are solid, trendlines for KLST specimens are dotted.

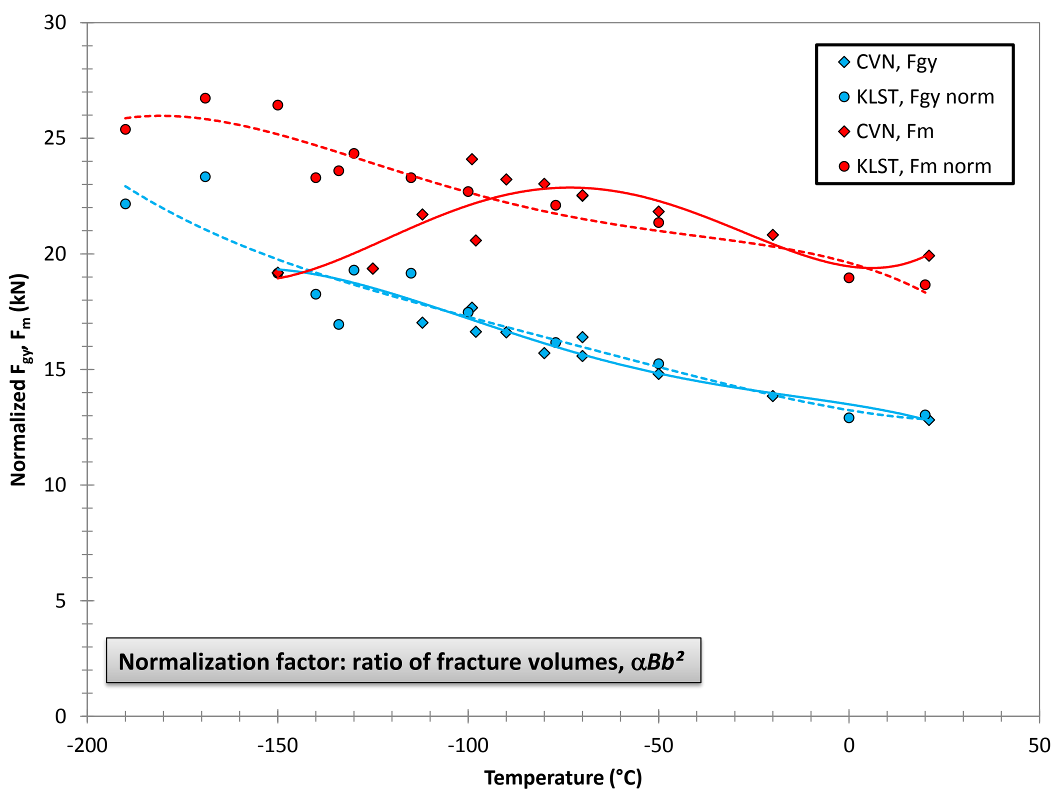

Figure 44 - Normalization of F_{gy} and F_m for KLST specimens of X70 steel with an optimized ratio of fracture volumes. Trendlines for CVN specimens are solid, trendlines for KLST specimens are dotted.

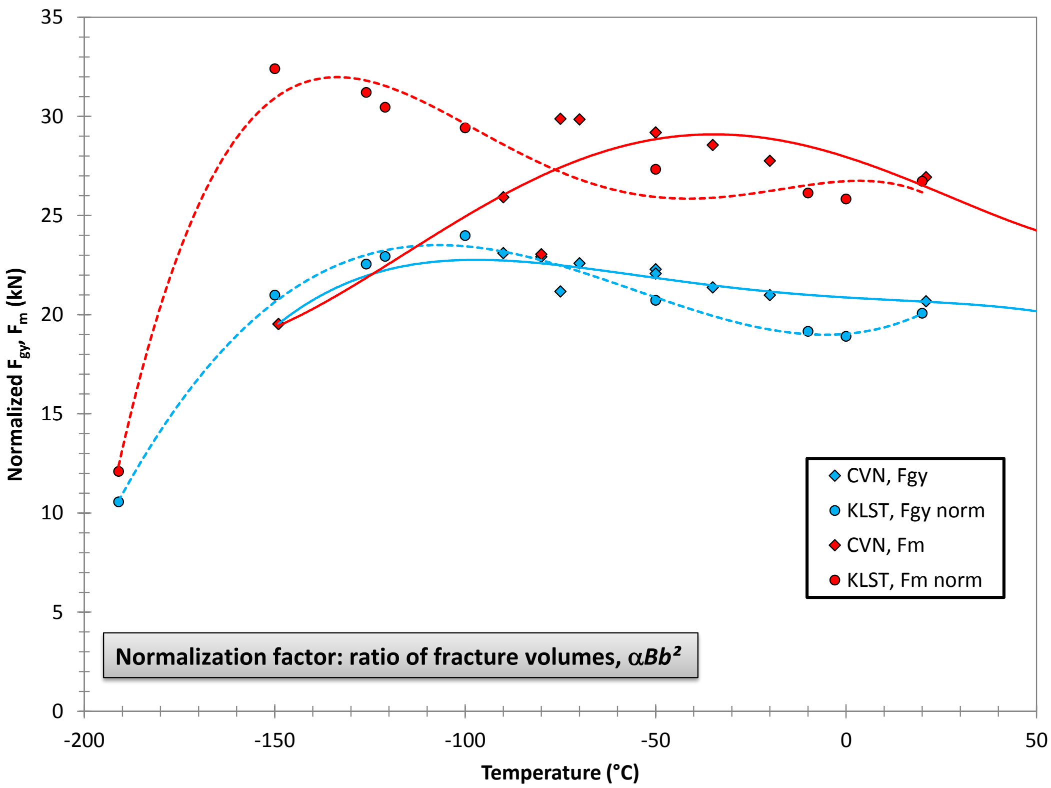

Figure 45 - Normalization of F_{gy} and F_m for KLST specimens of X100 steel with an optimized ratio of fracture volumes. Trendlines for CVN specimens are solid, trendlines for KLST specimens are dotted.

In summary, the following can be concluded.

- For SCVN specimens, forces at general yield and maximum forces should be normalized by the ratio of either nominal fracture areas, expressed as Bb, or nominal fracture volumes, expressed as Bb^2 (which are identical as shown in Table 15).
- Values of F_{gy} and F_m for RHS specimens should be normalized by the ratio of nominal fracture volumes, expressed either as Bb^2 or $(Bb)^{3/2}$ (which are identical as shown in Table 15).
- For KLST specimens, a nominal fracture volume normalization is recommended in the form αBb^2, where α = 0.55 for F_{gy} and $\alpha = 0.63$ for F_m.
- Normalization does not appear very effective under low toughness conditions (low test temperatures and/or low toughness materials).

All these recommendations could be unified by assuming a general form of the nominal fracture volume expressed by αBb^2, with the empirical coefficient α having different values as a function of specimen type according to Table 16.

Table 16 – Recommended values of the empirical coefficient α for normalization of characteristic force values.

Specimen type	Coefficient α F_{gy}	Coefficient α F_m
SCVN	1	
RHS		
KLST	0.55	0.63

4.3 Different measures of absorbed energy (*KV* and W_t)

The ratio KV/W_t (last column in Tables 9 to 13) is plotted as a function of measured *SFA* in Figure 46 (CVN and SCVN specimens), Figure 47 (KLST specimens), and Figure 48 (RHS specimens). Each plot refers to a specific combination of impact machine and instrumented striker.

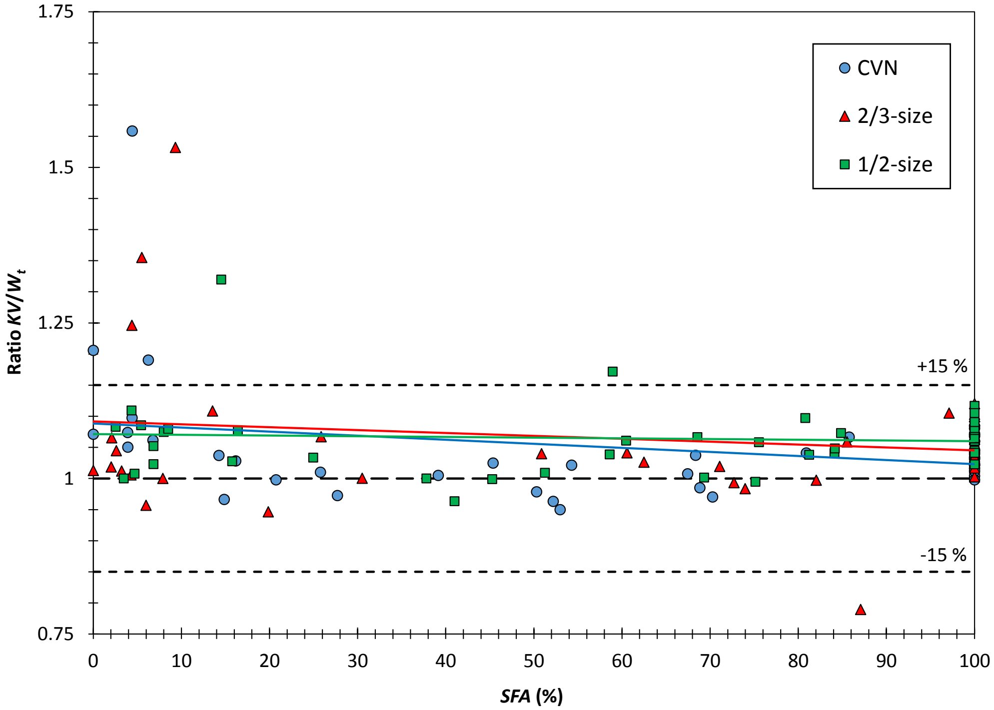

Figure 46 - Values of KV/W_t as a function of SFA for CVN and SCVN tests.

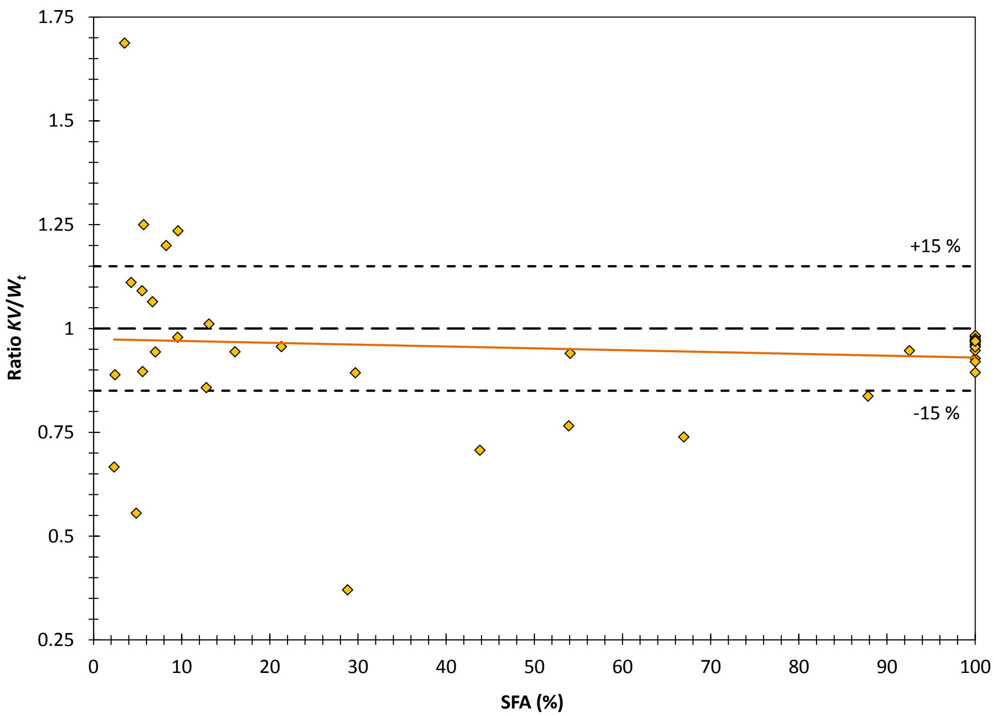

Figure 47 - Values of KV/W_t as a function of SFA for KLST tests.

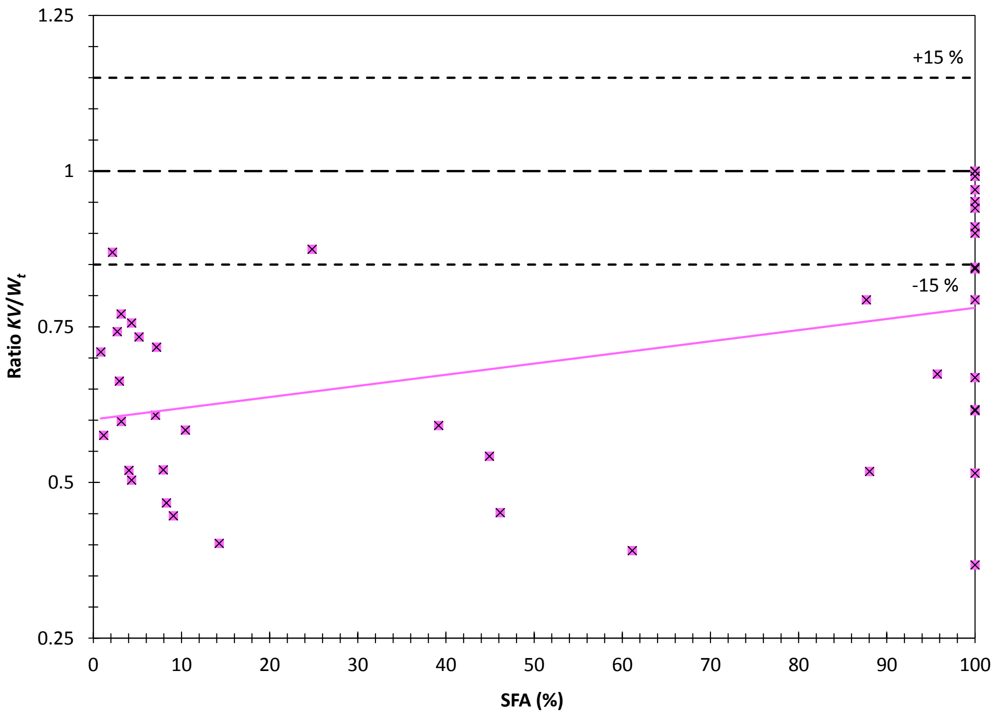

Figure 48 - Values of KV/W_t as a function of SFA for RHS tests.

For CVN, SCVN and KLST specimens, the vast majority of the tests yielded values of KV/W_t within ±15 % (0.85 to 1.15), which according to ASTM E2298-13a is the acceptable range inside which no correction to instrumented forces is required. Most of the outliers correspond to low *SFA* values, *i.e.*, brittle tests which are typically more difficult to analyze[§].

In the case of RHS tests, the difference between the two measures of absorbed energy is generally much larger, and a large portion of the KV/W_t values actually fall below the line corresponding to -25 % (0.75), irrespective of material or ductility level. For RHS tests, instrumented force values were corrected by imposing equality between W_t and *KV*, as prescribed by ASTM E2298-13a. This approach, commonly used in instrumented Charpy testing, is denominated "dynamic force adjustment" [10].

5. Correlations between specimen types

5.1 Ductile-to-brittle transition temperatures

The values of *DBTT* calculated from SCVN and MCVN specimens for *KV* ($DBTT_{KV}$), *LE* ($DBTT_{LE}$), and *SFA* ($T_{50\%}$) are plotted in Figures 49 to 51 as a function of the corresponding transition temperatures for full-size specimens. Substantially linear relationships are observed in all cases. However, particularly for $DBTT_{KV}$ values (Figure 49), X65 tends to behave as an outlier with comparatively larger shifts then the other line pipe steels. The cause of this behavior is the $DBTT_{KV}$ measured for X65 (-34.8 °C), which is much higher than $DBTT_{LE}$ (-75.7 °C) and $T_{50\%}$ (-65.1 °C), and therefore yields larger shifts than expected. Note that a similar tendency for X65 to

[§]According to several researchers, brittle tests that feature less than 3 dynamic force oscillations before specimen fracture should be analyzed, since the striker signal does not accurately represent the true specimen behavior [9].

provide larger shifts than the other steels can also be observed for *LE* (Figure 50) and *SFA* (Figure 51), although to a lesser degree. We therefore decided to exclude X65 results in the calculation of the average *DBTT* shifts and their standard deviations in Table 17 and Figure 52.

Table 17 - Shifts of ductile-to-brittle-transition temperature calculated for different steels (excluding X65), specimen types and Charpy parameters.

		Specimen type			
Parameter	Material	⅔-size	½-size	RHS	KLST
KV	X52	-11.4	-16.0	-17.2	-46.7
	X65	*-35.3*	*-45.7*	*-76.8*	*-76.2*
	X70	-5.8	-9.3	-32.1	-42.2
	X100	-13.2	-7.1	-33.4	-48.2
	Mean	-10.1	-10.8	-27.6	-45.7
LE	X52	-9.2	-13.7	-13.2	-38.1
	X65	*-18.9*	*-26.9*	*-38.4*	*-35.2*
	X70	-4.0	-16.9	-23.2	-35.9
	X100	-11.2	-4.7	-29.0	-41.5
	Mean	-10.8	-15.5	-26.0	-37.7
SFA	X52	-8.8	-17.4	-25.8	-54.4
	X65	*-38.8*	*-45.4*	*-74.2*	*-62.8*
	X70	-6.5	-16.4	-31.1	-41.7
	X100	-16.0	-10.8	-35.9	-45.3
	Mean	-17.5	-22.5	-41.7	-51.0
Overall mean		**-9.6**	**-12.5**	**-26.8**	**-43.8**
Overall st. dev.		**3.8**	**4.7**	**7.6**	**5.6**

As expected, the magnitude of the downward shift increases as the specimen size decreases, which confirms the well-known shift of *DBTT* to lower temperatures due to a reduction in specimen size [8,11].

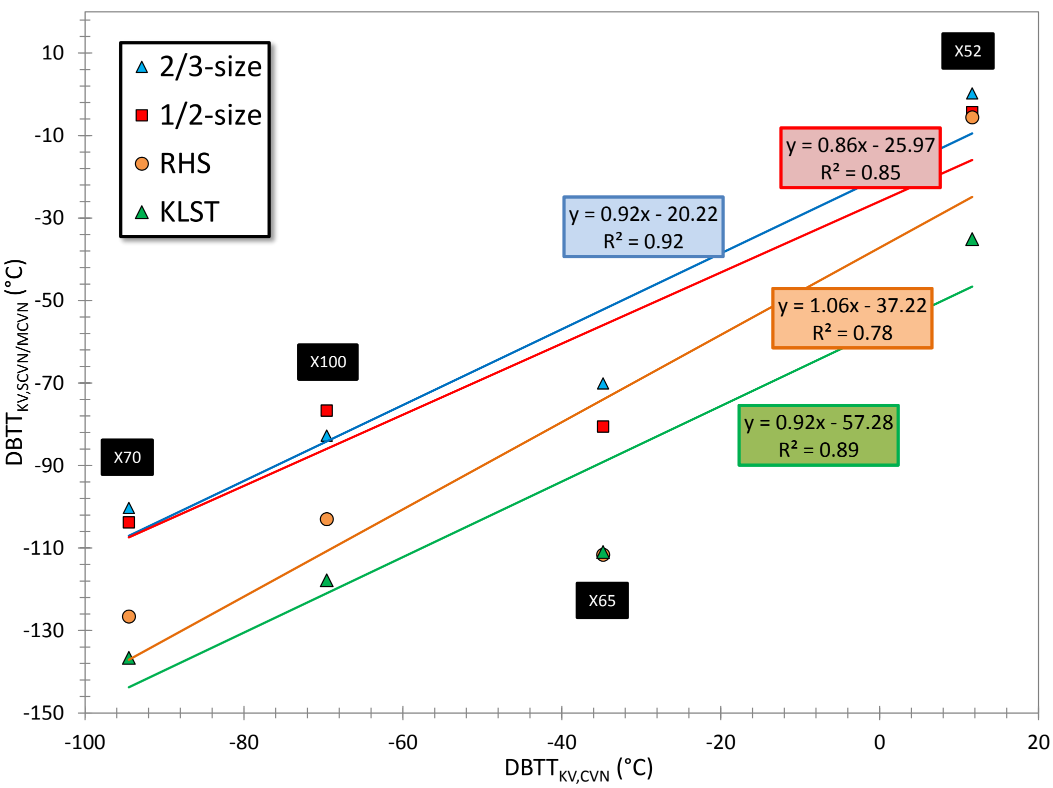

Figure 49 - Values of *DBTT_KV* calculated from different specimen types.

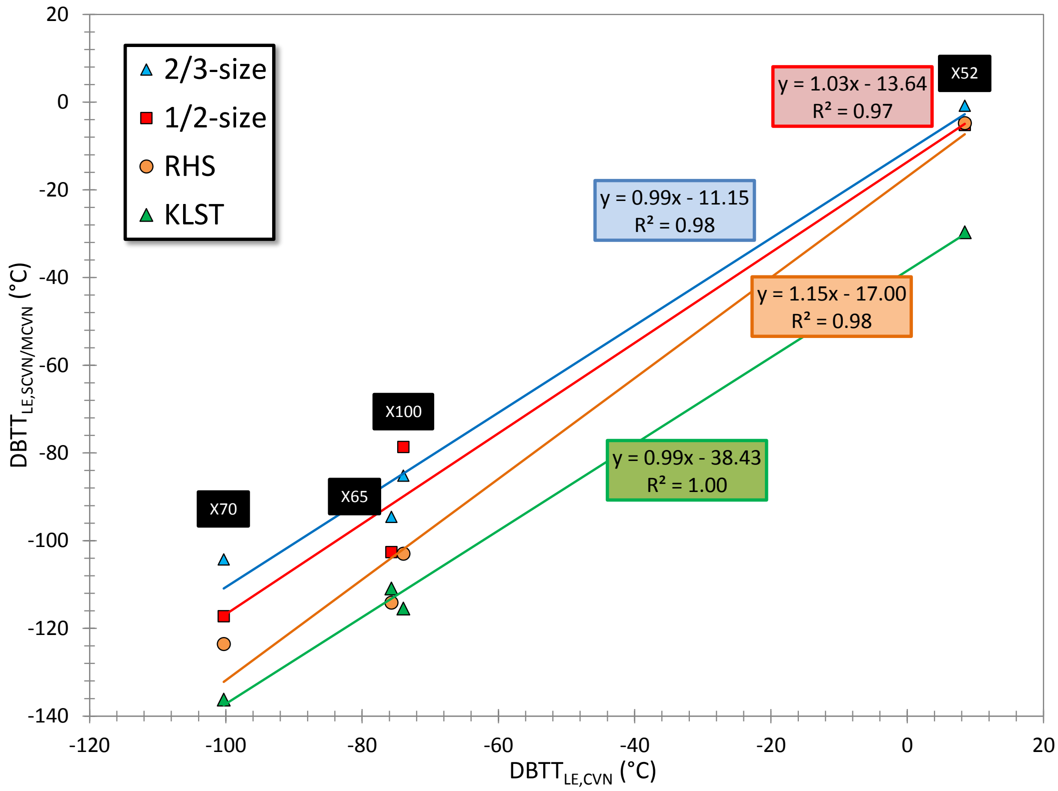

Figure 50 - Values of *DBTT_LE* calculated from different specimen types.

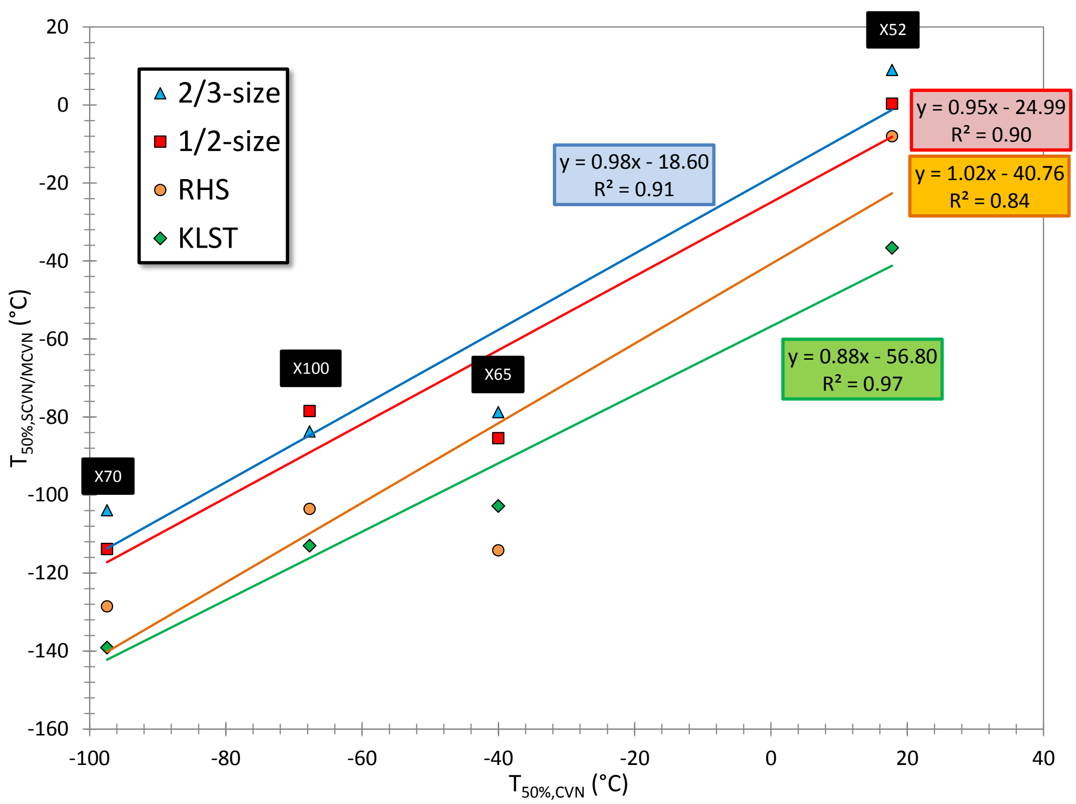

Figure 51 - Values of *T_50%* calculated from different specimen types.

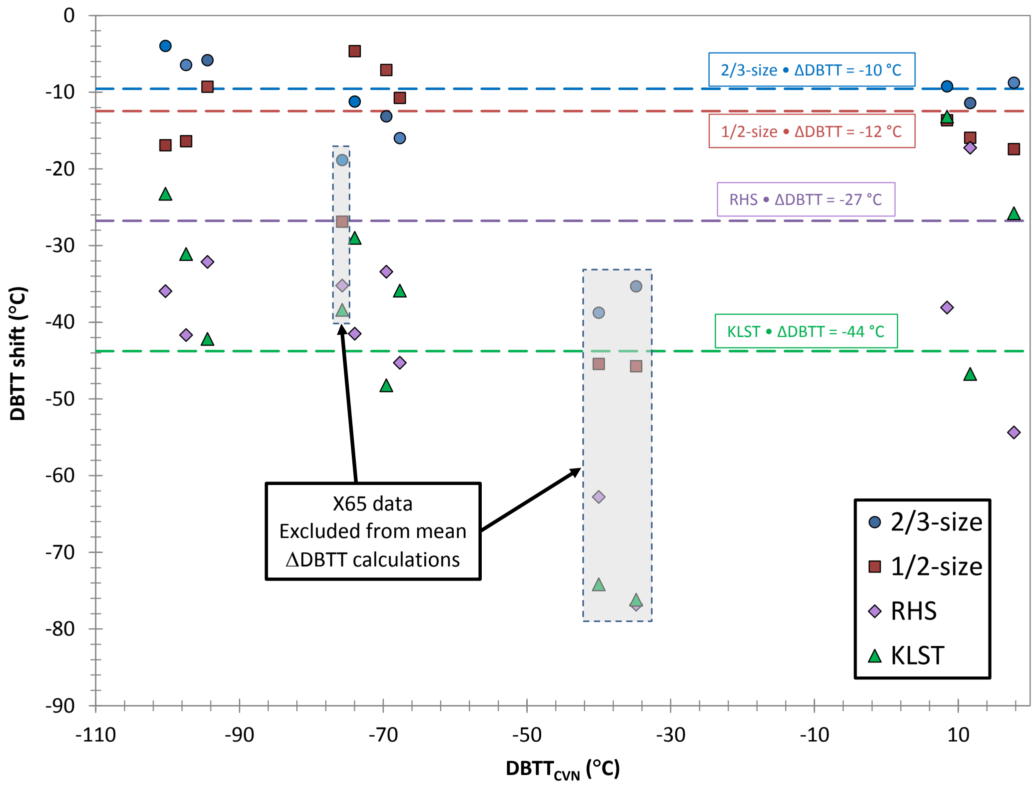

Figure 52 - Values of *DBTT* shift (from *KV*, *LE*, and *SFA*) obtained from different specimen types.

The feasibility of using a simple empirical model such as:

$$DBTT_{CVN} = DBTT_{SCVN/MCVN} + M \tag{2}$$

(where M is the *DBTT* shift due to specimen size reduction) was verified by performing a statistical t-test on the slope of the linear fits correlating all values of $DBTT_{SCVN/MCVN}$ and $DBTT_{CVN}$ (Figures 49 to 51). In all cases except for RHS specimens (see Table 18 and Figure 53), the calculated slope is not statistically different from 1 at a confidence level of 95 % (α = 0.95), and therefore the use of eq.(2) is justified. The degree of linear correlation is high in all cases (R^2 = 0.99).

Table 18 - Results of the *t*-test on the slope of the linear correlations shown in Figure 53. The slope is not statistically different from 1 if $t_0 < t_{crit,\alpha=0.95}$.

X-variable	Y-variable	Specimen	Slope (1/°C)	Intercept (°C)	t_0	$t_{crit,\alpha=0.05}$	Result of *t*-test
$DBTT_{SCVN/MCVN}$	$DBTT_{CVN}$	⅔-size	1.015	10.514	0.536	1.895	Slope is not statistically different from 1
		½-size	1.027	14.174	0.753		Slope is not statistically different from 1
		RHS	0.896	18.642	2.981		Slope is statistically different from 1
		KLST	1.046	48.181	1.124		Slope is not statistically different from 1

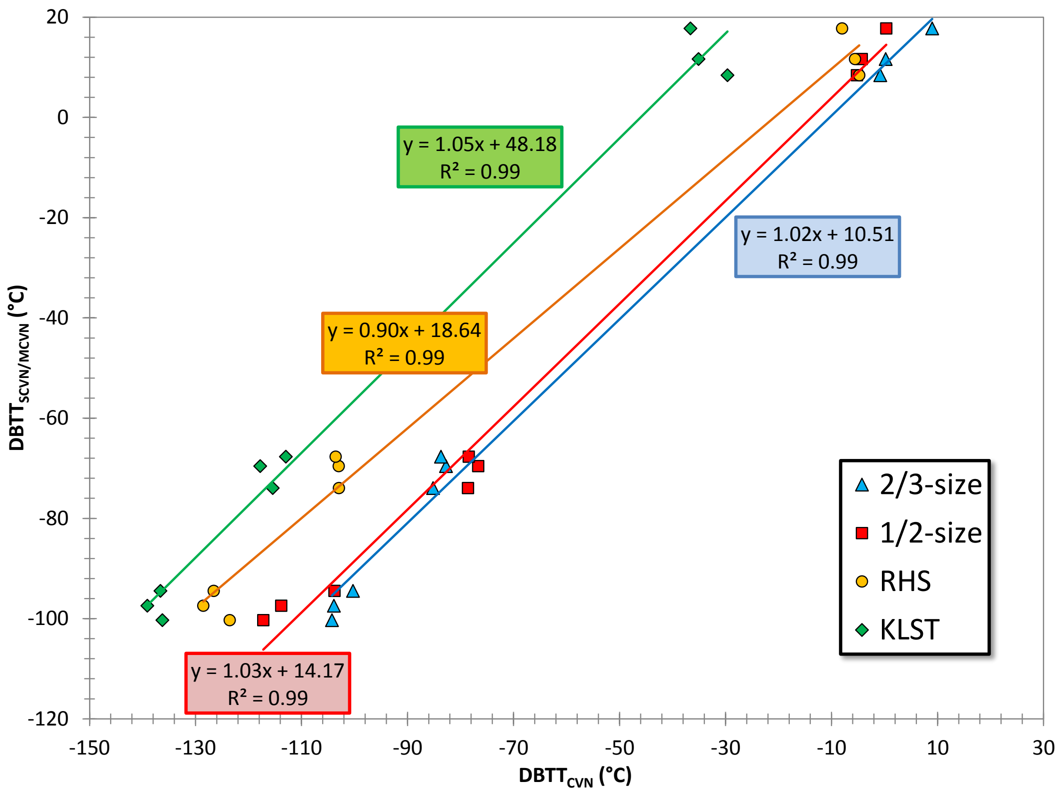

Figure 53 - Linear correlations between *DBTT* values from SCVN, MCVN, and CVN specimens. NOTE: data from X65 are not included.

5.1.1 Comparison with the literature

By analyzing test results obtained from CVN and four types of MCVN specimens** for 10 base and weld metals from reactor pressure vessel steels, Sokolov and Alexander [8] proposed the following correlation between the factor M in eq.(2) and the nominal fracture volume, expressed as Bb^2 (B = specimen thickness, b = ligament size):

$$M = 98 - 15.1 \cdot \ln\left(Bb^2\right) \tag{3}$$

In [8], eq.(3) was obtained by fitting values of M corresponding to four different definitions of transition temperature: (a) 41J-temperature; (b) 68J-temperature; (c) temperature at the midpoint of the transition curve; (4) 50 %-SFA temperature.

The values of *DBTT* shift obtained in this investigation and listed in Table 17 are compared to eq.(3) in Figure 54, where excellent agreement with Sokolov/Alexander's original fit can be observed. We recalculated the coefficients of eq.(3) using both sets of results, subject to the constraint M = 0 for Bb^2 = 640 mm^3 (*i.e.*, for CVN specimens), and the following modified relationship was obtained:

$$M = 92.7 - 14.34 \cdot \ln\left(Bb^2\right) \tag{4}$$

**Type 1: B = 5 mm, b = 4.2 mm; type 2: B = 3.3 mm, b = 2.83 mm; type 3: B = 5 mm, b = 4 mm; type 4 (KLST): B = 3 mm, b = 3 mm.

Figure 54 illustrates our test results, the data points obtained by Sokolov/Alexander in [8] for MCVN specimens of 4 different geometries, their original relationship, eq.(3) and the modified fitting line, eq.(4).

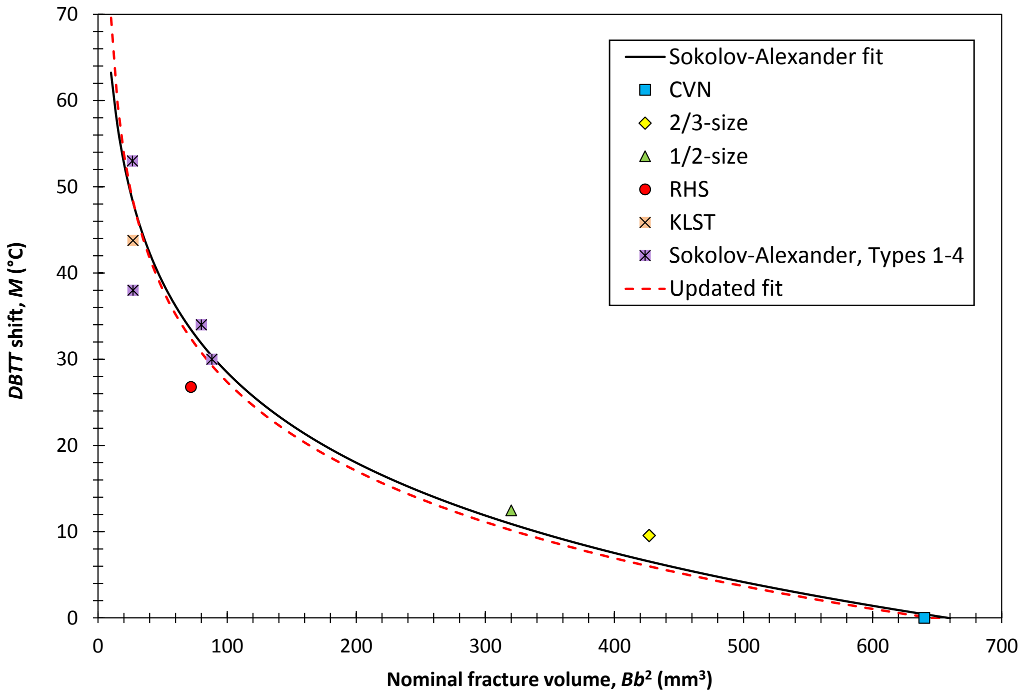

Figure 54 - Transition temperature correction for SCVN/MCVN specimens as a function of nominal fracture volume.

An earlier investigation by Gross [12] studied the relationship between different measures of transition temperature obtained from standard and sub-size Charpy specimens of five structural steels of different strength and ductility. The sub-size geometries considered were ½-size (denominated HW, or *half-width*[††]) and ¼-size (QW, *quarter-width*). Specimens with B = 20 mm were also used (DW, *double-width*). The criteria used to define and calculate *DBTT*s referred to absorbed energy [*KV* = 15 ft.lb (20.3 J) and 3.8 ft.lb/0.1 in. (5.2 J/2.5 mm) thickness], lateral expansion [*LE* = 10 mil (0.25 mm), 15 mil (0.38 mm), and 20 mils (0.51 mm)], and shear fracture appearance (*SFA* = 10 %, 30 %, and 50 %). In addition, Nil-Ductility Temperature (*NDT*) values measured by drop-weight testing in accordance with ASTM E208 were also reported. The average values of M for each steel investigated in [12] and the overall mean shift values are given in Table 19.

[††]Note that in [10], the specimen dimension parallel to the notch is denominated "width". However, in this investigation the same dimension (B) is called "thickness", following the conventional fracture toughness designation.

Table 19 - *DBTT* shifts measured by Gross [12] on five structural steels using different types of Charpy specimens.

Steel	Specimen type	Mean *M* (°C)
ABS-C	QW	-37
	HW	-14
	DW	4
A302-B	QW	-36
	HW	-15
	DW	2
HY-80	QW	-44
	HW	-12
	DW	-3
A517-F	QW	-67
	HW	-23
	DW	4
HY-130	QW	-56
	HW	-8
	DW	-2
All	**QW**	**-48**
	HW	**-14**
	DW	**1**

The only sub-size specimen in common with our investigation is the ½-size, or HW: the average shift reported by Gross (-14 °C) is in agreement with our calculated value *KV*, *LE*, and *SFA* transition curves (see Table 17), M = -12.5 °C. Note that the shift for ¼-size specimens (-48 °C) is much larger than the shift we obtained for RHS specimens (-26.8 °C), and quite close to the shift we obtained for KLST specimens (-43.8 °C). Note also that the change in *DBTT* was negligible (1 °C) when the thickness of the specimen was doubled.

If we add Gross' data to the M vs. Bb^2 plot shown in Figure 54, the value for ¼-size (QW) specimens is clearly an outlier with respect to both Sokolov/Alexander's original fit and our modified fit (Figure 55).

However, examination of Figure 55 leads to formulate a different hypothesis. We observe that all data points corresponding to SCVN specimens (⅔-size, ½-size, ¼-size) lie above the fitting lines. One could therefore speculate that SCVN specimens might follow a different trend than MCVN specimens, and therefore it might be appropriate to separately fit SCVN and MCVN data.

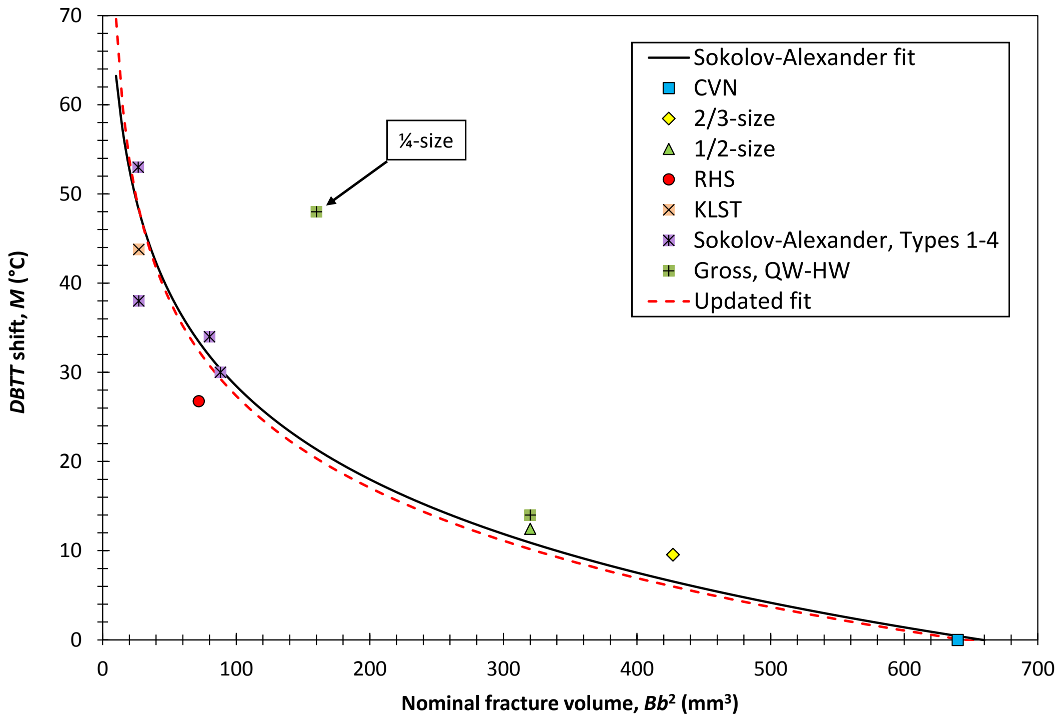

Figure 55 - Transition temperature correction for SCVN/MCVN specimens, with Gross' results added.

In Figure 56 we present an attempt at separately fitting SCVN and MCVN data, using the same formulation as eqs.(3) and (4) and still imposing $M = 0$ for CVN specimens. The quality of the SCVN fit appears to be poor, and a simple exponential fit of the type $M = C_1 \exp(-C_2 \cdot Bb^2)$ (green dashed line in Figure 56) appears to provide a better fit. Additional data from sub-size specimens are needed to confirm or disprove these observations.

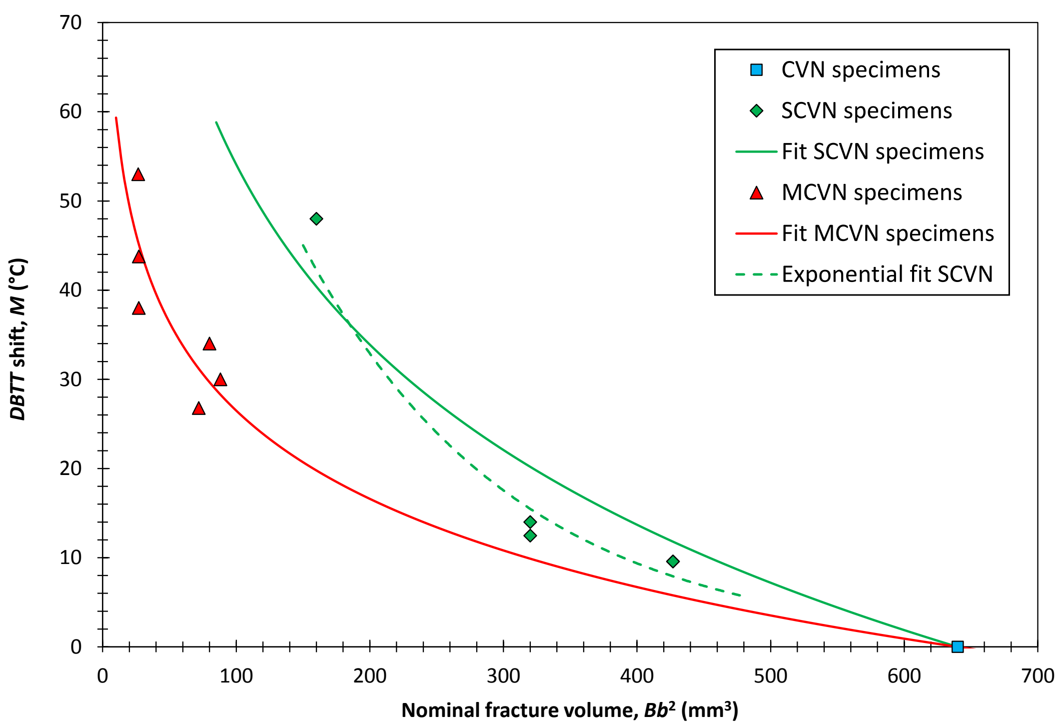

Figure 56 – *DBTT* shifts from [8], [12], and this investigation, fitted separately for SCVN and MCVN specimens.

5.2 Upper Shelf Energy

The most commonly used approach for correlating *USE* values between Charpy specimens of different geometry involves the use of a normalization factor, *NF*, which can be empirically derived from experimental data or calculated as the ratio between specific geometric parameters (see also Section 4.2.1):

$$USE_{CVN} = NF \times USE_{SCVN/MCVN} \tag{5}$$

Published values of *NF* include:

- NF_1 = ratio of fracture areas, expressed as Bb [13,14];
- NF_2 = ratio of nominal fracture volumes, expressed as $(Bb)^{3/2}$ [13,14];
- NF_3 = ratio of nominal fracture volumes, expressed as Bb^2 [15,16];
- NF_4 = ratio of Bb^2/SK_t (with S = span, or distance between the anvils, and K_t = elastic stress concentration factor, which depends on ligament size and notch root radius) [17];
- NF_5 = ratio of $(Bb)^{3/2}/QK_t$ (with Q = plastic stress concentration factor, given by $Q = 1 + (\pi - \theta)/2$, where θ is the notch angle in radians) [18].

Additionally, empirical normalization factors were published by Sokolov and Alexander for 4 types of miniaturized Charpy specimens [8] (NF_6) and by Lucon for KLST specimens [11] (NF_7).

In this investigation, the empirical normalization factors NF_8 obtained by fitting *USE* values with eq.(5), see Figure 57, are listed in Table 20, where they are compared with all the previously listed geometrical and empirical factors.

Table 20 - Normalization factors published in the literature (NF_1 to NF_7) and calculated in this investigation (NF_8). For the definition of NF_1 to NF_7, see above.

Specimen type	NF_1	NF_2	NF_3	NF_4	NF_5	NF_6	NF_7	$\boldsymbol{NF_8}$
⅔-size	1.50	1.84	1.50	1.50	1.50	-	-	**1.70**
½-size	2.00	2.83	2.00	2.00	2.00	-	-	**3.24**
RHS	4.29	8.89	8.89	3.30	6.84	6.3[‡‡]	-	**8.89**
KLST	8.89	26.50	23.70	30.00	51.26	24.9	21.6	**36.77**

Across the board, the best agreement for the measured data is achieved with NF_2 (ratio of nominal fracture volumes, expressed as $(Bb)^{3/2}$). Only for KLST specimens, the calculated factor NF_8 is closest to NF_4.

[‡‡]This value corresponds to Type 3 in [6], which is dimensionally almost identical to a RHS specimen (thickness = 5 mm, width = 5 mm, length = 27 mm, notch angle = 45°, notch depth = 1 mm, notch root radius = 0.25 mm).

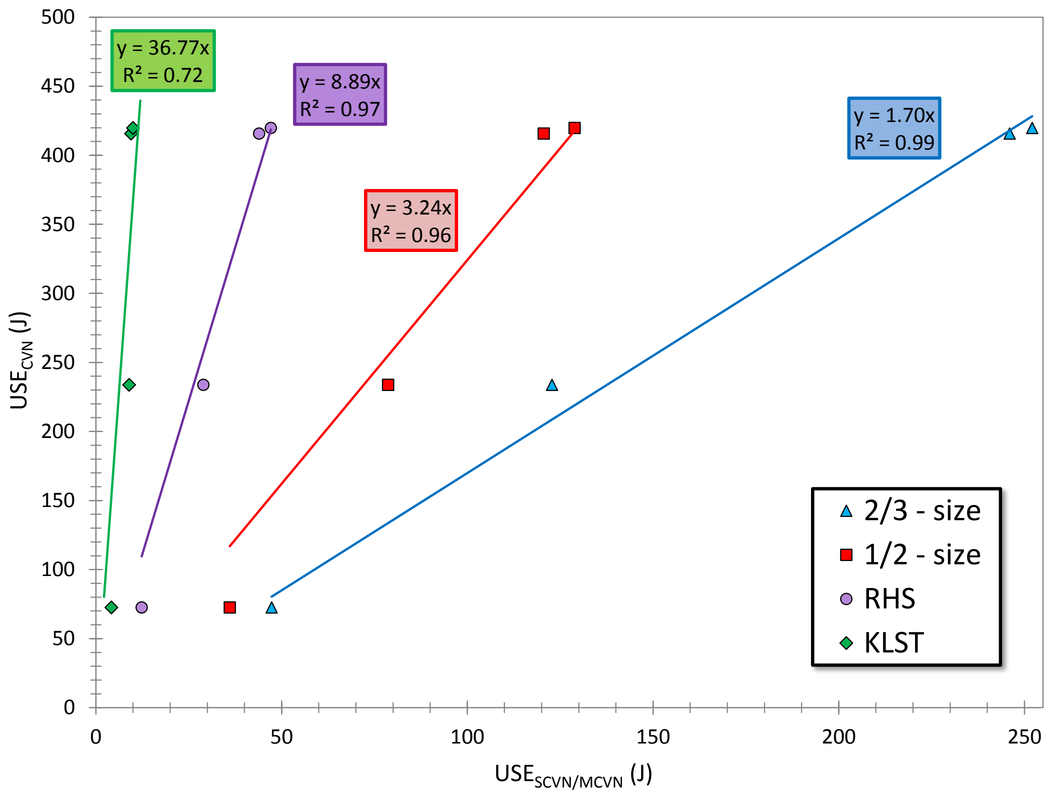

Figure 57 - Correlation between USE values measured on CVN, SVCN, and MCVN specimens.

The correlation coefficients *r*, which quantify the degree of linear relationship between two variables, are very high for ⅔-size (0.996), ½-size (0.998), and RHS specimens (0.997), but lower for KLST specimens (0.915). See also the coefficients of determination R^2 for the fitting lines in Figure 57.

The latter observation might also indicate that the actual relationship between *USE* values from CVN and KLST specimens is not linear, as suggested in [11] where the following exponential fit was proposed:

$$USE_{CVN} = 29.454 \cdot e^{0.2378 USE_{KLST}} \tag{6}$$

We have compared the results from this investigation to eq.(6) in Figure 58. Good agreement was found for X52 and X100, where material fracture actually occurred in upper shelf tests. For X65 and X70, the measured absorbed energy for KLST specimens is much higher than predicted by eq.(6). For these two steels, USE_{CVN} is higher than 400 J. Under these conditions, specimens tested in the fully ductile region dissipate large amounts of plastic deformation at the support points, due to the specimen squeezing between the anvils. All interactions between specimen and anvils will require additional energy, and specimens with high *USE* values will have significant amounts of energy associated with the anvil interactions in addition to the fracture process at the notch.

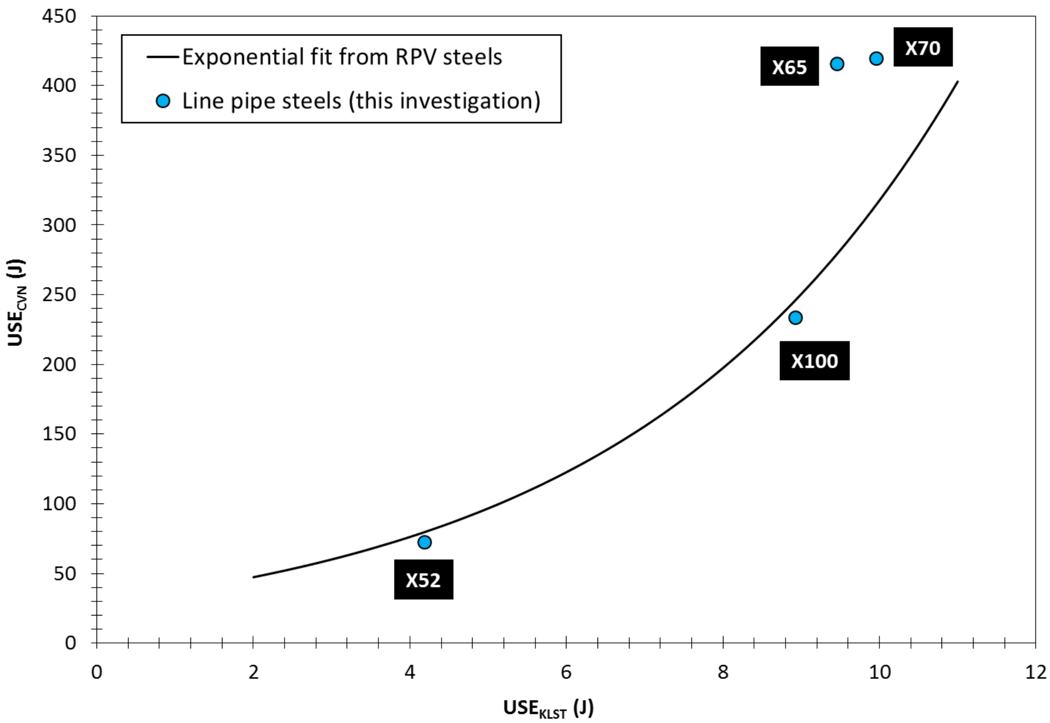

Figure 58 - Correlation between USE values measured on CVN and KLST specimens.

6. Conclusions

(1) Ductile-to-brittle transition temperatures ($DBTT_{KV}$, $DBTT_{LE}$, $T_{50\%}$) and upper shelf energies generally tend to decrease with decreasing specimen size, *i.e.*, the smaller the specimen, the more ductile it tends to behave. This confirms what has been published by many authors.

(2) Transition temperatures measured from *KV*, *LE*, and *SFA* are generally in good agreement (within ±10 °C). This is particularly the case for miniaturized specimens (KLST and RHS).

(3) Based on the results obtained for the four line pipe steels investigated:
   - X52 is the least tough and exhibits the widest ductile-to-brittle transition region;
   - X65 and X70 are the toughest, in terms of lowest *DBTT*s and highest upper shelf energies;
   - X70 has the narrowest ductile-to-brittle transition region;
   - X100 has lower *USE* than X65 and X70, but its *DBTT*s are lower than X65.

(4) Instrumented characteristic forces at general yield (F_{gy}) and maximum forces (F_m) tend to decrease with increasing test temperature and obviously with size. Instrumented forces can be effectively normalized, although the optimal normalization factor (ratio of different geometrical parameters) depends on the specimen type:
   - for SCVN specimens (⅔-size and ½-size), nominal fracture areas (Bb) or volumes (Bb^2) should be used;
   - for RHS specimens, the most effective normalization is by the use of nominal fracture volumes, expressed either in the form Bb^2 or $(Bb)^{3/2}$;
   - for KLST, we have developed an alternative expression of the nominal fracture volume, given by αBb^2, where $\alpha = 0.55$ for F_{gy} and $\alpha = 0.63$ for F_m.

(5) The ratio between the two measures of absorbed energy (KV and W_t) is quite consistent and independent of test temperature or specimen type for both the instrumented striker used for testing CVN and SCVN specimens, and the instrumented striker used for testing KLST specimens. In the case of RHS tests, however, discrepancies between KV and W_t were much larger and the so-called “dynamic force adjustment” had to be applied.

(6) Consistent *DBTT* shifts between CVN, SCVN and MCVN specimens were observed, except for X65 which had to be removed from the analyses. The relationship between *DBTT*s measured from CVN specimens and sub-size or miniaturized samples can be effectively expressed by a temperature shift M, which increases with decreasing specimen size. Its dependency from the nominal fracture volume Bb^2 was found to be consistent with previous investigations, although the empirical relationship between M and Bb^2 might be different for SCVN and MCVN specimens.

(7) For Upper Shelf Energy, the values measured on the different specimen types show the best correlation with the ratio of nominal fracture volumes, expressed as $(Bb)^{3/2}$, except for KLST specimens, whose *USE* appears to be exponentially correlated to USE_{CVN}, at least when the specimen fractures totally or partially in upper shelf conditions, *i.e.*, in the case of X52 and X100, but not in the case of X65 or X70.

In general, the applicability of both sub-size and miniaturized Charpy specimens to the characterization of line pipe steels has been confirmed, as well as the feasibility of establishing reliable empirical correlations between parameters measured from specimens of different types, such as ductile-to-brittle transition temperatures and upper shelf energies. Materials which do not exhibit particularly high levels of toughness and ductility (such as X65 and

X70 in this study) are however easier to correlate, since the values of absorbed energy measured in a Charpy test substantially correspond to the energy spent for fracturing the specimens. For steels like X65 and X70, the significant amount of energy dissipated in the interaction between specimen and machine anvil/supports makes the Charpy test more similar to a plastic bend test.

Bibliography

[1] ASTM A370-14, *Standard Test Methods and Definitions for Mechanical Testing of Steel Products*, ASTM Book of Standards 01.03, 2014.

[2] API Specification 5L, *Specification for Line Pipe*, American Petroleum Institute, Forty-Third Edition, March 2004.

[3] ISO 14556:2000, *Steel -- Charpy V-notch pendulum impact test -- Instrumented test method*, International Standards Organization, 2000.

[4] ASTM E2248-13, *Standard Test Method for Impact Testing of Miniaturized Charpy V-Notch Specimens*, ASTM Book of Standards 01.03, 2014.

[5] ASTM E2298-13a, *Standard Test Method for Instrumented Impact Testing of Metallic Materials*, ASTM Book of Standards 01.03, 2014.

[6] C. N. McCowan, E. Lucon, and R. L. Santoyo, "*Comparison of Charpy V-notch Specimens: Full Size, Sub-Size, and Mini – Part 2: Shear Fracture*," to be submitted to *Materials Performance and Characterization*, 2014 (in preparation).

[7] W. Oldfield, "*Curve Fitting Impact Test Data: A Statistical Procedure*," ASTM Standardization News, November 1975, pp. 24-29.

[8] M. A. Sokolov and D. J. Alexander, "*An Improved Correlation Procedure for Subsize and Full-Size Charpy Impact Specimen Data*," NUREG/CR-6379, ORNL-6888, Oak Ridge National Laboratory, March 1997.

[9] D. R. Ireland, "*Procedures and Problems Associated with Reliable Control of the Instrumented Impact Test*," in ASTM STP 563, "*Instrumented Impact Testing,*" 1974, pp. 3-29.

[10] E. Lucon, "*On the Effectiveness of the Dynamic Force Adjustment for Reducing the Scatter of Instrumented Charpy Results*," Journal of ASTM International, Vol. 6, No. 1, January 2009.

[11] E. Lucon, R. Chaouadi, A. Fabry, J.-L. Puzzolante, and E. van Walle, "*Characterizing Material Properties by the Use of Full-Size and Subsize Charpy Tests: An Overview of Different Correlation Procedures*," in ASTM STP 1380, "*Pendulum Impact Testing: A Century of Progress*," T. A. Siewert and M. P. Manahan, Eds., ASTM, West Conshohocken, PA, 2000, pp.146-163.

[12] J. H. Gross, "*Effect of Strength and Thickness on Notch Ductility*," in ASTM STP 466, "*Impact Testing of Metals*," D. E. Driscoll, Ed., ASTM, Philadelphia, 1970, pp. 21-52.

[13] W. R. Corwin and A. M. Hougland, "*Effect of Specimen Size and Material Condition on the Charpy Impact Properties of 9Cr-1Mo-V-Nb Steel*," in ASTM STP 888, "*The Use of Small-scale Specimens for Testing Irradiated Material,*" W. R. Corwin and G. E. Lucas, Eds., ASTM, Philadelphia, 1986, pp. 325-338.

[14] W. R. Corwin, R. L. Klueh, and J. M. Vitek, "*Effect of Specimen Size and Nickel Content on the Impact Properties of 12 Cr-1 MoVW Ferritic Steel*," Journal of Nuclear Materials **122-123**, 1984, pp. 343-348.

[15] G. E. Lucas, G. R. Odette, J. W. Sheckherd, P. McConnell, and J. Perrin, "*Subsized Bend and Charpy V-Notch Specimens for Irradiated Testing*," in ASTM STP 888, "*The Use of Small-scale Specimens for Testing Irradiated Material,*" W. R. Corwin and G. E. Lucas, Eds., ASTM, Philadelphia, 1986, pp. 304-324.

[16] G. E. Lucas, G. R. Odette, J. W. Sheckherd, and M. R. Krishnadev, "*Recent Progress in Subsized Charpy Impact Specimen Testing for Fusion Reactor Materials Development*," Fusion Technology **10**, 1986, pp. 728-733.

[17] B. S. Louden, A. S. Kumar, F. A. Garner, M. L. Hamilton, and W. L. Hu, "*The Influence of Specimen Size on Charpy Impact Testing of Unirradiated HT-9*," Journal of Nuclear Materials **155-157**, 1988, pp. 662-67.

[18] H. Kayano, H. Kurishia, A. Kimura, M. Narui, M. Yamazaki, and Y. Suzuki, "*Charpy Impact Testing Using Miniature Specimens and Its Application to the Study of Irradiation Behavior of Low-Activation Ferritic Steels*," Journal of Nuclear Materials **179-181**, 1991, pp. 425-88.